博士論文

# Development of Earthquake Risk Assessment System for Nepal

# （ネパールを対象とした地震リスク評価システムの開発）

by

Ramesh GURAGAIN

**ラメッシュ グラガイン**

The University of Tokyo

January 2015

# Abstract

Earthquake is one of the most significant natural hazards in Nepal. There is a long history of destructive earthquakes that damaged large number of buildings and killed many people. Earthquake risk evaluation is the first step for realistic and effective planning and implementation of earthquake risk reduction as well as preparedness initiatives as it helps understanding the underlying problems and its magnitude. Different risk assessment methods are used in Nepal in some cities but the need is to do the risk assessment work at the national level and also at the large number of cities. Therefore, a need for a study on development of earthquake risk assessment system in Nepal which suggests appropriate tool/s for conducting earthquake risk assessment at different scale in Nepal, provides/recommend appropriate fragility functions for different types of Nepalese buildings and also suggest how much risk can be reduced if the risk reduction activities are implemented.

Eight different earthquake risk assessment methodologies and tools used in different cities and communities in Nepal were compared for their characteristics in terms of stakeholders' involvement, provisions of detail input and output, resources required for assessment works, simplicity for use, appropriateness for use at city level and national level and the tools and accessories are open source or not. HAZUS and Open Quake are found better options for national level risk assessment and RADIUS is found comparatively better for cities where there is no GIS information of buildings and infrastructures while as CAPRA GIS is found better for cities where GIS information of individual buildings and infrastructures are available.

Computation of fragility functions for non-engineered low strength brick masonry buildings in Nepal through time history analysis using Applied Element Method (AEM) was done. Extreme Loading for Structures (ELS) tool is used for AEM simulation. Key parameter required for non-linear analysis like shear strength of existing masonry buildings was obtained through direct shear test in actual field condition. The result obtained from AEM was compared with shaking table test results and a good agreement on experimental and numerical simulation result was found. Numerical models of several buildings with different configuration and number of stories for three different category of brick masonry buildings were prepared and analyzed with different mortar properties and different input motions. Damage state of all the buildings at the given input motions are recorded and cumulative probability of damage at each level of Peak Ground Acceleration (PGA) are recorded and a set of fragility functions for four damage state namely "Slight",

"Moderate", "Extensive" and "Complete" are computed for three different types of brick masonry buildings prevalent in Nepal.

For the development of fragility functions for stone masonry buildings, a new approach of clustering randomly generated triangular meshes to form random shaped stones is proposed in this study. Numerical models of two experimental cases, one for monotonic load case and the other for dynamic load case, were prepared applying the proposed new approach of modeling. The numerical simulation results obtained were compared with the experimental results. In monotonic loading case, the force-displacement relation and the crack patterns were compared with experimental results and a good agreement was found. While, in case of the shaking table test, the initiation and propagation of cracks, acceleration output at different stage of loading and overall damage of the building till collapse were compared. The experimental and numerical results showed a good agreement in all these compared parameters. The study found that the stone masonry structures can be simulated accurately in AEM using this technique of triangular meshing and clustering. Numerical models of representative stone masonry buildings with different configuration and mortar strength were prepared, analyzed and fragility functions were developed.

Retrofitting of masonry buildings in developing country like Nepal is a challenge because of the retrofitting cost. A combined system of using reinforced concrete bands and PP-bands together is proposed in this study and shaking table tests were conducted to compare the effectiveness. Two identical two-story stone masonry buildings of quarter scale were constructed and tested to compare the benefit of this proposed concept of retrofitting through shaking table test. One building model was retrofitted only with reinforced concrete bands and the other with the proposed combined system. Both the models were tested on shaking table with sinusoidal motions of different frequencies and amplitude. The result obtained were compared in terms of crack patterns and damage level, total mass loss at different stage of loading, hysteresis behavior and the cumulative energy dissipation. The comparison clearly shows that the model with combined system performed much better in terms of overall damage and loss of mass, better hysteresis behavior and also better energy dissipation capacity while the additional cost of PP-bands is negligible.

Numerical Simulation of masonry buildings with code recommended practices were conducted to discuss the change in fragility functions of earthquake resilient masonry buildings with the existing buildings. A remarkable change in safety as well as fragility functions were noticed from the comparison.

Finally, comparative study on earthquake damage assessment at the same scenario earthquake with existing buildings information was conducted using existing fragility functions and the newly developed fragility functions. The comparison clearly shows the use of the newly developed fragility functions gives more specific damage at the given location considering the varieties of buildings available in that location.

# Acknowledgements

I am grateful to the Japan Society for the Promotion of Science (JSPS) for providing me the RONPAKU fellowship through which this research in Nepal and Japan was possible. I am indebted to Meguro Laboratory, Institute of Industrial Science, The University of Tokyo for allowing me to conduct this off campus PhD. I am obliged to National Society for Earthquake Technology-Nepal (NSET) for providing all necessary support for my research in Nepal, allowing me to use research data from different programs and projects and also providing me three months study leave every year in last four years to visit The University of Tokyo to conduct this research.

This study has been done under the supervision of Prof. Kimiro Meguro at Institute of Industrial Science, The University of Tokyo and I would like to express my sincere gratitude to him for his inspirational guidance, permanent support and encouragement throughout the study. In fact, without his encouragement, I would not have started this research. I am thankful to Prof. Muneyoshi Numada for his academic guidance as well as fruitful professional discussions. I am grateful to Prof. Yoshiaki NAKANO, Director General of Institute of Industrial Science, The University of Tokyo for his guidance and critical suggestions during consultations. My sincere thanks to Prof. Kohei Nagai and Prof. Kazumasa Ozawa for providing me feedbacks to my research.

My special thanks go to Dr. Amod Mani Dixit, Executive Director of NSET for continuous motivation, kind guidance and supervision of my work while conducting research in Nepal. I am thankful to Mr. Shiva Bahadur Pradhanang, Chairman of the Management Committee of NSET for his encouraging words, to Mr. Surya Narayan Shrestha, Mr. Tika Sharma, Ms. Hima Shrestha, Mr. Bijay Krishna Upadhyay, Mr. Surya Prasad Acharya, Mr. Ganesh Jimee, Ms. Bhubaneshwari Parajuli, Mr. Khadga Sen Oli, Mr. Sujan Adhikari all of NSET, for helping me to collect field information as well as for their intellectual and moral support.

I am thankful to Ms. Niva Upreti and Ms. Rita Thakuri at NSET and Ms. Mina Takahashi, Ms. Miki Ogawa, Ms. Sayaka Minemoto and Ms. Masako Sakai from Meguro Laboratory for their administrative and logistic support throughout the study.

I sincerely appreciate the kind support and friendship of all colleagues in Meguro laboratory during all the stages of the present study. My special thanks to Dr. Makoto Fujiu who provided kind support to me every year when I visited Japan. I would like to remember the long-term friendship and continuous support by Mr. Daisuke Itoh for

sharing special moments of friendship.

Last but not least, I gratefully acknowledge the continuing patience and vital sacrifices of my parents and family members whose love and supports are always a constant source of encouragement and guidance to me. I am especially thankful to my wife Pankaja for her continuous love and understanding. I am thankful to my daughters Parima and Paridhi for their sweet smiles and love which energized me to work even in adverse situation.

Ramesh Guragain
Tokyo, Japan
January, 2015

# List of Publications

1. Ramesh GURAGAIN, Muneyoshi NUMADA and Kimiro MEGURO; Development of Fragility Functions for Brick Masonry Buildings in Nepal using Applied Element Method; *SEISAN KENKYU* Vol. 65 (2013) No. 6 p. 745-752
2. Ramesh GURAGAIN, Amod Mani DIXIT and Kimiro MEGURO; Development of Fragility Functions for Low Strength Masonry Buildings in Nepal using Applied Element Method, *15th World Conference on Earthquake Engineering* (CD-ROM), September 24-28, 2012, Lisbon, Portugal
3. Hima SHRESTHA, Suman PRADHAN, Ramesh GURAGAIN; Experiences on Retrofitting of Low Strength Masonry Buildings by Different Retrofitting Techniques in Nepal, *15th World Conference on Earthquake Engineering* (CD-ROM), September 24-28, 2012, Lisbon, Portugal
4. Ramesh GURAGAIN, Ganesh JIMEE, Amod Mani DIXIT; Earthquake Awareness and Effective Planning through Participatory Risk Assessment: an Experience from Nepal, *14th World Conference on Earthquake Engineering, (CD-ROM),* October 12-17, 2008, Beijing, China
5. Ramesh GURAGAIN and Kimiro MEGURO; Numerical Simulation of Random Shaped Stone Masonry House using Applied Element Method, *Earthquake Spectra* (Submitted on November, 2014)

# Curriculum Vitae

**Name:** Ramesh GURAGAIN

**Date of birth:** August 26, 1973

**Nationality:** Nepalese

**Education:**

| | |
|---|---|
| 1994 - 1998 | Bachelor's Degree, Department of Civil Engineering, Institute of Engineeering, Tribhuvan University, Nepal |
| 2004 - 2006 | Master Degree, Department of Civil Engineering, The University of Tokyo, Japan |
| 2011 - 2015 | Doctoral Course, Department of Civil Engineering, The University of Tokyo, Japan |

**Professional and Research Experience:**

| | |
|---|---|
| 1998 - 2000 | Site Engineer, TAEC Consult Pvt. Ltd, Nepal. |
| 2000 - 2004 | Structural Engineer, National Society for Earthquake Technology-Nepal (NSET) |
| 2006-2009 | Senior Structural Engineer/Senior Researcher, National Society for Earthquake Technology-Nepal (NSET) |
| 2009-2012 | Director, Earthquake Engineering Research and Training Division of National Society for Earthquake Technology-Nepal (NSET) |
| 2012-Till Now | Deputy Executive Director, National Society for Earthquake Technology-Nepal (NSET) |

**Academic Awards:**

FURUICHI Award from the Department of Civil Engineering, The University of Tokyo for best research in Master Degree in 2004-2006 batch

# Table of Contents

# List of Figures

# List of Tables

# 1. Introduction

## *1.1 Earthquake Risk in Nepal*

Earthquake is one of the most significant natural hazards in Nepal. There is a long history of destructive earthquakes in the Himalayan region. Many studies have been carried out in the past to evaluate the earthquake hazard, and in later times, the risk in Nepal. Figure 1-1 shows the distribution of Peak Horizontal Acceleration at bedrock that has a 10% probability of being exceeded over 50 years prepared by Department of Mines and Geology, National Seismological Centre, Nepal (Pandey et al., 2002). The PGA distribution is varied from area to area and high PGA values can be seen along the western and central region of Nepal with most part of the country with more than 300 gal. The values given are for bedrock and with amplification at surface it will be higher.

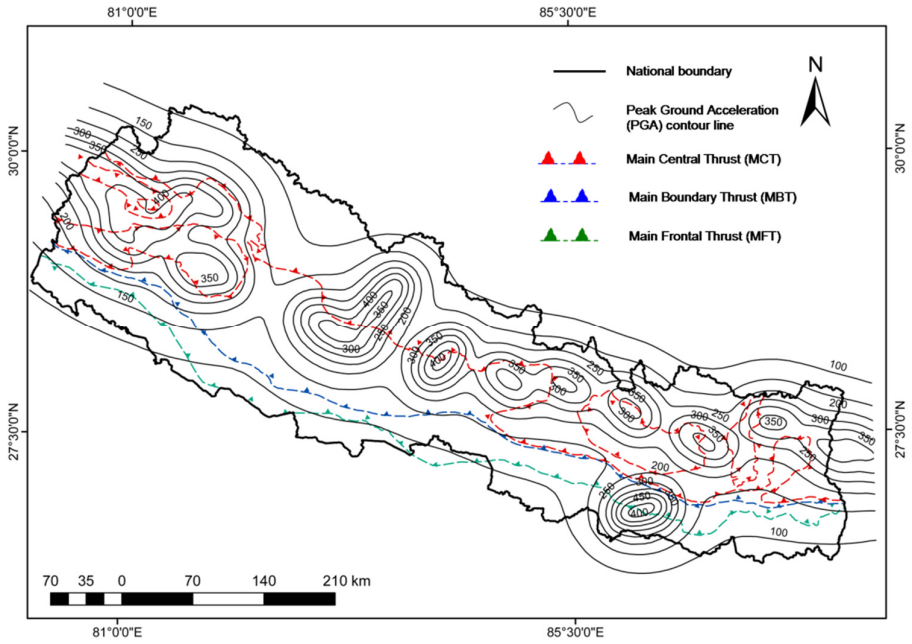


Figure 1-1: Seismic Hazard Map of Nepal (Pandey et al., 2002)

An Earthquake scenario for Kathmandu valley prepared by Kathmandu Valley Earthquake Risk Management Program (KVERMP) by National Society for Earthquake technology-Nepal (NSET) and Geo-Hazards International (GHI) in 1998 estimated about 40,000 deaths and about 95,000 injuries should there be a MMI IX level of shaking in Kathmandu Valley (NSET, 1999). The estimate was revised by NSET in 2010 and it estimates the probability of about 100,000 deaths and about

300,000 injuries in Kathmandu Valley.

Global Earthquake Safety Initiative (GESI) by GHI and United Nation Center for Regional Development (UNCRD) conducted comparative risk of 21 cities in earthquake hazard zone around the world and Kathmandu has been found with the highest per capita risk of casualty among those 21 cities studied (GESI, 2001). Figure 1-2 shows the comparison of per capita risk of casualty among the cities conducted by GESI (2001).

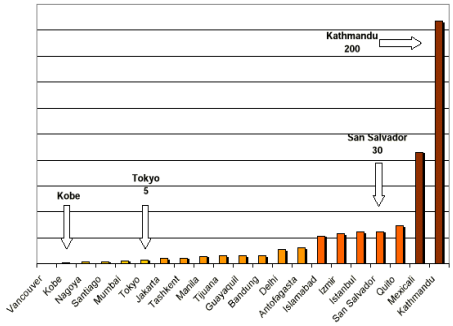


Figure 1-2: Comparison of Per Capita Risk of Casualty in different Cities (GESI, 2001)


Figure 1-3: Source of Earthquake Risk in Kathmandu (GESI, 2001)

Figure 1-3 shows the source of earthquake risk based on the study by GESI (2001). It clearly shows that the risk comes from vulnerable buildings stock in Kathmandu valley. The buildings scenarios in other cities in Nepal are similar. Therefore, Nepal is in a high earthquake risk with high potential casualty in future earthquakes. However, systematic earthquake risk assessment is required to quantify the risk for better earthquake risk management planning.

## 1.2 Earthquake Risk Assessment Practices in Nepal and use of Risk Assessment Results

Earthquake risk evaluation is the first step for realistic and effective planning and implementation of earthquake risk reduction as well as preparedness initiatives as it helps understanding the underlying problems and its magnitude. The first earthquake risk assessment at city level carried out in Nepal was in Kathmandu Valley under Kathmandu Valley Earthquake Risk Management Project (KVERMP) implemented jointly by National Society for Earthquake Technology–Nepal (NSET) and Geo-Hazards International (GHI) in 1997. Detail earthquake scenario of Kathmandu Valley based on KVERMP work is given in NSET (1999).

Different earthquake risk assessment studies in different cities/communities are

continued in Nepal with different approaches and methodologies. Starting from simple earthquake loss estimation based on secondary information on general building typology distribution in the city combined with intensity distribution of past earthquake (NSET, 1999), to comprehensive one with detail analysis of individual buildings (Jimee, 2006) were carried out. Assessments were carried out in small communities with population of a couple of thousands to the mega cities with Millions.

Use of earthquake risk assessment results for earthquake risk management planning and also for awareness raising has been studied by Guragain, Jimee, and Dixit (2008). They summarize the main lessons of earthquake risk assessment works in Nepal and highlights that earthquake risk assessment can be considered as a strong awareness raising and planning tool if concerned stakeholders are involved in the process of assessment. Study on different risk assessment works conducted in Nepal shows that the risk assessment conducted using simplified tool helped to create demand from the cities and communities for detail evaluation. There are different cases found in which communities started risk management initiatives after the assessment and there are cities which conducted systemic earthquake risk management action planning and there are cases of influence to higher level authorities that cause formulation of related policies (Guragain, Jimee and Dixit, 2008).

However, there is no recommended tools/methodology to be used for national as well as city level. A comparative study of these tools in terms of stakeholders involvement, provisions for detail Input/ output, resource required, simplicity to use, appropriateness of use at city and national level and easiness to customize and update so that tools for national level risk assessment and city level risk assessment can be recommended.

In addition, whatever the risk assessment tools, one of the important parameter on which the risk assessment result depends is fragility functions of the existing buildings. Thus, use of appropriate fragility function is very important to obtain reasonable risk assessment result.

In Nepal most of the buildings are masonry. A survey conducted by JICA (2002) shows more than 70% of the buildings in Kathmandu Valley are masonry, this ratio will be more in rural area. Therefore, accuracy of earthquake risk assessment results in Nepal depends on accuracy of fragility function of masonry buildings.

## *1.3 Fragility Functions for Masonry Buildings*

Review of seismic fragility functions of masonry buildings from different sources are studied to identify appropriate fragility functions for masonry buildings in Nepal.

Different fragility functions/curves for masonry buildings are suggested by various authors like ATC-13 (1985), NBC (1994), RADIUS (2000), GESI (2001) and HAZUS (2003). This sub-section describes different fragility functions analyze the pros and cons for their use for buildings in Nepal.

**ATC-13 Fragility Functions**

Applied Technology Council (ATC) developed earthquake damage evaluation data for facilities in California as a project contracted by Federal Emergency Management Agency (FEMA) from 1982 and published ATC-13 (1985) document with Earthquake Damage Evaluation Data for California in 1985.

The fragility functions developed under ATC-13 (1985) were primarily based on experience and judgment of seasoned earthquake engineers. Project Engineering Panel composed of senior-level specialists in earthquake engineering and 58 additional earthquake specialists involved in the process and prepare consensus earthquake damage database. ATC-13 fragility functions are developed for facilities in California but they have been widely used for earthquake evaluation of urban areas even in developing countries till now.

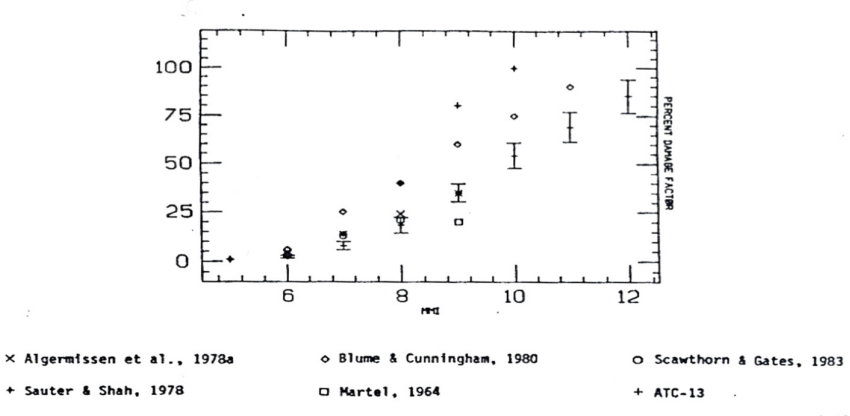


Figure 1-4: ATC-13 Fragility function for Unreinforced Masonry Buildings with standard deviation bars including damage data from literatures (ATC-13,1985)

Figure 1-4 gives ATC-13 fragility function for Unreinforced Masonry Buildings with standard deviation bars including damage data from literatures. It is on Modified Mercally Intensity (MMI) in X-axis and percentage of damage in Y-axis (In terms of repair cost).

Limitations for ATC-13 fragility functions to be used in Nepal are:

- Only one type of Low-raised Unreinforced Masonry buildings leading to only one damage probability matrix. However, in case of developing countries there are varieties of masonry buildings and their responses during earthquakes are also quite different.
- The database itself is mainly from experts opinions and not based on either direct damage data or analysis

**RADIUS Fragility Functions**

Risk Assessment tool for Diagnosis of Urban areas against Seismic disasters (RADIUS) methodology has been described in RADIUS (2000). It has used 10 classifications of buildings based on building materials, construction type, building age, story or height and usage, etc. RADIUS Tool uses 10 classification categories, adopted by sample Latin American countries.

Classifications of building types used in RADIUS are as follows:

1. RES1: Informal construction: mainly slums, row housing etc. made from unfired bricks, mud mortar, loosely tied walls and roofs
2. RES2: URM-RC composite construction: substandard construction, not complying with the local building code provisions. Height up to 3 stories. URM = Unreinforced Masonry, RC = Reinforced Concrete
3. RES3: URM-RC composite construction: old, deteriorated construction, not complying with the latest building code provisions. Height 4 - 6 stories
4. RES4: Engineered RC construction: newly constructed multi-story buildings, for residential and commercial purposes
5. EDU1: School buildings, up to 2 stories: generally, the percentage of this type of building should be very low
6. EDU2: School buildings, greater than 2 stories: office buildings should also be included in this class; generally, the percentage of this type of buildings should be very low

7. MED1: Low to medium rise hospitals: generally, the percentage of this type of building should be very low
8. MED2: High rise hospitals: generally, the percentage of this type of building should be very low.
9. COM: Shopping Centers
10. IND: Industrial facilities: both low and high risk

The tool gives fragility functions for each building categories above. Figure 1-5 gives the fragility functions given in RADIUS tool. The masonry buildings fall in to RES1, RES2 and RES3 type buildings above.

The limitations of choosing RADIUS fragility functions for use in Nepal are:

- Too general as both the RC and Masonry buildings are given common fragility functions, which in Asian region are quite different
- The categories are from Latin American countries and may not represent the case in Nepal
- Different damage state in relation to damage rate is not described

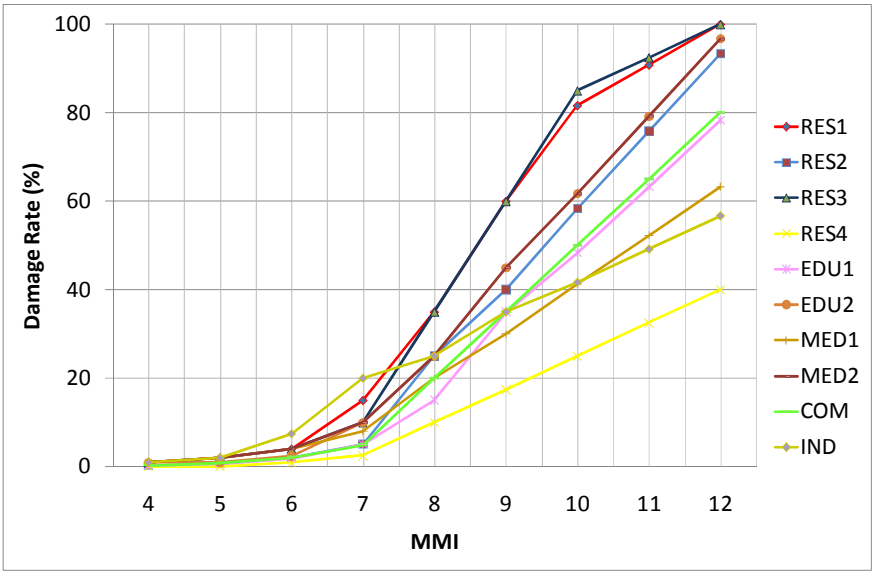


Figure 1-5: RADIUS fragility functions for different types of buildings

**GESI Fragility Functions**

Global Earthquake Safety Initiative (GESI), a program implemented by Geo-Hazards International (GHI) and United Nations Centre for Regional Development (UNCRD), Japan (GESI, 2001), developed and used a set of fragility functions for 9 different types of buildings. They used 9 typical fragility functions named A to I and used them

for different type of buildings combined with "quality of design", "quality of construction" and "quality of materials". So, same building type sometimes get one fragility curve and another time another. Figure 1-6 gives the GESI typical fragility curves.

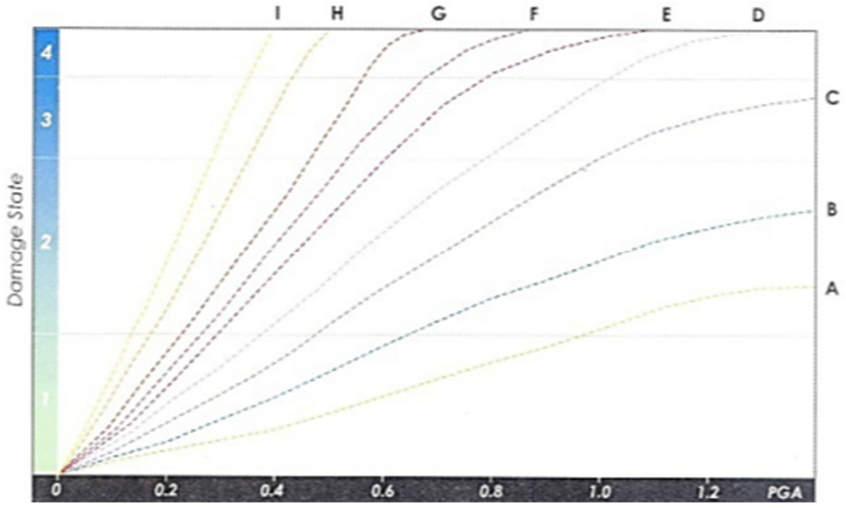


Figure 1-6: GESI fragility functions (GESI, 2001)

Limitations on using GESI fragility functions are:

- In GESI fragility functions, it has only one category of URM even for low rise or medium/high rise
- The different fragility functions are based on design, supervision and material quality but difficult to define these attributes for small geographical areas as they are too subjective
- The damage states for slight to moderate has only one category and difficult to separate

**Fragility Functions in Nepal National Building Code**

NBC (1994) has fragility functions for different types of masonry and reinforced concrete buildings in India, Nepal and other countries with similar building typology based on observed behavior of limited buildings in past earthquakes mainly in North Yemen, India and Iran.

It has primarily three major categories buildings:

Type A: Low strength masonry like field stone, adobe etc. (Mud based)

Type B: Cement mortar ordinary brick buildings

Type C: Reinforced concrete and steel buildings

Further sub classifications like "A-", "A+", "A++", "B-", "B+", "B++" etc. are done based on other properties of the buildings like number of stories, mortar, seismic resistant elements etc. Figure 1-7 gives the fragility functions given in NBC (1994)

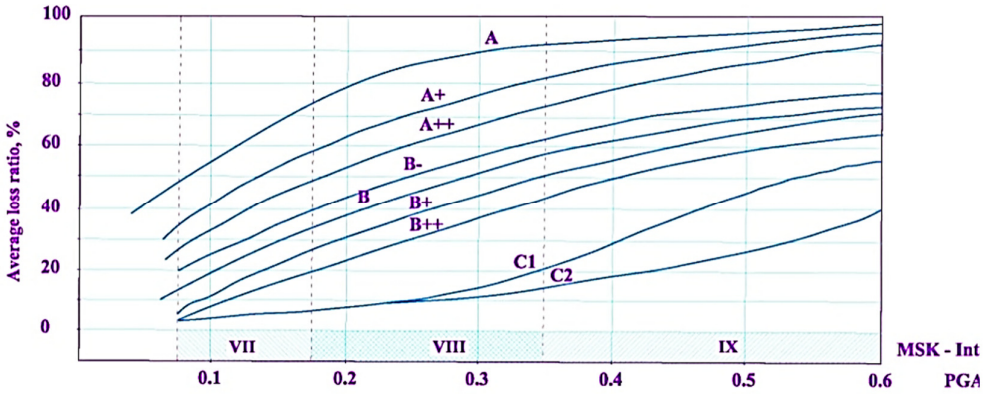


Figure 1-7: Fragility curves for different types of masonry and concrete buildings (Redrawn after NBC, 1994)

These fragility functions are given in terms of average loss ratio in different intensities and peak ground acceleration.

Limitations on using NBC fragility functions are as follows:

- The damage ratio are not known what level of damage (Complete collapse, extensive, moderate or all) they represent
- There is only one function (curve) for one type of building and cannot be segregated for different damage state
- The functions are based on qualitative judgment of acceleration and with limited survey

**Fragility Functions in HAZUS (2003) for Masonry Buildings**

HAZUS (2003) gives a set of fragility function for low raised unreinforced masonry buildings. It gives the probability of different damage state like "Slight", "Moderate", "Extensive" and "Heavy" damage. So, at any point of given peak ground acceleration, probability of damage to any damage state is known.

HAZUS (2003) has given only one set of function for all type of low raised unreinforced masonry buildings. However, in developing countries like Nepal, there are different type of unreinforced low rise masonry buildings which are different in configuration, materials properties and construction practices. The strength and ductility of these masonry buildings varies a lot and thus only one function is not

applicable.

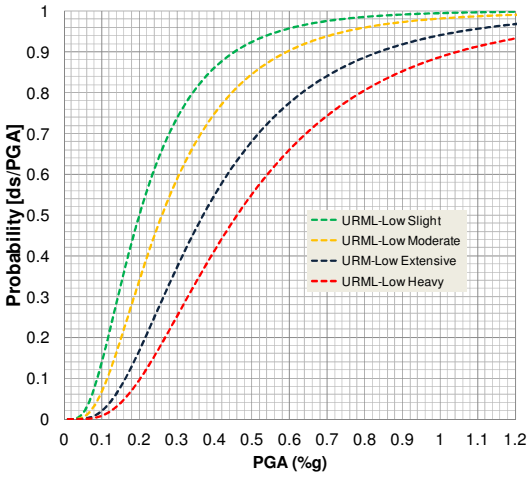


Figure 1-8: Fragility Functions for Low Rise Masonry Buildings (Redrawn after HAZUS, 2003)

Review of fragility functions for masonry buildings suggested by different authors it is found that some literatures like NBC(1994) covers many types of masonry buildings but does not have different function for different damage state. In other case like HAZUS (2003), a set of function for different damage state is given but it is only for one type of masonry.

Thus, it was found that whatever risk assessment methodology is chosen to use in Nepal, development of a set of fragility functions, especially for masonry buildings is required for conducting reasonable risk assessment work.

## *1.4 Research Objectives and Structures*

Earthquake risk evaluation is the first step for realistic and effective planning and implementation of earthquake risk reduction as well as preparedness initiatives as it helps understanding the underlying problems and its magnitude. Different risk assessment methods are used in Nepal in some cities but the need is to do the risk assessment work at the national level and also at the large number of cities. Therefore, a need for a study on development of earthquake risk assessment system in Nepal which suggest appropriate tool/s for conducting earthquake risk assessment at different scale in Nepal, provides/recommend appropriate fragility functions for different types of Nepalese buildings and also suggest how much risk can be reduced if the risk reduction activities are implemented is realized.

So, the overall Goal of this research is "Development of Earthquake Risk Assessment System in Nepal" and the specific objectives are:

1. Study and compare different tool/s for earthquake risk assessment and recommend to use at city and national level
2. Develop and recommend fragility functions for prevalent vulnerable type of buildings in Nepal
3. Compare effectiveness of retrofitted buildings in relation to the developed fragility functions

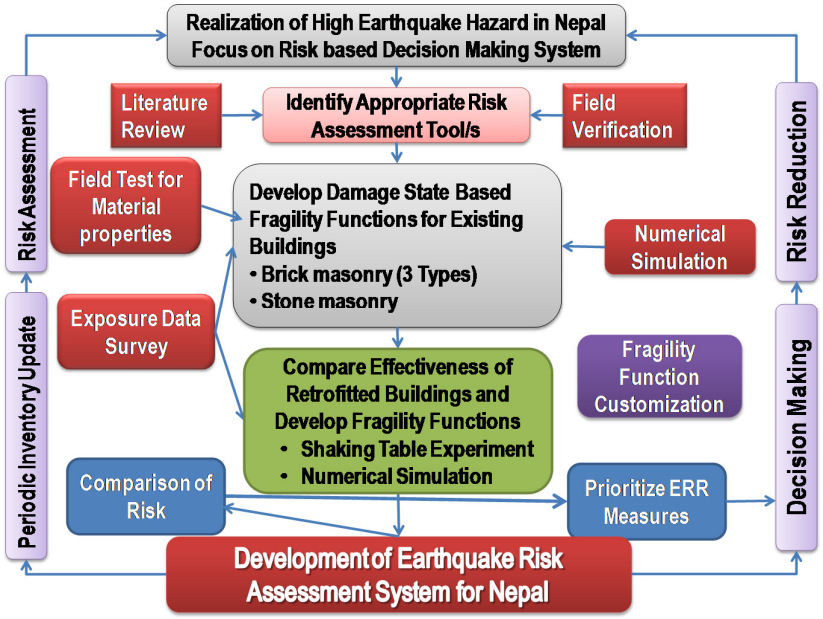


Figure 1-9: Overall Research Flow

## REFERENCES

ATC-25. (1991). "Seismic Vulnerability and Impact of Disruption of Lifelines in the Conterminous United States." *Applied Technology Council*, California, USA.

NBC. (1994). "Seismic Hazard Mapping and Risk Assessment for Nepal." *Nepal National Building Code (NBC)*, Ministry of Physical Planning and Works, Nepal.

ATC-13. (1995). "Earthquake Damage Evaluation Data for Probable Maximum Loss Studies of California Buildings." *Applied Technology Council*, California, USA.

NSET. (1999). "Earthquake Scenario of Kathmandu Valley." *National Society for Earthquake Technology-Nepal (NSET)*, Kathmandu, Nepal.

NSET. (1999b). "Kathmandu Valley Earthquake Risk Management Action Plan." *National Society for Earthquake Technology-Nepal (NSET)*, Kathmandu, Nepal.

RADIUS. (2000). "Risk Assessment Tools for Diagnosis of Urban Areas against Seismic Disasters (RADIUS)– an initiative of the International Decade for Natural Disaster Reduction

(IDNDR)" *Secretariat of the International Strategy for Disaster Reduction (ISDR),* (CD-ROM) Geneva, Switzerland.

GESI (2001), Global Earthquake Safety Initiative Pilot Project (GESI), Final report, GHI and UNCRD, 2001

Pandey MR, Chitrakar GR, Kafle B, Sapkota SN, Rajaure SN, Gautam UP (2002) Seismic hazard map of Nepal. Department of Mines and Geology, Kathmandu, Nepal

Amod Mani Dixit, Mahesh Nakarmi, Shiva Bahadur Pradhanang, Jitendra Bothara, Jyoti Prasad Pradhan, Brian Tucker and Laura Dwelley Samant. (2002a). "Hazard Mapping and Risk Assessment: Experiences of KVERMP." *Proceedings on Regional Workshop on Best Practices in Disaster Mitigation*, 24-26 September 2002, Bali, Indonesia.

Amod Mani Dixit, Mahesh Nakarmi, Shiva Bahadur Pradhanang, Jitendra Bothara, Bishnu Hari Pandey, Ramesh Guragain, Ram Chandra Kandel, Surya Narayan Shrestha and Brian Tucker, Laura Dwelley Samant. (2002b). "Promoting Safer Building Construction: Experiences of KVERMP." *Proceedings on Regional Workshop on Best Practices in Disaster Mitigation*, 24-26 September 2002, Bali, Indonesia.

Amod Mani Dixit, Shiva Bahadur Pradhanang, Ramesh Guragain, Ram Chandra Kandel, Surya Narayan Shrestha, Brian Tucker, Laura Dwelley Samant, Yogeshwor Krishna Parajuli. (2002c). "Promoting Safer Building Construction: Experiences of KVERMP." *Proceedings on Regional Workshop on Best Practices in Disaster Mitigation*, 24-26 September 2002, Bali, Indonesia.

JICA. (2002). "The study on Earthquake Disaster Mitigation in the Kathmandu valley Kingdom of Nepal." Final report, Vol - II, *Japan International Cooperation Agency*, Kathmandu, Nepal.

HAZUS-MH. (2003). "Multi-hazard Loss Estimation Methodology." Department of Homeland Security, Emergency Preparedness and Response Directorate, *Federal Emergency Management Agency (FEMA)*, Washington D.C.

Guragain, J. (2004). "GIS for Seismic Building Loss Estimation: A Case Study from Lalitpur Sub-Metropolitan City Area Kathmandu, Nepal." M. Sc. Thesis, International Institute for Geo-information Science and Earth Observation, Enschede, Netherland

Guragain, R., Pandey, B., and Shrestha, S. (2004). "Guideline for Seismic Vulnerability Assessment of Hospitals in Nepal." *National Society for Earthquake Technology-Nepal (NSET)*, Kathmandu, Nepal

Jimee, G. (2006). "Seismic Vulnerability and Capacity Assessment at Ward Level: A Case Study of Ward No. 20, Lalitpur Sun-metropolitan City, Nepal", M. Sc. Thesis, International Institute for Geo-information Science and Earth Observation, Enschede, Netherland

Ramesh Guragain, Ganesh Jimee and Amod Mani Dixit. (2008). "Earthquake Awareness and Effective Planning Through Participatory Risk Assessment: An Experience from Nepal", *Proceedings on 14th World Conference on Earthquake Engineering*, (CD-ROM), October 12-17, 2008, Beijing, China

CAPRA (2012). "CAPRA Probabilistic Risk Assessment Program", <http://www.ecapra.org/capra-gis achieved on 2014/10/16 > (19 October, 2014)

GEM. (2014). "Open Quake", < http://www.globalquakemodel.org/openquake/about/> (19 October, 2014)

# 2. Comparative Study of Earthquake Risk Assessment Tools Implemented in Nepal

## *2.1 Introduction*

Earthquake risk evaluation is the first step for realistic and effective planning and implementation of earthquake risk reduction as well as preparedness initiatives as it helps understanding the underlying problems and its magnitude. The first earthquake risk assessment at city level carried out in Nepal was in Kathmandu Valley under Kathmandu Valley Earthquake Risk Management Project (KVERMP) implemented jointly by National Society for Earthquake Technology–Nepal (NSET) and Geo-Hazards International (GHI) in 1997. Detail earthquake scenario of Kathmandu Valley based on KVERMP work is given in NSET (1999a).

Different earthquake risk assessment studies in different cities/communities are continued in Nepal with different approaches and methodologies. Starting from simple earthquake loss estimation based on secondary information on general building typology distribution in the city combined with intensity distribution of past earthquake (NSET, 1999a), to comprehensive one with detail analysis of individual buildings (Jimee, 2006) were carried out. Assessments were carried out in small communities with population of a couple of thousands to the mega cities with Millions.

Guragain, Jimee, and Dixit (2008) summarize the main lessons of earthquake risk assessment works in Nepal and highlights that earthquake risk assessment can be considered as a strong awareness raising and planning tool if concerned stakeholders are involved in the process of assessment. Study on different risk assessment works conducted in Nepal shows that the risk assessment conducted using simplified tool helped to create demand from the cities and communities for detail evaluation. There are different cases found in which communities started risk management initiatives after the assessment and there are cities which conducted systemic earthquake risk management action planning and there are cases of influence to higher level authorities that cause formulation of related policies (Guragain, Jimee and Dixit, 2008).

This chapter focuses on six different earthquake risk assessment tools and methodologies used in Nepal as well as two more tools that are in the process of use. This chapter further discusses the lessons learned from different earthquake risk assessment activities and compare the risk assessment tools in terms of stakeholders involvement, provisions for detail Input/ output, resource required, simplicity to use, appropriateness of use at city and national level,

easiness to customize and update and open source or not.

## 2.2 Earthquake Risk Assessment Methodologies used in Nepal

Different earthquake risk assessment methodologies are used in Nepal for evaluation of earthquake risk of cities and communities in Nepal. They not only differ in details of input and output but also on the approaches and process too. The brief description of each earthquake risk assessment methodologies implemented in Nepal are discussed in the following sub-sections.

### 2.2.1 KVERMP Methodology

The first earthquake risk assessment at city level was conducted by NSET and GHI in 1997 under the program called Kathmandu Valley Earthquake Risk Management Program (KVERMP). KVERMP used an approach of using existing information on earthquake hazard than investing resources on refining it with new tools and equipment (Dixit, Nakarmi, Pradhanang, Bothara, Pradhan, Tucker and Samanta, 2002a). The program used the previous documented largest earthquake shaking to the study area as the worst case scenario in terms of hazard. Intensity distribution of 1934 Nepal-Bihar Earthquake in Kathmandu as shown in Figure 2-1, which was published in 1936 by geological survey of India, was used as the basis of potential earthquake hazard for loss estimation. In addition, liquefaction susceptibility map given in NBC (1994) was used for estimating potential loss of lifelines and critical infrastructures.

General information on building typology and their distribution based on census data and limited survey carried out for other projects was used as the building and population information. Earthquake risk in terms of damage to buildings and infrastructures was calculated based on fragility functions in ATC-13(1995) and ATC-25 (1991) respectively. In addition, possible death and injury figures were determined by looking at statistics from previous comparable earthquakes from around the world (Dixit et al, 2002a).

The main focus of KVERMP methodology was on process of involving cities and communities not only in mitigation planning and risk reduction but also in the risk assessment activities. According to Dixit et al (2002a), translation of technical outcome of risk assessment to common people languages was another major approach that KVERMP took as an approach.

All sectors of society, technical community, decision makers/authorities, lifelines, schools, hospitals etc. were involved in the process of earthquake scenario preparation. Program conducted series of interactions with stakeholders including all lifeline facilities for their opinion on estimated damage and also their preparedness level and recovery capacities. After

the realistic assessment of capacities of all concerned stakeholders, the risk maps were interpreted in common people language. For example, the number of possible breaks to water supply pipelines combined with repair capacity of Water Supply Corporation interpreted to water system functionality map showing the availability of water in different part of the city after different time of scenario earthquake as shown in Figure 2-2 (NSET, 1999a).

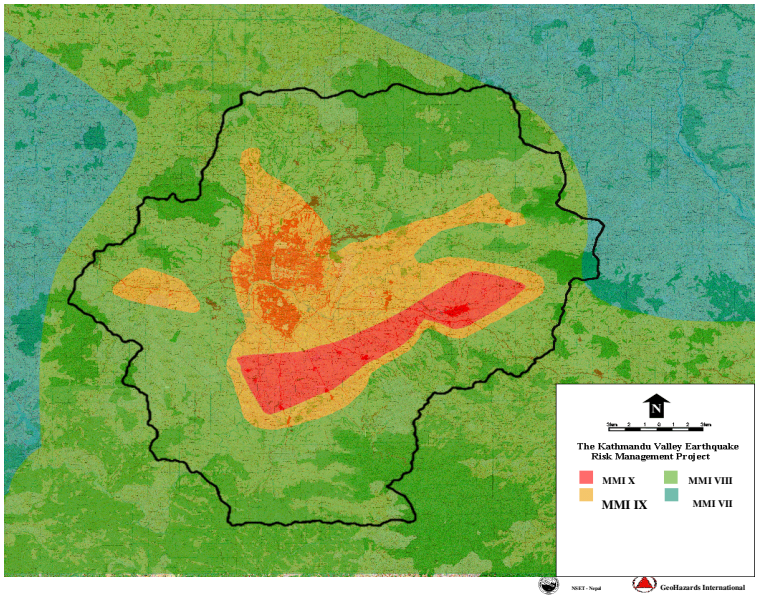


Figure 2-1: Intensity Distribution of 1934 Nepal-Bihar Earthquake in Kathmandu Valley compiled by KVERMP (NSET, 1999a)

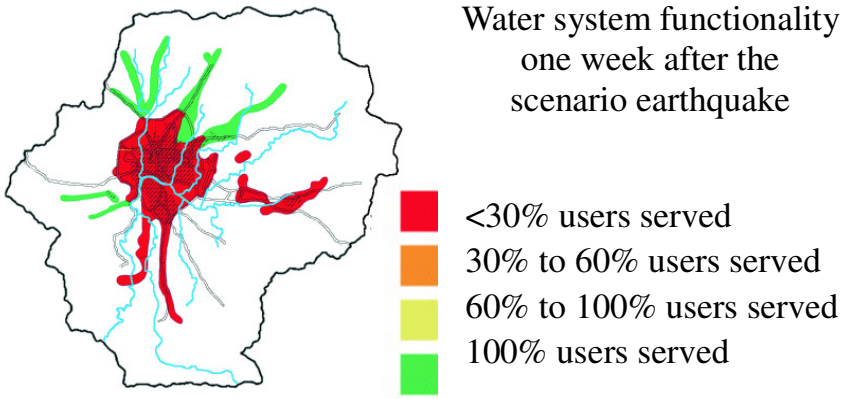


Figure 2-2: Water Supply System Functionality in Kathmandu Valley One week after Scenario Earthquake [NSET, 1999a]

The participation of all concerned stakeholders in the risk assessment process itself was

educatory for them on possible consequence of potential earthquake to their daily life and helped to planning some risk management activities (Dixit et al, 2002a). A scenario document explaining the results of the earthquake loss estimation study in layman's terms was written and published in English and Nepali languages (NSET, 1999a). This document includes a description of possible damages to various lifelines systems in Kathmandu and an explanation of the repercussions of this damage in the society. The document also presents a story of a representative citizen, "Bhaicha", for an entire year after the scenario earthquake, illustrating how his life is impacted. A part of script just with impact to "Bhaicha" just after an earthquake as documented in NSET (1999a) is given in Figure 2-3.

***Bhaicha is running …***

Bhaicha is a friendly, lower middle-class man who works as a clerk in a financial company. He is riding his bicycle on an errand for his branch chief. As he reaches Durbar Marg, his bicycle suddenly loses its balance and he falls over. Bhaicha is confused because his bicycle has not collided with anything, nor has it hit a bump in the road. He notices that other people around him have also fallen down and he is surprised to see that motorbikes and other vehicles are swerving and shaking. While trying to determine what is happening, he hears a low rumbling sound like that of a storm and sees many people running in all directions and he notices the swaying of buildings and trees. Only then he realizes that he is experiencing an earthquake. He leaves his bicycle on the roadside and starts running. He thinks of his family and, forgetting his errand, runs towards home.

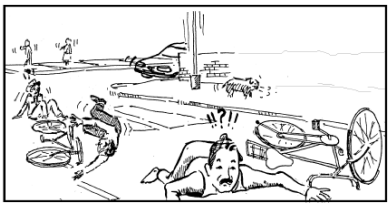

It is difficult to run because the ground is still shaking strongly and there are many frightened and confused people in the streets. A house collapses directly in front of Bhaicha, blocking his path. He realizes that he could be crushed by falling debris and starts to move with a little more caution. Bhaicha is scared, but he stumbles on in the direction he thinks is towards home, trying to avoid other people and falling objects. Bhaicha reaches an open space and stops, unsure of where he is. The shaking has stopped, but the collapsing buildings are no longer recognizable and the air is thick with dust. He takes a deep breath, realizing that it will be difficult to find his way home.

Figure 2-3: Part of Earthquake Scenario of Kathmandu Valley prepared by KVERMP [NSET, 1999a]

After this process of scenario, the project worked with over 80 government and non-government institutions to develop an action plan to systematically reduce the risk over time (Dixit, Nakarmi, Pradhanang, Bothara, Pandey, Guragain, Kandel, Shrestha, Tucker and Samanta, 2002b). The main purpose of the plan was to assist the Government of Nepal, concerned agencies and the municipalities of the Kathmandu Valley to reduce the earthquake risk over time by implementing earthquake risk reduction and preparedness activities. The specific objectives of the plan according to NSET (1999b) were: improving emergency response planning and capability, improving awareness of issues relating to earthquake risk, integrating seismic resistance into new construction processes, improving safety in school buildings, improving the seismic performance of existing structures, improving the seismic performance of utility and transportation systems, increasing experts' knowledge of the earthquake phenomenon, vulnerability, consequences and mitigation techniques, and preparing for long-term community recovery following damaging.

Some of the important actions of the action plan were implemented by NSET in collaboration with central and local government in Nepal. Among them activities like school earthquake

safety program, masons training, earthquake safety day etc. initiated as the activities of the plan are key programs in Nepal and the region in the field of earthquake risk management. The earthquake scenario was helpful on raising awareness and finally leading to implementation of such earthquake risk management activities according to Dixit, Pradhanang, Guragain, Kandel, Shrestha, Tucker, Samant and Parajuli (2002c).

### 2.2.2 RADIUS methodology

UN IDNDR (UN ISDR) implemented the project called Risk Assessment Tools for Diagnosis of Urban Areas against Seismic Disasters (RADIUS) during 1996-1999. The project included development of earthquake damage scenarios and action plans for earthquake disaster mitigation for nine different cities which were Bandung, Tashkent, Zigong, Addis Ababa, Izmir, Skopje, Antofagasta, Guayaquil, and Tijuana. RADIUS has produced a tool for earthquake damage estimation. The scenario preparation methodology developed under KVERMP was adopted by the RADIUS project for implementation in the RADIUS cities around the world (RADIUS, 2000).

A computer program in MS-Excel for simplified Earthquake Damage Estimation was developed as a component of the RADIUS project. The program requires input of a simple data set and provides visual results with user-friendly prompts and help functions. Input data are scenario earthquake (Magnitude, distance, depth and attenuation relation), population, building types, ground types, and lifeline facilities and outputs are seismic intensity (MMI), building damage, lifeline damage and casualties, which are shown with tables and maps. The concerned city needs to be divided to specific grid and the input data has to be provided for all grids (RADIUS, 2000).

NSET implemented Municipal Earthquake Risk Management Project (MERMP) in 2003-2004 and used the RADIUS tool for earthquake loss estimation in three selected cities, Banepa, Vyas and Dharan, under the project. As the RADIUS tool was easy-to-use and does not require detail technical knowledge on earthquake engineering to use it, the municipality officials conducted the risk assessment with small guidance from NSET. They run the tool for different possible earthquake scenarios. The difference of earthquake impact, if it is small or large; it occurs in day time and night time etc. was analyzed. The city officials also analyzed the impact of implementing earthquake risk management activities like building code implementation by developing different scenario after a certain period of time (Guragain, Jimee, and Dixit, 2008).

Figure 2-4 and Figure 2-5 show example of converting any available base map of city to excel grids. Different cities continue updating their risk assessment and also develop different scenarios to compare changes in building damage and casualties if any risk reduction

activities are implemented. Figure 2-6 shows a comparison of casualty scenario calculated in 2011 by Dharan Municipality after 10 years of building code implementation, i.e. projection of casualty scenario in 2021 for two cases with and without building code implementation calculated in 2011. Such comparison has been found helpful on motivating cities and communities to focus on important risk reduction initiatives.

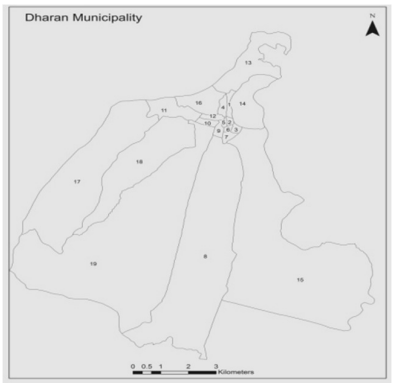


Figure 2-4: Example base map of a city for analysis in RADIUS

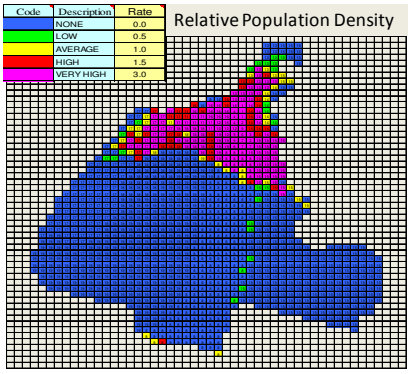


Figure 2-5: Example on Conversion of base map to Excel-Grids in RADIUS

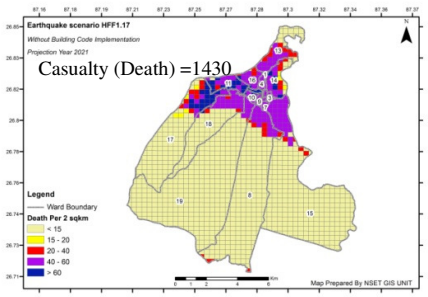


(a) Casualty Scenario in case of without Building Code Implementation

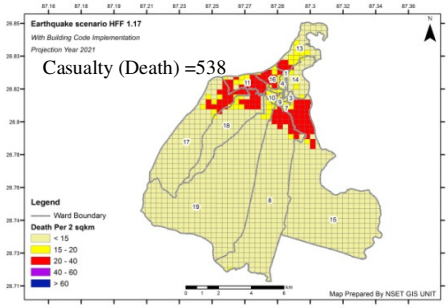


(b) Casualty Scenario in case of Building Code Implementation

Figure 2-6: Comparison of casualty scenario for building construction with and without building code

### *2.2.3 SEDM Methodology*

Ministry of Home Affairs (MOHA) the Government of Nepal with support from Japan International Cooperation Agency (JICA) implemented a project on "Study on Earthquake Disaster Mitigation in Kathmandu Valley (SEDM)" in 2001 (JICA, 2002). NSET worked with JICA study team for some components related to risk assessment. In this study, hazard and risk assessment was done in GIS environment. The whole Kathmandu valley was divided to 500m x 500m grid and distribution of seismic hazards and vulnerability were calculated for each grid.

The whole valley was divided to six different categories based on the buildings typology distributions, population density and the development pattern. First, the valley was divided to urban, sub-urban and rural areas based on development pattern and all three areas were further divided to core and fringe based on population density. Distribution of different building typologies in these different areas was then counted in some of the selected areas and extrapolated the similar distribution in other similar areas. Figure 2-7 shows a type of map prepared by JICA (2002).

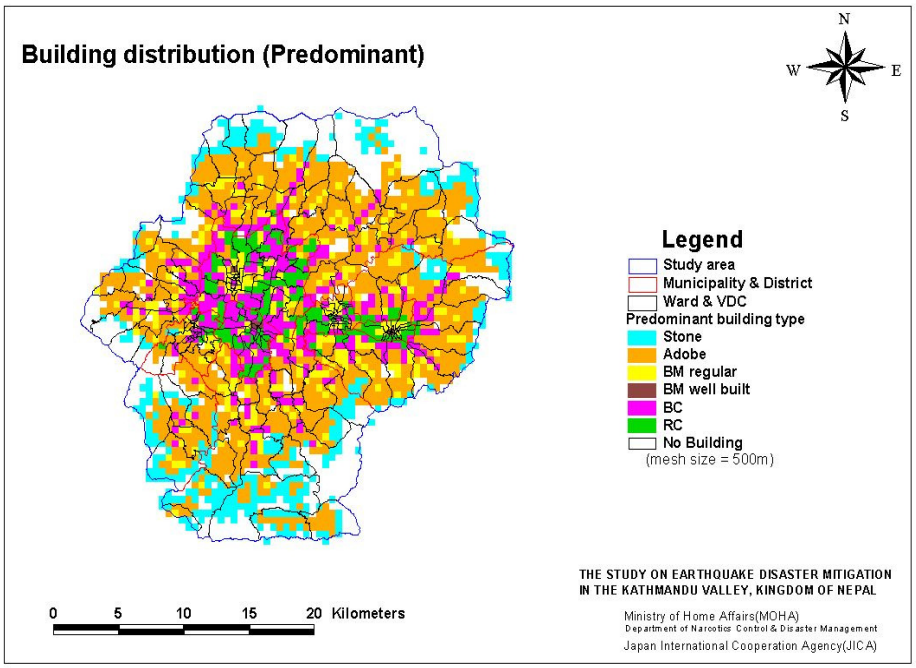


Figure 2-7: Building typology distribution in Kathmandu Valley (JICA, 2002)

About 1200 buildings were surveyed in detail to understand the vulnerabilities of different typology as well as use of the buildings. About 80 students from engineering institute were involved for the building inventory survey which gave them an exposure on earthquake risk assessment. The risk assessment work was done by professionals and the report was shared to central government and cities.

### *2.2.4 SLARIM Methodology*

In 2002 the International Institute for Geoinformation Science and Earth Observation (ITC) launched a research project with the acronym SLARIM, which stand for Strengthening Local Authorities in Risk Management. The SLARIM project in Nepal was implemented in collaboration with NSET. The main objective of this research project was to develop generic methodologies for GIS-based risk assessment and decision support that can be beneficial for

local authorities in medium-sized cities in developing countries. The project was implemented in three cities Naga city, Philippines; Lalitpur Sub-Metropolitan City, Nepal and Dehradun, India.

Many students from ITC worked under SLARIM in Lalitpur Sub-Metropolitan City, a city with about 300,000 populations, for different aspects of earthquake risk assessment and management. In terms of methodology, project took two approaches for buildings damage and casualty estimation. In the first method, the city was divided to different homogeneous clusters (Guragain, 2004). The clusters were made considering similar type of buildings by their number of stories, building use, building system and materials etc. In this study the same fragility functions developed during JICA project were used for damage calculation. Casualty ratios according to buildings damage were derived HAZUS-MH (Islam, 2004). The outcome of this risk assessment methodology was detail enough for city level planning for emergency response. It gives the detail information i.e. which roads are blocked by debris and which are open after an earthquake. Figure 2-8 gives the buildings distribution and Figure 2-9 gives the number of collapsed buildings in different clusters in Lalitpur sub-metropolitan city.

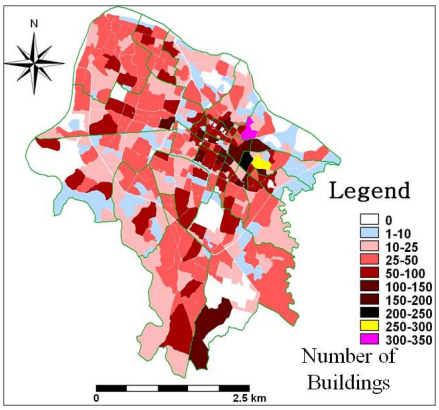


Figure 2-8: Buildings distribution in Lalitpur Sub-Metropolitan City area (Guragain, 2004)

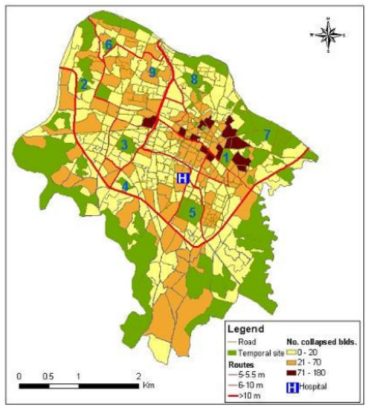


Figure 2-9: Buildings damage estimation in Lalitpur Sub-Metropolitan City area (Guragain, 2004)

In the second method, the information was collected at individual household level. Both the physical characteristics and socio-economic information of individual buildings were collected. Different building related vulnerability factors, socioeconomic conditions, public awareness, response capacity, risk perception and preparedness level of individual household were collected from the field survey (Jimee, 2006). Building damage matrix by Guragain, Pandey and Shrestha (2004) was used for building damage estimation.

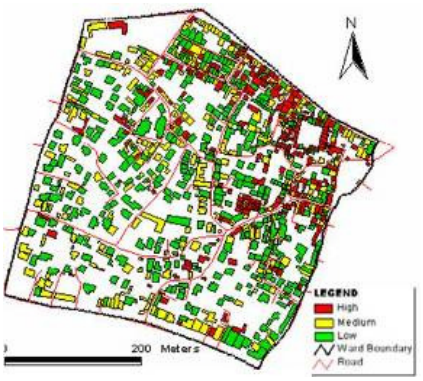


Figure 2-10: Buildings collapse probability at MMI IX level of shaking (Jimee, 2006)

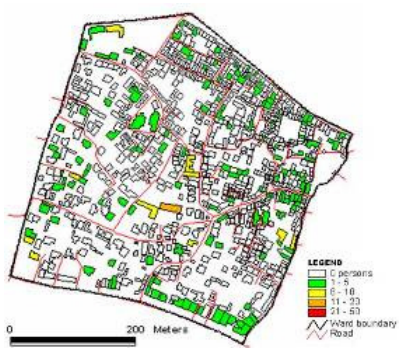


Figure 2-11: Possible casualty (death) at MMI IX level of shaking (Jimee, 2006)

Once the building damage was assessed, human casualties were estimated in relation of population distribution and building damage/collapse probability. Casualty ratios related to building damage were derived from HAZUS-MH. However, this detail study was done at ward level only. Figure 9 shows the buildings collapse probability at MMI IX level of shaking and Figure 10 shows the estimated casualty at the same level of shaking.

### *2.2.5 Community Watching*

NSET implemented Community Based Disaster Risk Management Program, which is exemplary to develop synergy of resources and understanding among the key players and stakeholders including central and local government, communities and civil society, in different parts of the country. As a part of community based program, the program was implemented in selected 5 wards of Lalitpur Sub-metropolitan City in Kathmandu. The major components of the project were establishing disaster risk management organization at community Level; hazard, vulnerability and capacity assessment by community; preparation of disaster scenario and participatory action planning and implementation of pilot activities as demonstration.

The communities conduct vulnerability and capacity assessment of their community after a 3 days training on vulnerability and capacity assessment. Concerned community members visit together to all individual buildings and infrastructures in their community and identify them as highly vulnerable, medium or low vulnerable directly in the field. They discuss will all households about the problem and also collect suggestions from individuals in the community on how to reduce the vulnerability and also on how to prepare. The community also collects the resources that can be helpful during emergency. The resources includes both the human resources i.e. doctors, nurses, emergency rescuer etc. and community infrastructures like well, open spaces etc.

Figure 2-12: Example of vulnerability and capacity map prepared by community

Figure 2-13: Leading community members finalizing the vulnerability and capacity assessment map prepared by community

Figure 2-12 shows an example of vulnerability and capacity assessment map prepared by one of the community in Lalitpur Sub-metropolitan City. After the vulnerability and capacity assessment work, the leading community members sit together and prepare a draft action plan. The draft plan then is discussed in a wider range of community members and finalized for implementation. Figure 2-13 shows leading community members analyzing the vulnerability and capacity assessment result for the formulation of action plan.

### *2.2.6 HAZUS Methodology*

The most advance loss estimation tool, which is publicly available, is HAZUS. It is interactive software released by the Federal Emergency Management Agency (FEMA) since 1997. Where the first version of HAZUS was only dealing with earthquake loss estimation, the recent HAZUS-MH is a multi-hazard loss estimation system, dealing with earthquakes (ground shaking, and earthquake induced hazards such as liquefaction, landslides, fires, floods, debris etc.) windstorms (hurricanes) and floods (coastal and river flooding) (HAZUS, 2003). However, HAZUS-MH need ArcGIS environment to work. Therefore, even if the HAZUS is a free tool, it is dependent on relatively expensive other system.

The HAZUS tool was used in Kathmandu Valley on a research basis to check if it is possible to use it with the available information in Nepal or not. It is found that HAZUS tool is relatively complex in comparison to other methodologies described above and requires detail information on buildings and infrastructures. Some technical difficulties like requirement of displacement based functions; limitations on building occupancy classes; lack of unit rate for calculation of indirect loss were noted as limitations during use of HAZUS in Kathmandu Valley. Further research is required to meet the local requirements. However, it was found that basic loss estimation especially direct damage to buildings and infrastructures and

calculation of casualty by direct damage can be done with the basic data available Thus, the study concluded that HAZUS can be used and can be a basis for a national level risk assessment system if the objective is to conduct detail assessment work by professionals. Figure 2-14 shows an example of use of HAZUS in Kathmandu Valley.

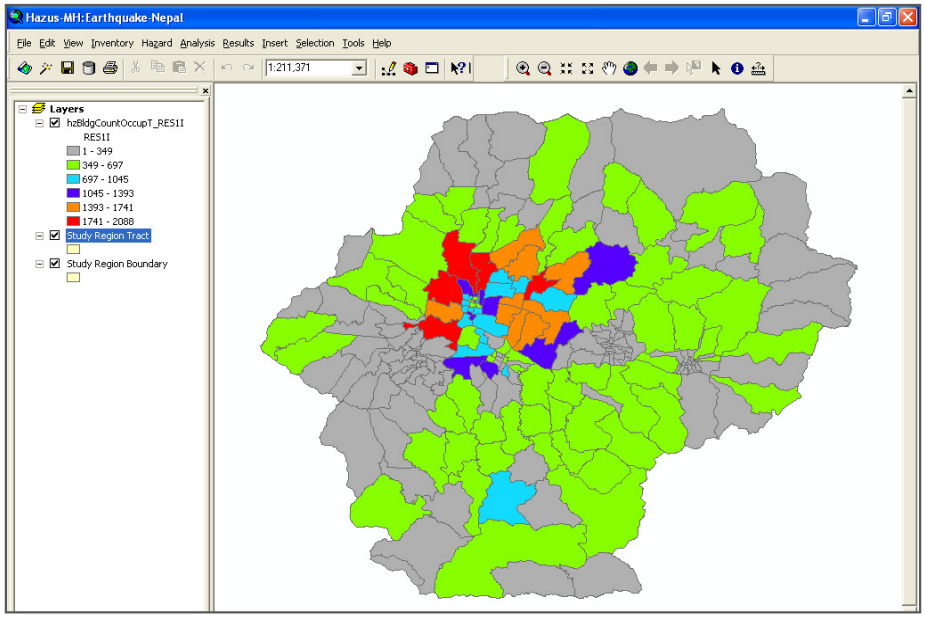


Figure 2-14: Residential buildings distribution in Kathmandu (Example of a Map in HAZUS)

## 2.3 Other Potential Earthquake Risk Assessment Tools that can be used in Nepal

Two more tools, CAPRA GIS and Open Quake, were introduced in Nepal by the developers of the tools through trainings to professionals in Nepal. These tools are not applied practically till the date of this research. However, while participating in the training, author found these are other potential tools that can be used in Nepal and considered for this comparative study. Short description of these tools is given below.

### 2.3.1 CAPRA GIS

The CAPRA (Probabilistic Risk Assessment) program was initiated with an aim to strengthen institutional capacity for assessing, understanding and communicating disaster risk, with the ultimate goal of integrating disaster risk information into development policies and programs (CAPRA,2012 ).

The CAPRA (2012) describes that it offers a modular and free software platform to support experts and practitioners in probabilistic risk analysis related to natural hazards such as earthquakes and hurricanes. There are four different modules for hazards, exposure,

vulnerability and loss. The input and output are ArcGIS compatible and it has the capacity to analyze at individual buildings and infrastructures level. This system can be used in the cities where information of individual buildings and infrastructures are available in GIS.

### *2.3.2 Open Quake*

The Open Quake platform is web-based and offers an interactive environment for modeling, viewing, exploring, and managing earthquake risk (GEM, 2014). It is open-source but at this stage only risk professionals can use the system for risk assessment. The computer interface is not user friendly for general user and thus this platform can be used only at the national level by experts and professionals. However, it has different level of analysis starting at national level to individual buildings level, so it is one of the good tool to establish at national level.

## *2.4 Comparison of Risk Assessment Methodologies*

A comparison of earthquake risk assessment methodologies and tools used in different cities and communities in Nepal are compared for their characteristics in terms of different stakeholders involved, provisions of detail input and output, resources required for assessment works in terms of trained manpower and cost, simplicity for use, appropriateness for use at city level and national level and the tools and accessories are open source or not. Table 2-1 shows a comparison of different earthquake risk assessment tools for these parameters.

Table 2-1. Comparison of risk assessment methodologies for applicability in Nepal

| Methodologies | Stakeholders Involvement | | | Provisions for detail input/ output | Resource required | Simplicity | Appropriate for city level | Appropriate for national level | Ease to customize and update | Open source or not |
|---|---|---|---|---|---|---|---|---|---|---|
| | Professional | Local authorities | Community | | | | | | | |
| KVERMP | M | H | M | L | L | S | H | L | H | YES |
| RADIUS | M | H | M | M | L | S | H | L | H | YES |
| GIS GRID | H | L | L | H | H | C | M | L | L | NO |
| SLARIM | H | M | L | H | H | C | H | L | L | NO |
| COMMUNITY WATCHING | L | M | H | L | L | S | L | L | - | YES |
| HAZUS | H | L | L | H | H | C | H | H | M | NO |
| CAPRA | H | M | L | H | H | C | H | L | H | YES |
| Open Quake | H | M | L | H | M | C | H | H | M | YES |

H: High, M: Medium, L: Low, S: Simple, A: Average, C: Complex

The comparison of risk assessment tools in Table 2-1 shows that HAZUS and Open Quake are better options for national level risk assessment though they are relatively complex to use; different level of analysis is possible in these tools and are appropriate for national level. RADIUS is comparatively better for cities where there is no GIS information of buildings and

infrastructures and CAPRA GIS is better for cities where there is GIS information of individual buildings and infrastructures.

## 2.5 Conclusions and Recommendations

Different earthquake risk assessment tools are used for evaluation of earthquake risk in cities and communities in Nepal. Some tools are easy-to-use and insure involvement of community and local authorities in the assessment process. Planning and implementation of earthquake risk management activities at local level depends more on the involvement of concerned stakeholders than the accuracy of the assessment result. Comprehensive and resource demanding detail tools can better serve to develop the system at national level than the local level.

**REFERENCES**

ATC-25. (1991). "Seismic Vulnerability and Impact of Disruption of Lifelines in the Conterminous United States." *Applied Technology Council*, California, USA.

NBC. (1994). "Seismic Hazard Mapping and Risk Assessment for Nepal." *Nepal National Building Code (NBC)*, Ministry of Physical Planning and Works, Nepal.

ATC-13. (1995). "Earthquake Damage Evaluation Data for Probable Maximum Loss Studies of California Buildings." *Applied Technology Council*, California, USA.

NSET. (1999a). "Earthquake Scenario of Kathmandu Valley." *National Society for Earthquake Technology-Nepal (NSET)*, Kathmandu, Nepal.

NSET. (1999b). "Kathmandu Valley Earthquake Risk Management Action Plan." *National Society for Earthquake Technology-Nepal (NSET)*, Kathmandu, Nepal.

RADIUS. (2000). "Risk Assessment Tools for Diagnosis of Urban Areas against Seismic Disasters (RADIUS)– an initiative of the International Decade for Natural Disaster Reduction (IDNDR)" *Secretariat of the International Strategy for Disaster Reduction (ISDR),* (CD-ROM) Geneva, Switzerland.

Amod Mani Dixit, Mahesh Nakarmi, Shiva Bahadur Pradhanang, Jitendra Bothara, Jyoti Prasad Pradhan, Brian Tucker and Laura Dwelley Samant. (2002a). "Hazard Mapping and Risk Assessment: Experiences of KVERMP." *Proceedings on Regional Workshop on Best Practices in Disaster Mitigation*, 24-26 September 2002, Bali, Indonesia.

Amod Mani Dixit, Mahesh Nakarmi, Shiva Bahadur Pradhanang, Jitendra Bothara, Bishnu Hari Pandey, Ramesh Guragain, Ram Chandra Kandel, Surya Narayan Shrestha and Brian Tucker, Laura Dwelley Samant. (2002b). "Promoting Safer Building Construction: Experiences of KVERMP." *Proceedings on Regional Workshop on Best Practices in Disaster Mitigation*, 24-26 September 2002, Bali, Indonesia.

Amod Mani Dixit, Shiva Bahadur Pradhanang, Ramesh Guragain, Ram Chandra Kandel, Surya Narayan Shrestha, Brian Tucker, Laura Dwelley Samant, Yogeshwor Krishna Parajuli. (2002c). "Promoting Safer Building Construction: Experiences of KVERMP." *Proceedings on Regional Workshop on Best Practices in Disaster Mitigation*, 24-26 September 2002, Bali, Indonesia.

JICA. (2002). "The study on Earthquake Disaster Mitigation in the Kathmandu valley Kingdom of Nepal." Final report, Vol - II, *Japan International Cooperation Agency*, Kathmandu, Nepal.

HAZUS-MH. (2003). "Multi-hazard Loss Estimation Methodology." Department of Homeland Security, Emergency Preparedness and Response Directorate, *Federal Emergency Management Agency (FEMA)*, Washington D.C.

Guragain, J. (2004). "GIS for Seismic Building Loss Estimation: A Case Study from Lalitpur Sub-Metropolitan City Area Kathmandu, Nepal." M. Sc. Thesis, International Institute for Geo-information Science and Earth Observation, Enschede, Netherland

Guragain, R., Pandey, B., and Shrestha, S. (2004). "Guideline for Seismic Vulnerability Assessment of Hospitals in Nepal." *National Society for Earthquake Technology-Nepal (NSET)*, Kathmandu, Nepal

Jimee, G. (2006). "Seismic Vulnerability and Capacity Assessment at Ward Level: A Case Study of Ward No. 20, Lalitpur Sun-metropolitan City, Nepal", M. Sc. Thesis, International Institute for Geo-information Science and Earth Observation, Enschede, Netherland

Ramesh Guragain, Ganesh Jimee and Amod Mani Dixit. (2008). "Earthquake Awareness and Effective Planning Through Participatory Risk Assessment: An Experience from Nepal", *Proceedings on 14th World Conference on Earthquake Engineering*, (CD-ROM), October 12-17, 2008, Beijing, China

CAPRA (2012). "CAPRA Probabilistic Risk Assessment Program", <http://www.ecapra.org/capra-gis achieved on 2014/10/16 > (19 October, 2014)

GEM. (2014). "Open Quake", < http://www.globalquakemodel.org/openquake/about/> (19 October, 2014)

# 3. Field Study on Mortar Strength of Existing Masonry Buildings in Nepal

## *3.1 Introduction*

Understanding existing strength of materials is very important as that will be the key input for any numerical analysis. Identification of existing strength of low-strength masonry is challenging as the specimen get damaged during the extraction process.

In addition, the extraction process may damage the building as well. So, it is impractical to extract specimen from existing low-strength masonry buildings and test in lab. Thus, in-situ test at field is a better option for identification of existing capacity of low strength masonry with mud mortar or weak cement-sand mortar. Different type of non-destructive tests for masonry structures are discussed by different researchers including Schuller (2003), Hans, Boutin, Ibraim and Roussillon (2005) and FEMA-273 (2003).

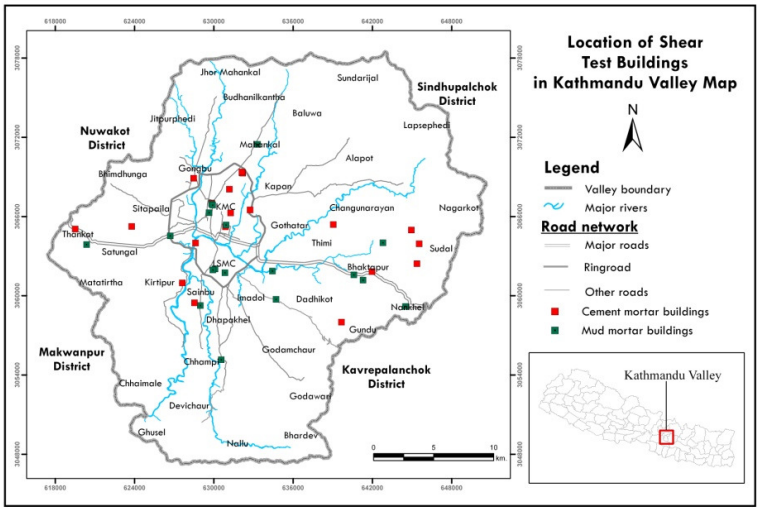


Figure 3-1: Locations of buildings with direct shear test in Kathmandu Valley

This study conducted two types of non-destructive tests, one for determining mortar joint shear strength and the other one for determining compressive strength. The shear test was carried out for about 100 masonry buildings at different locations of Kathmandu Valley to determine representative mortar strength of masonry buildings using hydraulic jack. Figure 3-1 shows the locations of buildings where the direct shear test was conducted in Kathmandu Valley. The tests were carried out for both the buildings with brick in mud mortar as well as buildings with brick in cement mortar. In some locations shown in the figure, more than one test was conducted. Limited numbers of flatjack test for identification of compressive strength

especially for brick masonry buildings with mud mortar were also conducted.

## 3.2 Masonry Mortar Bond Strength Test

### 3.2.1 Test Methodology

Procedures for three different methods on in-situ measurement of masonry mortar joint shear strength are given in ASTM 1531-09 (2011). The method "B" in ASTM 1531-09 (2011), which gives the procedures for determining mortar joint shear strength index using an estimate of the normal compressive stress from overburden pressure at the location of the test site without Flat jacks controlling normal compressive stress, is used in this study. In this test procedure, a single masonry unit and a head joint are removed from opposite ends of the chosen test unit. It is ensured that the bed joints are not disturbed in the unit to be tested. The test unit is then displaced horizontally relative to the surrounding masonry using a hydraulic jack. The horizontal force required to cause first movement of the test unit provides a measured index of the mortar joint bond strength.

Following steps are used for conducting these tests:

Step 1: Selection brick for direct shear test. A wall panel with minimum of Minimum of 8 full bricks in horizontal and 11 layer of bricks in vertical is selected to avoid any other pattern of failure. Two bricks are marked at centre horizontally and at the base of the selected wall panel.

Step 2: Remove plaster from two selected bricks.

Step 3: Remove one of the brick and a vertical joint using drill machine

Step 4: Keep Hi-Force Jack in the cavity with steel bearing plates in proper position

Step 5: Apply pressure by hydraulic pump manually and observe pressure value along with failure mode.

Hydraulic pump by Hi Force-HP 110 with single speed hand pump of 700 bar working pressure capacity was used for this study. Figure 3-2 shows the test set-up for conducting in-situ testing of brick masonry for shear.

The average bed joint shear strength was calculated as below:

$$\tau = \frac{P_h}{A_j}$$

Where:

$\tau$ = Measured bed joint shear strength

$P_h$= maximum horizontal force resisted by the test unit and

$A_j$ = gross area of upper and lower bed joints

The shear index, "τ", is reduced to the value that would have been obtained under zero axial loads, $\tau_0$, using the relation:

$\tau_{0=}\tau-\mu(\sigma_v)$

Where:

$\tau_0$ = Bed joint shear strength at zero axial load condition

τ = Measured bed joint shear strength

μ = coefficient of friction for masonry

$\sigma_v$=estimated normal compressive stress at the test unit

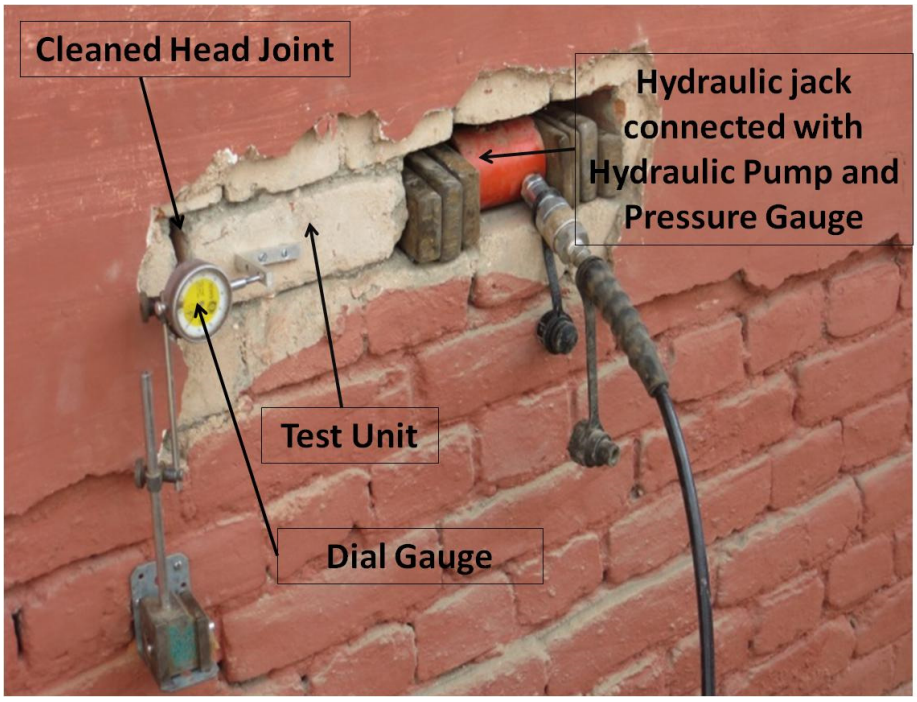


Figure 3-2: Test set-up for conducting in-situ testing of brick masonry for shear

### *3.2.2 Test Result of Brick in Cement-Sand Mortar Buildings*

Direct shear test of brick masonry buildings in Kathmandu valley was carried out as per the methodology described in Section 3.2.1 above. Total of 43 numbers of buildings with brick in cement-sand mortar were tested for bond strength. The location of buildings tested for bond strength in Kathmandu Valley is shown in Figure 3-1. Figure 3-3 gives the histogram of the bond shear strength of the brick in cement mortar buildings in Kathmandu valley.

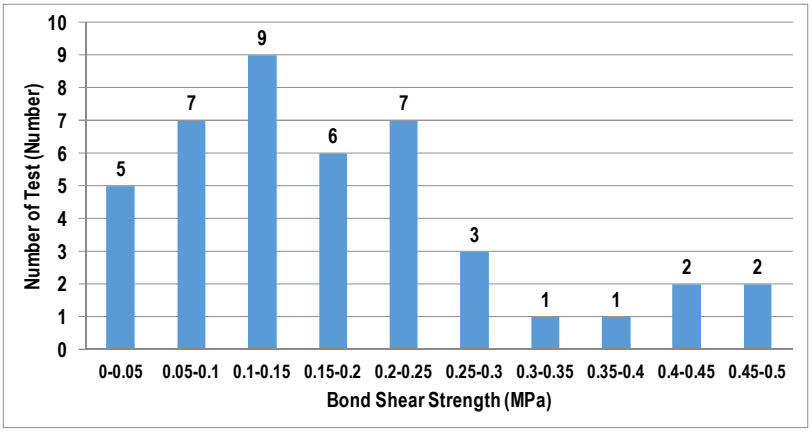


Figure 3-3: Histogram of Bond Shear Strength for Brick in cement mortar buildings in Kathmandu Valley

Table 3-1 gives the summary of bond shear strength obtained from field test on brick masonry with cement mortar buildings and Table 3-2 gives the lower bound brick masonry properties in FEMA-356 (2000). The average shear strength of the brick masonry in cement mortar has been found slightly more than the suggested shear strength for fair type of masonry. So, the values suggested in FEMA-356 (2000) are for the masonry buildings with cement mortar. These material properties of brick in cement mortar buildings are used for simulation of brick masonry buildings in the Section 4 of this thesis. The average value, $20^{th}$ percentile and $80^{th}$ percentile are used for average, weak and strong buildings during numerical simulation.

Table 3-1: Summary of field test on brick masonry in cement mortar

| SN | Particulars | Value |
|---|---|---|
| 1 | Total Number of Tests | 43 |
| 2 | Average Bond Strength (MPa) | 0.17 |
| 3 | $20^{th}$ Percentile (MPa) | 0.078 |
| 4 | $80^{th}$ Percentile (MPa) | 0.24 |
| 5 | Standard Deviation | 0.117 |
| 6 | Coefficient of Variation | 0.67 |

Table 3-2: Lower bound brick masonry properties in FEMA-356 (2000)

| Property | Masonry Condition | | |
|---|---|---|---|
| | Good | Fair | Poor |
| Compressive Strength, $f_m$,(MPa) | 6.2 | 4.14 | 2.07 |
| Elastic Modulus in Compression | 550 $f_m$ | 550 $f_m$ | 550$f_m$ |
| Flexural Tensile Strength (MPa) | 0.14 | 0.069 | 0 |
| Shear Strength for masonry with running bond lay-up | 0.19 | 0.14 | 0.09 |

Shear modulus of the mortar was also calculated based upon the measured shear stress and shear strain. The Young's modulus of elasticity was calculated the equation as below:

$$G = \frac{E}{(1+\vartheta)}$$

Where:

G=Shear Modulus

E=Young's Modulus

ϑ=Poisons ratio

In this study, the poisons ratio is considered as 0.2 (FEMA-356, 2000)

The average Young's modulus, 20$^{th}$ percentile and the 80$^{th}$ percentile are calculated to use with corresponding bond strength in numerical simulation and are presented in Table 3-3.

Table 3-3: Young's Modulus of Elasticity Calculated from Field Tests

| SN | Particulars | Value |
|---|---|---|
| 1 | Average Young's Modulus (MPa) | 263 |
| 2 | 20$^{th}$ Percentile (MPa) | 26 |
| 3 | 80$^{th}$ Percentile (MPa) | 350 |
| 4 | Standard Deviation | 332 |
| 5 | Coefficient of Variation | 0.79 |

The relation between the Shear Strength and the Young's Modulus of elasticity is shown in Figure 3-4. It shows a linear relation between shear strength and the Young's modulus of elasticity.

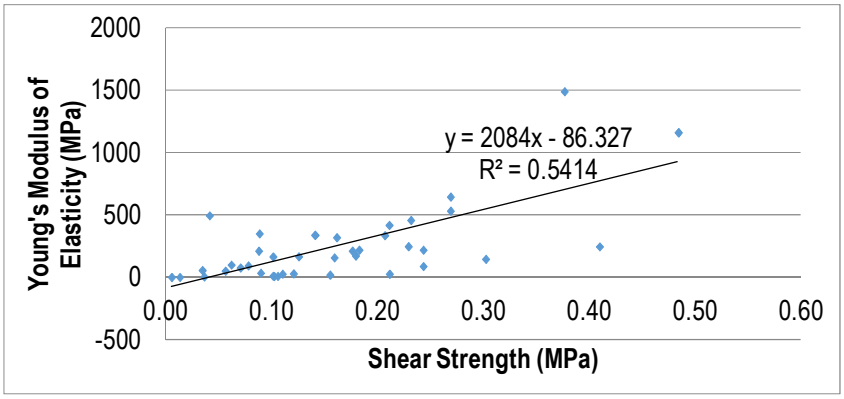


Figure 3-4: Relation between Shear Strength and Young's Modulus of Elasticity obtained from field test for Brick in Cement Buildings

### *3.2.1 Test Result of Brick in Mud Mortar Buildings*

Total number of 54 buildings with brick in mud mortar was tested for mortar bond strength in Kathmandu Valley. The location of mud-mortar buildings tested for mortar bond strength is shown in Figure 3-1. The test sites were distributed at different locations in Kathmandu Valley and in some cases more than one test were conducted in a same location.

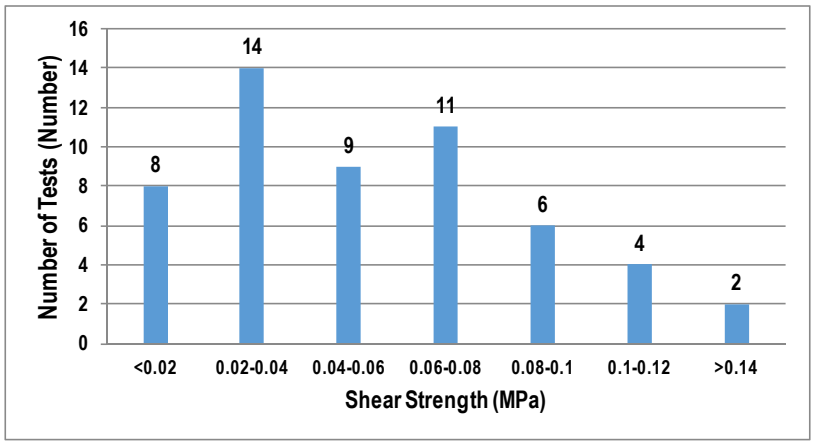


Figure 3-5: Histogram of Bond Shear Strength for Brick in mud mortar buildings in Kathmandu Valley

Figure 3-5 gives the histogram of the bond strength of the brick in mud mortar buildings in Kathmandu valley. The summary of the test results is given in Table 3-4. Comparison of the test data with the FEMA-356 (2000) lower bound values for masonry, which are presented in Table 3-2 above, shows that the strength of existing brick in mud mortar buildings is way below with about 3.5 times less than the values suggested in FEMA-356 (2000).

Table 3-4: Summary of field test on brick masonry in mud mortar

| SN | Particulars | Value |
|---|---|---|
| 1 | Total Number of Tests | 54 |
| 2 | Average Bond Strength (MPa) | 0.047 |
| 3 | $20^{th}$ Percentile (MPa) | 0.029 |
| 4 | $80^{th}$ Percentile (MPa) | 0.081 |
| 5 | Standard Deviation | 0.033 |
| 6 | Coefficient of Variation | 0.59 |

The average Young's modulus, $20^{th}$ percentile and the $80^{th}$ percentile are calculated to use with corresponding bond strength in numerical simulation and are presented in Table 3-5. The relation between the observed Shear Strength and the Young's Modulus of elasticity is shown in Figure 3-6. It shows a linear relation between shear strength and the Young's modulus of elasticity.

Table 3-5: Young's Modulus of Elasticity Calculated from Field Tests

| SN | Particulars | Value |
|---|---|---|
| 1 | Average Young's Modulus (MPa) | 45 |
| 2 | 20th Percentile (MPa) | 10 |
| 3 | 80th Percentile (MPa) | 73 |
| 4 | Standard Deviation | 49 |
| 5 | Coefficient of Variation | 0.9 |

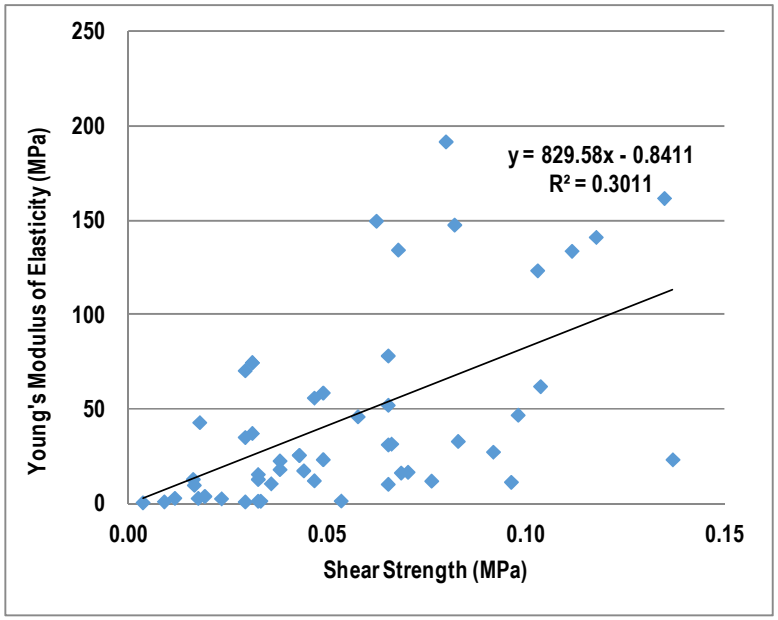


Figure 3-6: Relation between Shear Strength and Young's Modulus of Elasticity obtained from field test for Brick in Mud Buildings

## 3.1 Masonry Compressive Strength Test

Compressive strength test for brick masonry with mud-mortar was done using ASTM-C1196 (2013) and ASTM-C1197 (2013). The test was carried out using two flat jack palates of size R-6-16 (0.15" X 6" X 16"). Two slots of size 6.5" x 17" are prepared which are 18.5" apart (5 layers of brick) and gauge point pairs are selected to measure the deflection of the masonry units. Flat jacks are then inserted into both slots, and the initial distance between gauge points are measured. By giving pressure to the flat jacks by using hydraulic compressor, loads are applied to the wall specimen. With a pressure increase in the flat jacks, the distance between gauge point pairs decreases. The pressure and deformation are recorded and stress-strain curve is developed. The pressure is increased till the failure in the masonry specimen occurs. Figure 3-7 shows a test set-up for the flat-jack test to identify compressive strength and the modulus of elasticity for compression and the Figure 3-8 gives the specification of the flat-

jacks used for the test.

(a) Flat jacks inserted in the cut sluts

(b) Setting of dial gauge for deformation measurement

Figure 3-7: Test set-up for flat-jack test for masonry compressive strength and modulus of elasticity

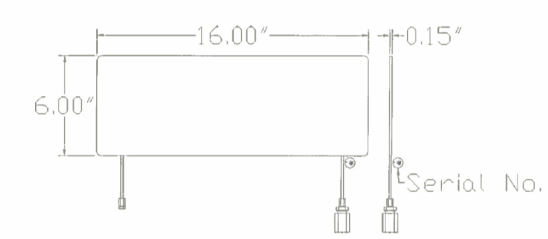


Figure 3-8: Specification of flat-jack used for test

The average compressive stress in masonry was calculated using the following equation as given in ASTM-C1197 (2013):

$f_m = K_m K_a p$

where:

$f_m$ = average compressive stress in masonry

$K_m$ = dimensionless constant which reflects the geometrical and stiffness properties of the flatjack. In this study, $K_m$ for the flatjacks used was 0.88

$K_a$ = the ratio of measured area of the flatjack to the average measured area of the slot, and

p = flatjack pressure, psi or MPa

Total of 3 tests were carried out and the average Modulus of Elasticity of Masonry was found as 943.8 MPa and the Average Compressive Strength of Masonry (Ultimate) was found as 1.21 MPa.

## 3.2 Conclusions

Understanding existing strength of materials is very important as that will be the key input for any numerical analysis. Identification of existing strength of low-strength masonry is challenging as the specimen get damaged during the extraction process. This study conducted two types of non-destructive tests, one for determining mortar joint shear strength and the other one for determining compressive strength. The shear test was carried out for about 100 masonry buildings at different locations of Kathmandu Valley to determine representative mortar strength of masonry buildings using hydraulic jack. Compressive strength test was carried out only to limited buildings. The test result shows that there is very high variation in strength and stiffness of different type of masonry buildings in Nepal. The variation in strength is found more in cement mortar buildings as very weak shear strength of 0.01 MPa to high strength of about 0.5 MPa was noted during the test. The average bond strength was found as 0.17 Mpa. In case of mud mortar, the range of the bond strength was from 0.004 MPa to 0.2 MPa and the average was found 0.047 MPa. A positive relation between shear strength and modulus of elasticity was found in both type of masonry. The $20^{th}$ percentile and $80^{th}$ percentiles for strength as well as modulus of elasticity and calculated and are recommended to use for further numerical simulation.

### References

Michael P. Schuller. (2003). "Nondestructive testing and damage assessment of masonry structures." *Prog. Struct. Engng Mater.* 5:239–251

S. Hans, C. Boutin, E. Ibraim, and P. Roussillon. (2005). "In situ experiments and seismic analysis of existing buildings. Part I: Experimental investigations." *Earthquake Engineering and Structural Dynamics* 34:1513–1529

FEMA-356. (2000). "Prestandard and Commentary for the Seismic Rehabilitation of Buildings." Federal Emergency Management Agency (FEMA), Washington D.C., USA

ASTM C1531-09. (2011). "Standard Test Methods for In Situ Measurement of Masonry Mortar Joint Shear Strength Index", *ASTM International,* 100 Barr Harbor Drive, PO Box C700, West Conshohocken, USA

ASTM C 1197-04. (2013). "Standard Test Method for In Situ Deformability Properties Using Flat Jack Measurements", ASTM International, 100 Barr Harbor Drive, PO Box C700, West Conshohocken, USA

ASTM C1196-09. (2013). "Standard Test Method for In Situ Compressive Stress Within Unit Masonry Estimated Using Flat Jack Measurements", ASTM International, 100 Barr Harbor Drive, PO Box C700, West Conshohocken, USA

# 4. Numerical Simulation of Brick Masonry Buildings and Development of Fragility Functions

## *4.1 Introduction*

Use of appropriate fragility functions for specific type of buildings is one of the main parameter for earthquake risk evaluation. Coburn, A. and Spence, R. (2002) gives the breakdown of the fatalities due to earthquakes in the period of 1900-1990 in the world and about 75% of the fatalities attributed to earthquakes are caused by the collapse of buildings and the greatest proportion is from the collapse of masonry buildings. This trend has been continued in recent earthquakes in developing countries as well. So, the accuracy of earthquake loss estimation depends more on accuracy of fragility functions of masonry buildings.

Different fragility functions/curves for masonry buildings in developing countries are suggested by various methods and authors like ATC-13 (1985), NBC (1994), RADIUS (2000), GESI (2001) and HAZUS (2003). These fragility functions are used in Nepal earthquake risk assessment at different cities as discussed by Guragain, Jimee and Dixit (2008).

All these methods give a single fragility curve defining potential damage ratio at a certain level of earthquake shaking for one type of buildings and do not differentiate different state of damage at the given level of shaking. New earthquake risk assessment tools like HAZUS (2003) gives a set of fragility functions like slight, moderate, extensive and complete damage for each type of building including unreinforced masonry buildings. However, these fragility functions are for buildings in United States and similar fragility functions for masonry buildings in Nepal are not available.

This study focuses on development of a set of fragility functions for masonry buildings in Nepal so that earthquake risk assessment can be done for different level of damage. Essential parameters required for numerical simulation are collected through field test and fragility functions are developed through numerical simulation using Applied Element Method (AEM). Computer software called Extreme Loading for Structures (ELS) is used for the AEM simulation.

Before doing numerical simulation of representative brick masonry buildings in Nepal, the ELS software was first used for an experimental model to verify the analysis result with the experimental data. This chapter discusses the numerical simulation of an experimental model; time history analysis of different type of brick masonry buildings and present the fragility

functions developed through numerical simulation.

## 4.2 Non-linear Simulation of Masonry Buildings

One way of developing fragility functions is through damage assessment after an earthquake in which it is required to wait for a large earthquake to occur. The other way is to develop fragility functions through numerical simulations. Authors like M. Rota et al (2010) and J. Park et al (2009) have developed fragility functions for different type of buildings through macro modeling. In case of masonry, as the main energy dissipation is through cracking as well as frictional sliding after cracking micro modeling with bricks and mortar is required. In the domain of numerical simulation of masonry buildings, the Applied Element Method (AEM) is more suitable than other approaches because of mainly three reasons. Firstly, the AEM is capable to follow complete structural response from initial stage of loading until total collapse behavior with reasonable accuracy so that inelastic responses after the cracks occur can be captured (Meguro K. and Tagel-Din H, 2001). Secondly, brick masonry which is composite of brick units and mortar and has discrete nature can easily be model in the AEM by a set of square elements connected at their contact edges either by 'Element springs' or 'Joint springs' according to their positions. Thirdly, the progressive failure of masonry i.e. cracks initiation, propagation and their distribution is simulated better by AEM (Guragain, R. 2006).

AEM has shown good result for analysis for different types of loading for brick masonry buildings. AEM has been used to simulate the behavior of masonry by Pandey et al (2004) and Mayorca et al (2004) for monotonic load case, Guragain et al (2006) for cyclic loading 2-D and Worakanchana et al (2008) for 3-D. This study focuses on time history analysis of brick masonry buildings.

## 4.3 Experimental Verification

The ELS software was first used for an experimental model to verify the analysis result with the experimental data. The shaking table test conducted by Sathiparan, N. (2008) in the Meguro Laboratory at the University of Tokyo was used for verification of numerical result obtained from ELS. Model A-4-NR-X which was for non-retrofitted without plaster Adobe model was chosen for numerical simulation.

### 4.3.1 Model Parameters

The specimen consisted of 18 rows of 44 bricks in each layer except openings. Material properties of masonry used in experiment are given in Table 4.1. The same material properties were used for numerical simulation also.

Table 4-1: Properties of Masonry used in Experiment

| | |
|---|---|
| Compressive Strength (Mpa) | 4.28 |
| Bond Strength (MPa) | 0.0046 |
| Diagonal Shear Strength | 0.041 |
| Modulus of Elasticity (MPa) | 2400 |

Figure 4-1 and Figure 4-2 give the photograph of experimental model and the Numerical Simulation model obtained from ELS respectively. The overall dimension of model was 933mm x 933mm x 720 mm without roof and the wall thickness was 50mm. The sizes of door and window in opposite walls were 243mm x 485mm and 325mm x 245mm respectively. In case of numerical model, the roof is simulated just by a layer of wooden beam as top layer which has assigned to same weight of the roof in experiment.

Figure 4-1: Experimental Model (Sathiparan, N. 2008)

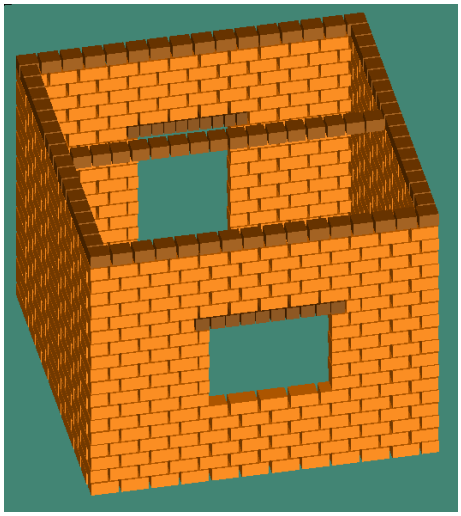

Figure 4-2: Numerical Model

### *4.3.2 Input Motions*

Sinusoidal motions of frequencies ranging from 2Hz to 35 Hz and amplitudes ranging from 0.05g to 0.8g were applied to obtain the dynamic response of the structures in the experiment. Figure 4.3 shows the typical shape of the applied sinusoidal wave.

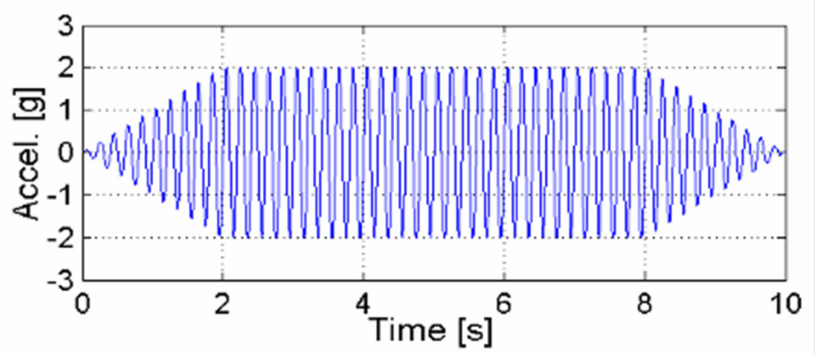


Figure 4-3: Typical shape of the applied sinusoidal wave

The numbers given in the Table 4-2 show the loading sequence followed for tests. General trend of loading was from high frequency to low frequency and from lower amplitude to higher amplitude. There was no significant damage until run 22, thus, the numerical simulation was performed only from run 22 to run 45. During experiment there was some gap between consequent run so that the model was in a static condition before another run of input motion. However, in case of numerical simulation the input motion was continuously provided one after another.

Table 4-2:Loading sequence of input motions

| **Amplitude** | **Frequency** | | | | | | | |
|---|---|---|---|---|---|---|---|---|
| | **2Hz** | **5Hz** | **10Hz** | **15Hz** | **20Hz** | **25Hz** | **30Hz** | **35Hz** |
| 0.8g | | | 43 | 40 | 37 | 34 | 31 | 28 |
| 0.6g | | 45 | 42 | 39 | 36 | 33 | 30 | 27 |
| 0.4g | | 44 | 41 | 38 | 35 | 32 | 29 | 26 |
| 0.2g | | 25 | 24 | 23 | 22 | 21 | 20 | 19 |
| 0.1g | 18 | 17 | 16 | 15 | 14 | 13 | 12 | 11 |
| 0.05g | 10 | 09 | 08 | 07 | 06 | 05 | 04 | 03 |
| sweep | 01,02 | | | | | | | |

### *4.3.3 Result Comparison*

The result of the experiment in terms of cracks patterns and extent of damage which are documented by Sathiparan, N. (2008) are compared with simulation result. The comparison of the result is done after run 28, 37 and 45. Figure 4-4 shows the crack patterns mapped after run 28 of the experiment. A large crack was observed in one top corner of the door, Some cracks at the bottom layer of the side of the door, cracks in all four corners of the window and some horizontal cracks near to top layer to other sides than the window and the door. Figure 4-5 shows the cracks pattern after run 28 from numerical simulation. Cracks were observed in

both side of the top corners of the door with one crack longer and another shorter similar to the experimental cracks. Similarly, cracks in all four corners of the window were observed and are found similar to the experimental result. The cracks at top corners of the windows reach to the top layer of the bricks.

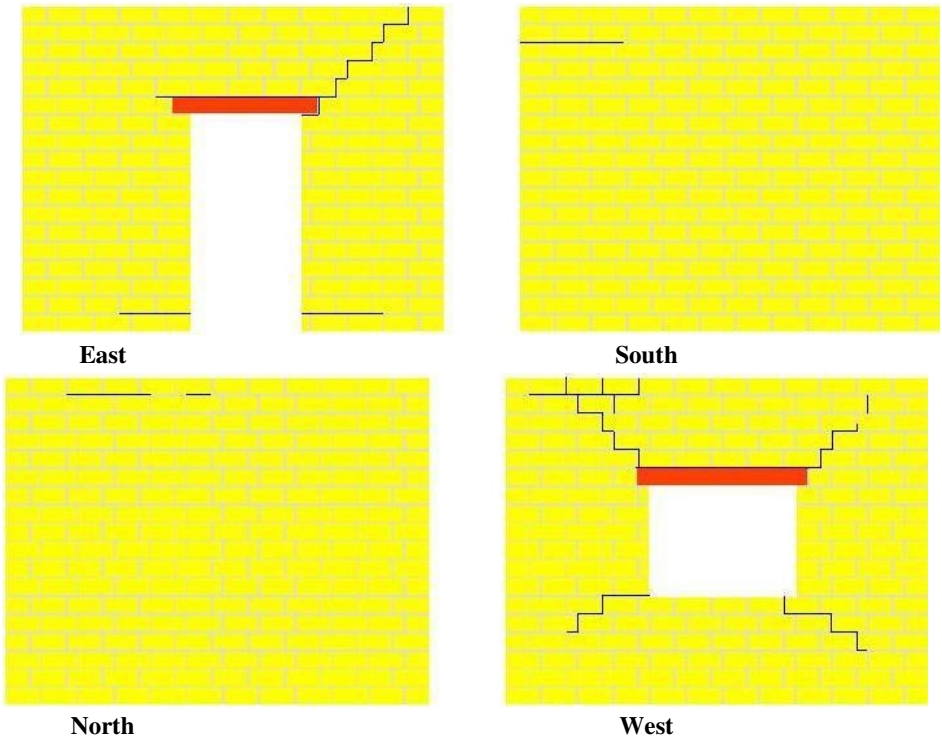


Figure 4-4: Crack patterns after Run 28 (35Hz-0.8g) from experiment (Sathiparan, N. 2008)

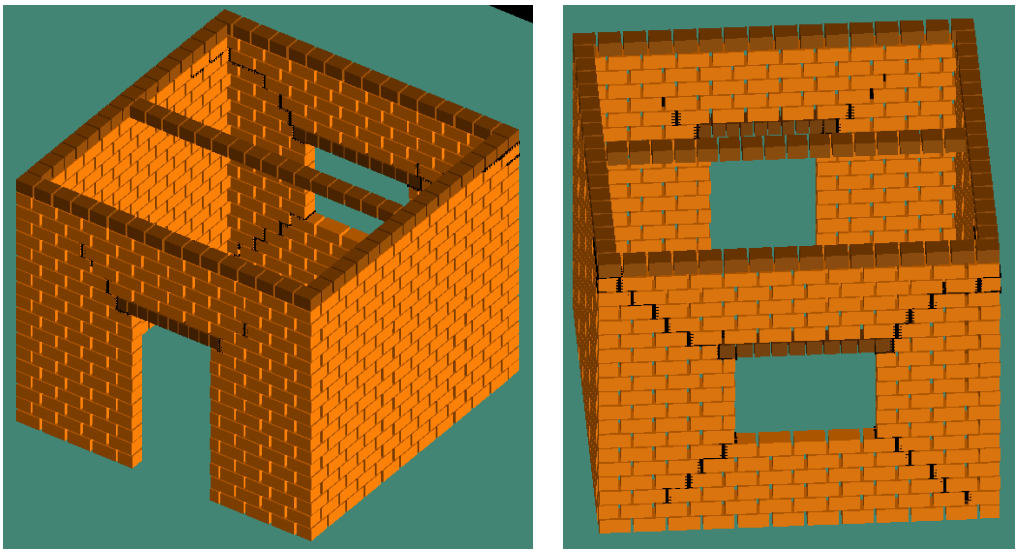

Figure 4-5: Crack patterns after Run 28 (35Hz-0.8g) from numerical simulation

Figure 4-6 and Figure 4-7 show crack patterns after run 37 from experiment and numerical simulation respectively. In both the cases, there are more cracks above the openings, more horizontal cracks in side walls and the horizontal cracks at top layer of the side walls almost passes through one side to other.

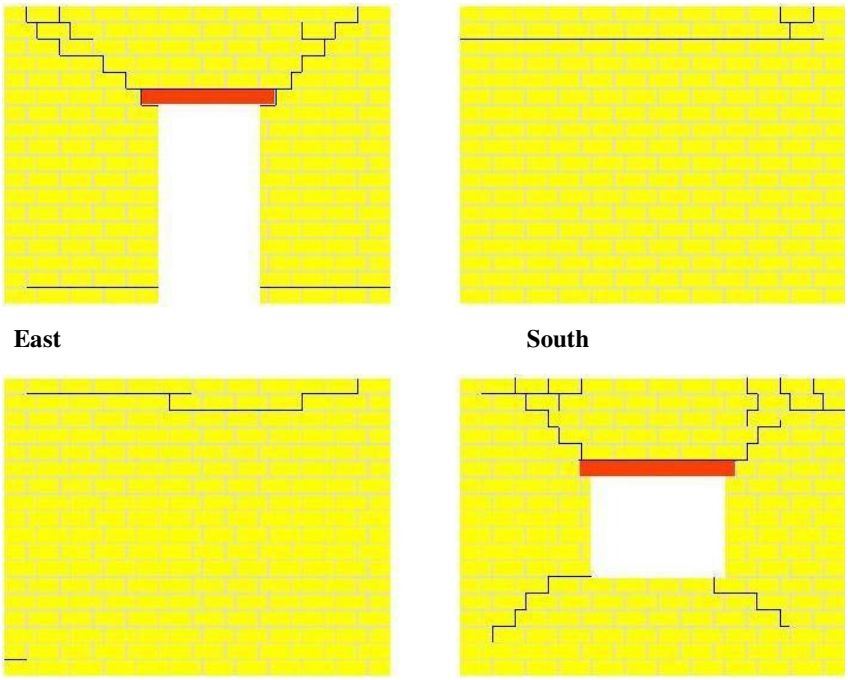


Figure 4-6: Crack patterns after Run 37 (20Hz-0.8g) from experiment by Sathiparan. (2008)

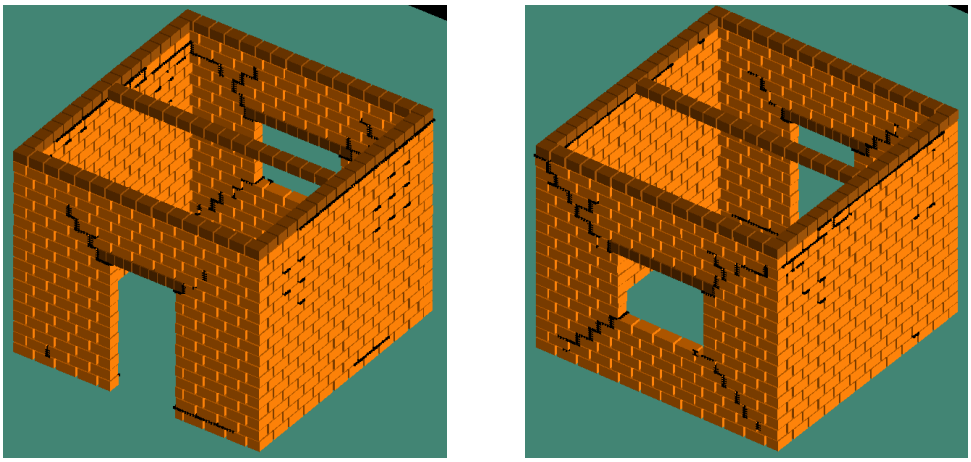

Figure 4-7: Crack patterns after Run 37 (20Hz-0.8g) from numerical simulation

Figure 3.1.8 and Figure 3.1.9 show the photographs of the experiment model after the final run 45 (5HZ-0.6g) and Figure 3.1.10 and Figure 3.1.11 show the numerical simulation results.

In both the cases, the masonry wall above the door and window is collapsed. Similarly, some portion of side walls has also fallen in both the experimental and numerical cases. In both the cases, the experiment as well as in numerical simulation, the initial cracks widened in further shaking ultimately leading to collapse. This behaviour is typical of non-retrofitted masonry buildings which has very limited ductility. So, the energy dissipation capacity is limited as there are few large cracks.

Figure 4-8: Door side photo after run 45 (5HZ-0.6g) of experiment (Sathiparan, N. 2008)

Figure 4-9: Window side photo after run 45 (5HZ-0.6g) of experiment (Sathiparan, N. 2008)

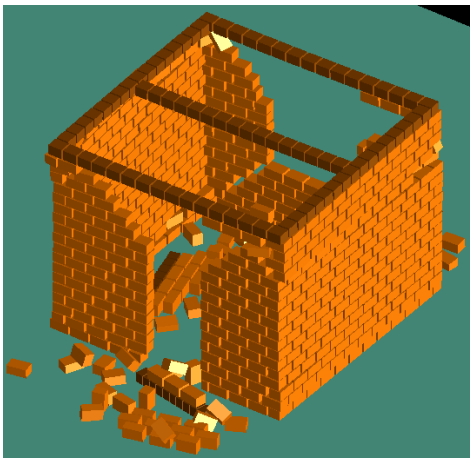

Figure 4-10: Numerical simulation result after run 45 (5HZ-0.6g) graphics from door side

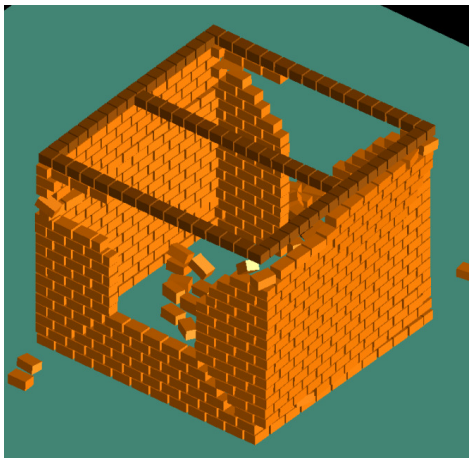

Figure 4-11: Numerical simulation result after run 45 (5HZ-0.6g) graphics from window side

The comparison of experimental result and the numerical simulation results at different stages of loading shows a good agreement for the cracks initiation, propagation and also the collapse of masonry structure even though the numerical simulation model was slightly simplified, specially the roof case.

## 4.4 Time History Analysis and Formulation of Fragility Functions

Numerical model of representative brick masonry buildings of different type with different geometry, number of stories and mortar strength are prepared and analyzed using different time history records. Total of five time history motions are used for the simulation of each buildings. There are not many strong motion records available for earthquakes in Nepal. Only one strong motion record of September 18, 2011 earthquake in east of Nepal recorded at Kathmandu was available and used for this research. Other four strong motions from different from earthquakes recorded in different countries are used for this study.

Figure 4-12 to Figure 4-16 show the different strong motions used for the simulation of masonry buildings in Nepal.

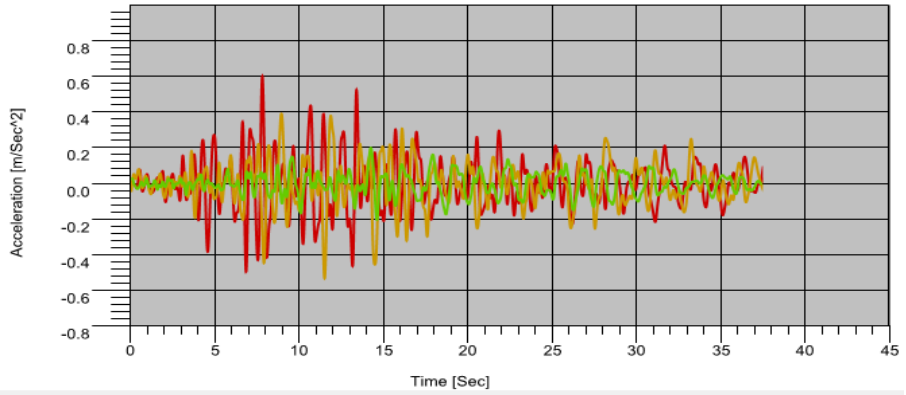


Figure 4-12: Time History Record of Taplejung Earthquake, Nepal; Date: 2011/09/18; Station: Kathmandu

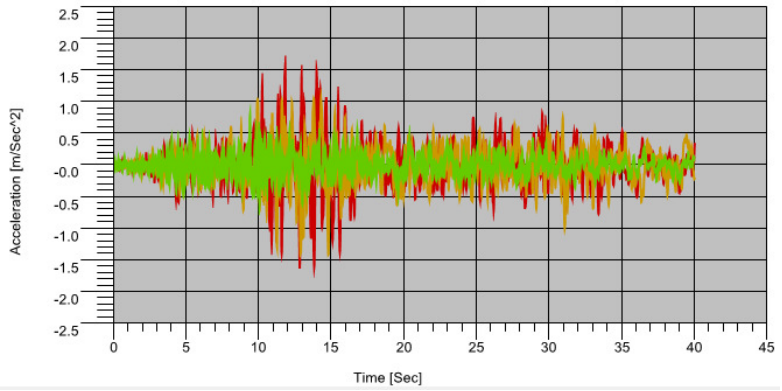


Figure 4-13: Time History Record of Chi-chi Earthquake, Taiwan; Date: 1999/09/20; Station: CHY004

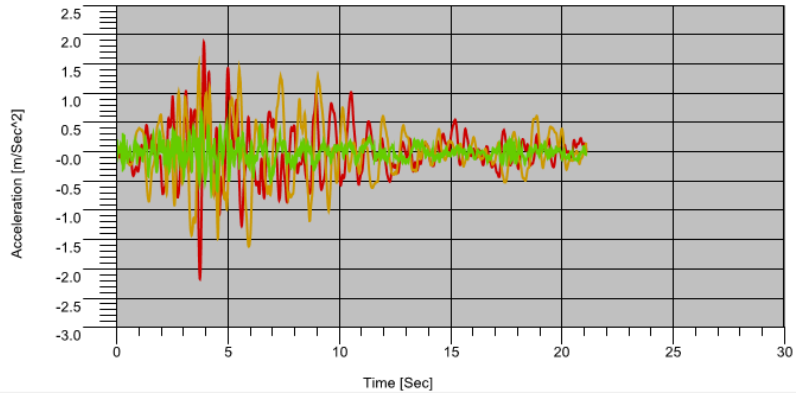


Figure 4-14: Time History Record of Kocaeli Earthquake , Turkey; Date: 999/08/17; Station: Ambarli

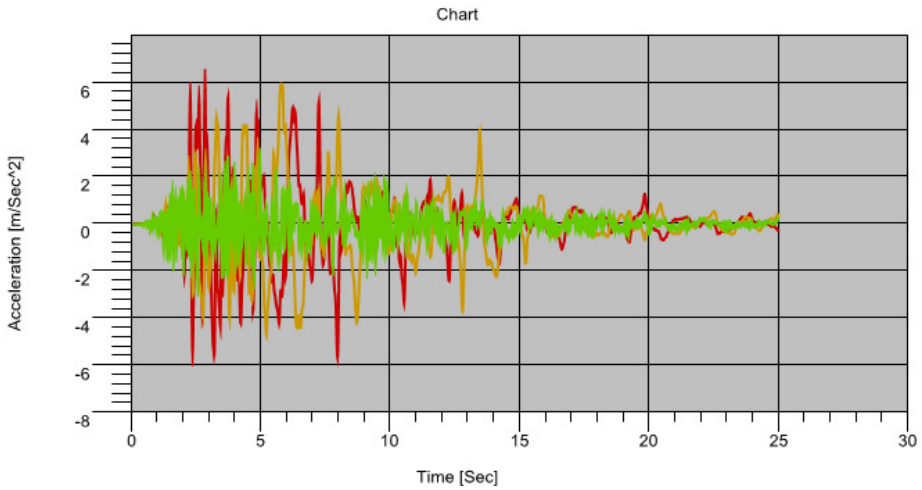


Figure 4-15: Time History Record of Kobe Earthquake, Japan; Date: 1995/01/16; Station: JR Takatori

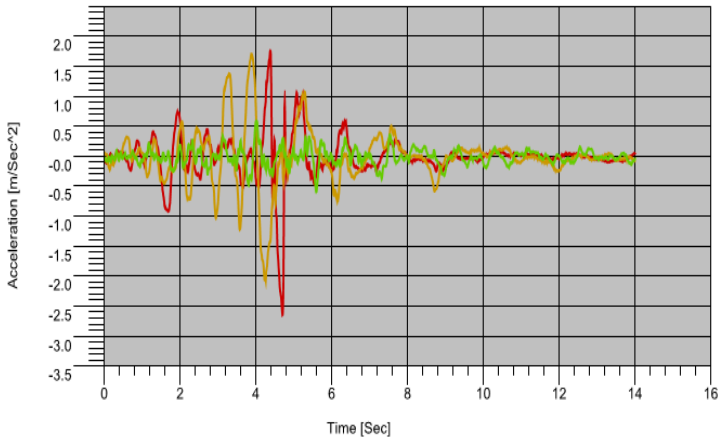


Figure 4-16: Time History Record of Loma Prieta Earthquake, USA; Date: 1989/10/18; Station: Alameda Naval Air Hanger 23

### *4.4.1 Fragility Functions for Brick in Cement Mortar Buildings with Flexible Floors and Roof*

**Preparation of Numerical Models**

Typical brick masonry buildings prevailing in Nepal are modeled numerically for non-linear simulation using ELS. Different size and geometry of the buildings are chosen on the basis building inventory survey carried out for JICA (2002) which considered the number of bays, typical wall thickness, floor height, number of bays, maximum bay size etc. Numerical model of the buildings representing these conditions are prepared and the simulation was conducted to get the average fragility functions. Figure 4-17 shows 8 different types of brick masonry buildings with flexible floor and roof for numerical simulation.

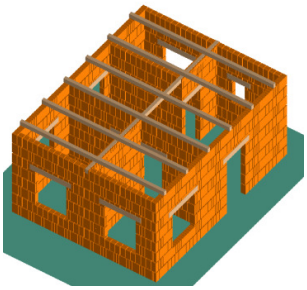

(a) BC1: One storey, multiple rooms, flat roof, No gable, many doors/windows

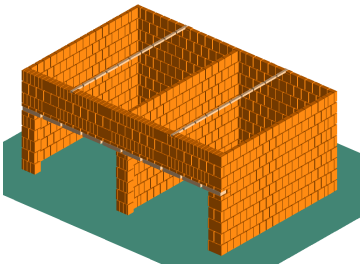

(b) BC2: One storey, two rooms, flat roof, No gable, One side open for shop

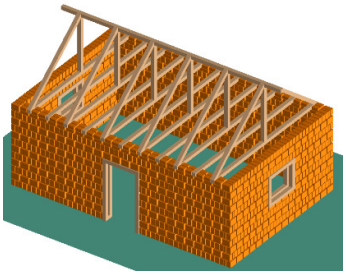

(c) BC3: One storey, One room, Slope roof, No gable, limited doors/windows

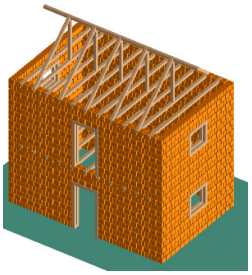

(d) BC4: Two storey, One room, Slope roof, No gable, limited doors/windows

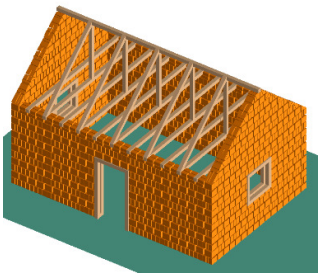

(e) BC5: One storey, One room, Slope roof, with gable, limited doors/windows

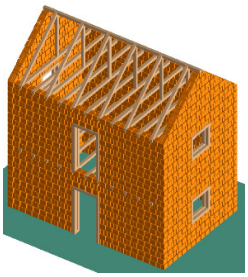

(f) BC6: Two storey, One room, Slope roof, With gable, limited doors/windows

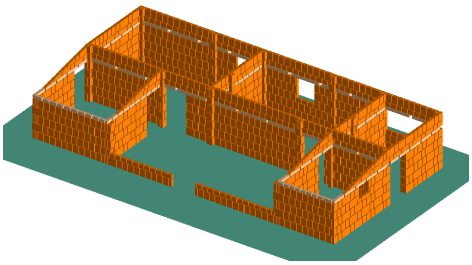

(g) BC7: One storey, Multiple room, Lintel band, Slight Slope roof, No gable, many doors/windows

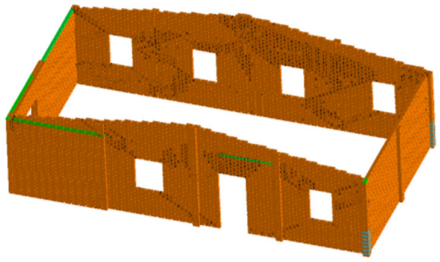

(h) BC8: One storey, One room, Lintel band, Slight Slope roof, No gable, many doors/windows

Figure 4-17: Numerical Models of Brick Masonry buildings with Flexible Floor and roof

The buildings are analyzed for different level of peak ground acceleration (PGA) by scaling the time history data given in Figure 4-12 to 4-16. The time history records are scaled to 0.2g, 0.4g, 0.6g and 1g PGA and applied to the buildings till the building is collapsed.

**Damage Classification**

Classification of damage state for unreinforced masonry buildings is given in FEMA-306 (1998), FEMA-307 (1998), FEMA-308 (1998) and HAZUS (2003). The damage states are identified considering the overall building damage definition according to HAZUS (2003) and the components level damage from FEMA-306 (1998) in this study. The damage definitions at different damage state according to HAZUS (2003) are given in Table 4-3. Different damage states at different level of PGA are noted observing the damage level at the respective peak ground acceleration.

Table 4-3:Definition of Damage Level at Different Damage State

| Damage State | Damage Definition |
|---|---|
| Slight | Diagonal, stair-step hairline cracks on masonry wall surfaces; larger cracks around door and window openings in walls with large proportion of openings; movements of lintels; cracks at the base of parapets. |
| Moderate | Most wall surfaces exhibit diagonal cracks; some of the walls exhibit larger diagonal cracks; masonry walls may have visible separation from diaphragms; significant cracking of parapets; some masonry may fall from walls or parapets. |
| Extensive | In buildings with relatively large area of wall openings most walls have suffered extensive cracking. Some parapets and gable end walls have |

| | |
|---|---|
| | fallen. Beams or trusses may have moved relative to their supports. |
| Complete | Structure has collapsed or is in imminent danger of collapse due to in-plane or out-of-plane failure of the walls. Approximately 15% of the total area of URM buildings with Complete damage is expected to be collapsed. |

**Observation of Damages according to Damage Classification**

The damage state of the building at the given level of input motion is done through observation of cracks, deformed shape and extent of damage to different structural members. Damage of the buildings at intermediate PGA level is noted at the respective time when the peak acceleration reached to the concerned value. For example, the damage state for PGA 0.05g, 0.1g, 0.15g and 0.2g are noted from a simulation of the building using time history with maximum 0.2g PGA while as the damage state at 0.25g, 0.3g, 0.35g and 0.4g are noted with another simulation with maximum acceleration of 0.4g.

Example of cracks and damages at different PGA for one of the building simulated are shown as an example here. Same building which was simulated with different type of mortars is presented for comparison. In the first case, a strong case is presented to show the damage patterns at different stage of loading from 0.15g to 0.7g PGA. Figure 4-18 to 4-25 show the different damage state according to HAZUS (2003) classification for this building. These damage patterns are obtained from four simulations conducted with Koceli earthquake of different scale as 0.2g, 0.4g, 0.6g and 1g as input motions. The crack patterns and damage up to 0.2g are obtained from first simulation with maximum 0.2g PGA earthquake. The damage patterns from 0.25g to 0.4g are obtained from the next simulation with maximum PGA of 0.4g and so on.

Figure 4-18 shows the damage patterns at 0.15g when vertical cracks at corners all orthogonal walls start. There are some cracks at the corners of the doors also. According to HAZUS (2003) classification of damage as given in Table 4-3, this level of damage is considered as slight damage.

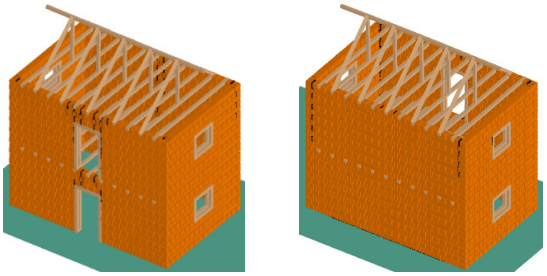

PGA: 0.15g

- Cracks at corners of building
- Cracks from corners of openings

"Slight Damage"

(a) Front side (b) Back side

Figure 4-18: Damage Patterns and Damage State at 0.15g for building with strong cement mortar

Figure 4-19 shows the damage patterns and damage state at 0.2g PGA. At this stage, the vertical cracks are extended throughout the floor height, additional vertical crack at the middle of the back side, cracks from corner of doors and windows and also horizontal cracks at bottom layer on side of the door. However, there are still limited cracks, no falling of any bricks and no shift of roof truss or other structural elements. Thus, the damage state is still "Slight Damage" at this stage.

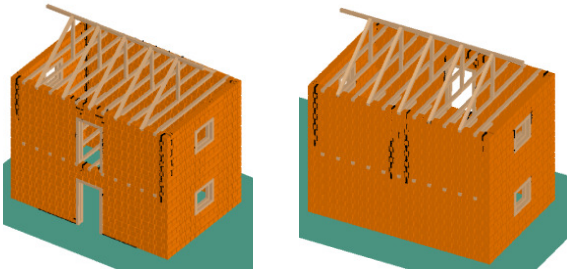

PGA: 0.2g

- Cracks at all corners of building
- Cracks from corners of openings
- Cracks at bottom layers near opening

"Slight Damage"

(a) Front side (b) Back side

Figure 4-19: Damage Patterns and Damage State at 0.2g PGA for building with strong cement mortar

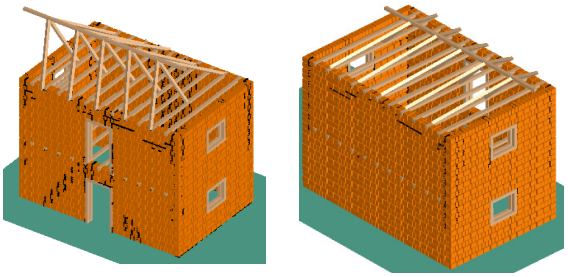

PGA: 0.25g

- Cracks at all corners of building extend throughout the floor height
- Two way diagonal Cracks from corners of openings
- Cracks at throughout the bottom layers
- Roof truss displaced from original position

"Moderate Damage"

(a) Front side (b) Back side

Figure 4-20: Damage Patterns and Damage State at 0.25g PGA for building with strong cement mortar

Figure 4-20 and Figure 4-21 show the damage patterns and damage state at PGA 0.25g and 0.35g respectively. At this stage, cracks at all corners of building extend throughout the floor height, Cracks at all corners of building extend throughout the floor height, there is throughout crack at bottom layer and roof truss is dislocated from the original position. In addition some bricks from top of the door are dropped off at 0.35g. The damage state at this stage is "Moderate Damage".

The damage continues with higher acceleration. At 0.4g PGA, some portion of the corner of the building, which is a critical location, loses some bricks and wider cracks appear in addition to the damage mentioned above. This level of damage is considered at Extensive Damage" according to the classification described above. The damage level of the building at 0.4g and 0.6g are presented in Figure 4-22 and 4-23 respectively. At 0.6 PGA, some portion of corner collapsed.

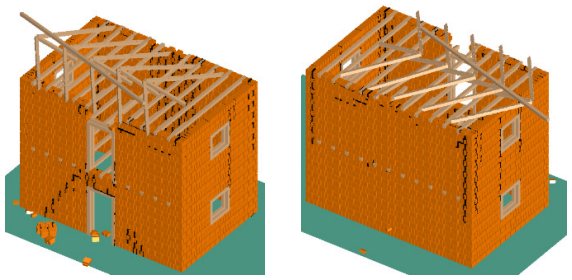

(a) Front side (b) Back side

PGA: 0.35g

- Some bricks from top of the door fall down
- Roof truss displaced
- Cracks at most of wall

"Moderate Damage"

Figure 4-21: Damage Patterns and Damage State at 0.35g PGA for building with strong cement mortar

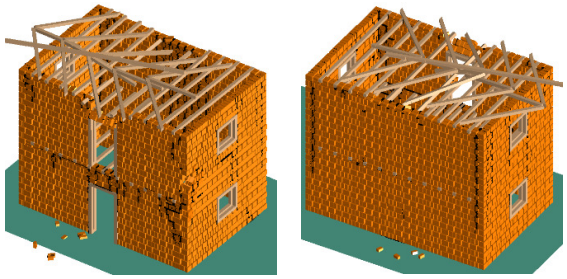

(a) Front side (b) Back side

PGA: 0.4g

- Severe cracks in all walls
- Some portion of corner collapsed

"Extensive Damage"

Figure 4-22: Damage Patterns and Damage State at 0.4g PGA for building with strong cement mortar

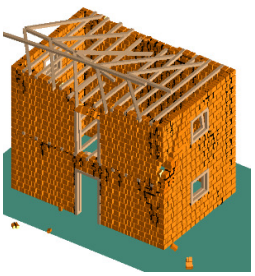

(a) Front Side

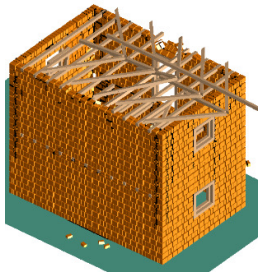

(b) Back Side

PGA: 0.6g

- Severe cracks in all walls
- Some portion of corner collapsed

"Extensive Damage"

Figure 4-23: Damage Patterns and Damage State at 0.6g PGA for building with strong cement mortar

The next simulation was with Koceli earthquake scaled to maximum 1g PGA, and the building was in the verge of collapse at 0.65 PGA and it was completely collapsed at PGA 0.7g. As the building was already at the verse of collapse at 0.65g, it was categorized as "Completely Damaged" as per the damage classification. The damage patterns of building at 0.65g and 0.7g PGA are shown in Figure 4-24 and 4-25 respectively.

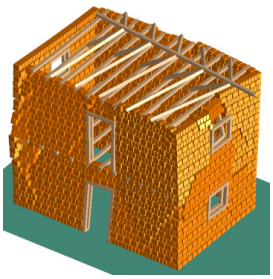

(a) Front Side

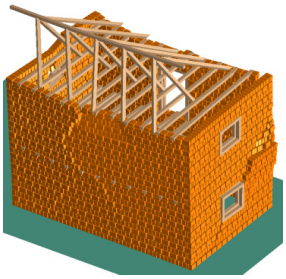

(b) Back Side

PGA: 0.65g

- The building is on the verge of collapse

"Complete Damage"

Figure 4-24: Damage Patterns and Damage State at 0.65g PGA for building with strong cement mortar

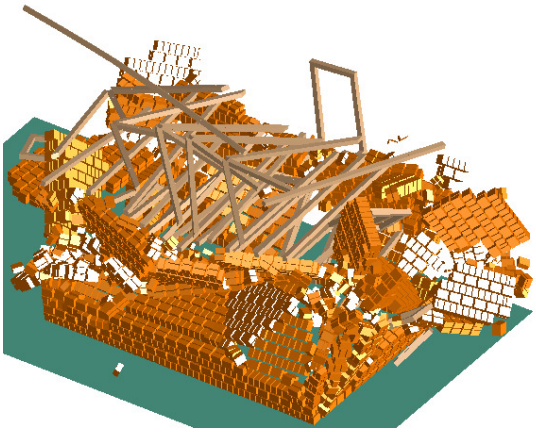

PGA: 0.7g

"Complete Damage"

Figure 4-25: Damage Patterns and Damage State at 0.7g PGA for building with strong cement mortar

Effect of mortar strength was found significant on stability of buildings against earthquakes. The building which suffered complete damage only at 0.65g was damaged completely at 0.35g when the average strength mortar was used. This large variation is due to a large variation in mortar strength also. Figure 4-26 shows the damage patterns and damage state of average strength cement mortar building for different acceleration. The building was slightly damaged at 0.1g PGA, moderately damaged at 0.25g PGA and completely damaged at 0.35g PGA.

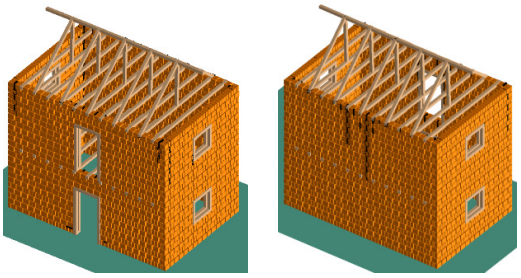

Front side Back side

PGA: 0.1g

- Cracks at corners of building
- Cracks from corners of openings

"Slight Damage"

(a) Damage Patterns and Damage State at 0.1g PGA for building with average cement mortar

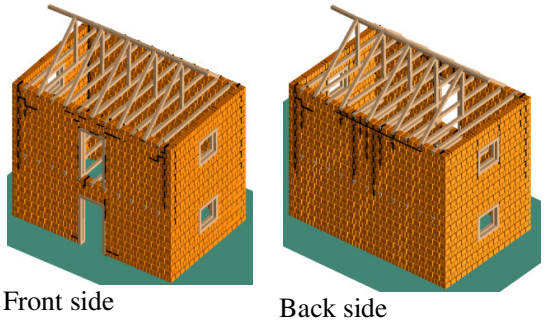

Front side Back side

PGA: 0.15g

- Throughout cracks at the corners of building
- Several vertical cracks at the back side of the building

"Moderate Damage"

(b) Damage Patterns and Damage State at 0.15g PGA for building with average cement mortar

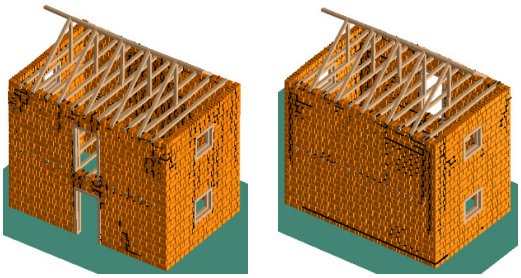

Front side Back side

PGA: 0.25g

- All walls severely cracked
- Significant deformation and damage at corners

"Extensive Damage"

(c) Damage Patterns and Damage State at 0.25g PGA for building with average cement mortar

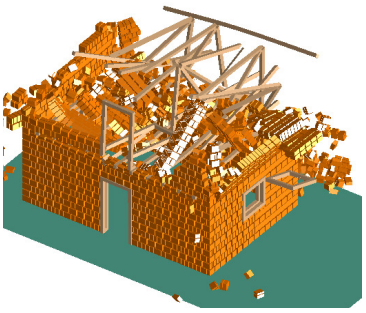

PGA: 0.35g

"Complete Damage"

(d) Damage Patterns and Damage State at 0.35g PGA for building with average cement mortar

Figure 4-26: Damage Patterns and Damage State of Average Strength Cement Mortar Building for Different Acceleration

In case of higher strength mortar (Figure 4-18 to 4-25), brick wall was very strong in comparison to roof truss connection and the dislocation of the roof had occurred before the building get significant damage. However, in case of average strength mortar building, damage to wall was occurred before the damage to roof truss.

**Analysis of Different Buildings and Compilation of Damage State**

Numerical simulations of all the buildings with different configurations as shown in Figure 4-17 are analyzed with different mortar properties for five different input motions. Each building was simulated with five cases. Out of the five cases, three cases (60%) were analyzed with the average mortar strength and also average energy content time histories. One case (20%) was analyzed to simulate the worst case when weak mortar strength and high energy content time history was used and the remaining one case (20%) was analyzed with strong mortar and weak energy content time history to simulate the best case. The mortar strength for average, strong and weak cases are taken based on field test which are presented in Table 3-1 in Section 3 of this thesis.

Total of 40 cases for the 8 buildings as shown in Figure 4-17 are analyzed at different PGA using five different input motions of different scale. The buildings were analyzed till complete

collapse and the damage state at different PGA are noted. The damage states were noted through observation of cracks, deformed shape and damage level. The damage state noted for each case is presented in Table 4-4.

The damage state is analyzed further for two different cases. In the first case, only the average cases are considered. The number of cases for each damage state from "None" to "Complete" is counted at each PGA level starting from 0.05g to 0.7g and given in Table 4-5. Cumulative probability of given damage state or more are calculated from it. For example, at 0.05g, there are 9 cases of slight damage and 1 case of moderate damage. In this case, the probability of damage for moderate and more is 1/24 and for slight level and more damage it is (1+9)/40. In this way, the cumulative probability of damage at different PGA for different damage state is calculated. The calculated cumulative probability of damage of all damage state and more damage considering only the average cases are given in Table 4-6.

In the second case, the number of cases and the cumulative probability includes two extreme cases for all the buildings with the worst case with very strong time history plus weak mortar and best case with weak strong motion plus strong mortar. The number of cases for different damage state including these extreme cases is presented in Table 4-7. The corresponding cumulative probability of damages is given in Table 4-8.

Table 4-4: Damage State of Different Cases of Brick in Cement Buildings with Flexible Floor and Roof

| Building | Acceleration (g) | | | | | | | | | | | | | |
|---|---|---|---|---|---|---|---|---|---|---|---|---|---|---|
| | 0.05 | 0.1 | 0.15 | 0.2 | 0.25 | 0.3 | 0.35 | 0.4 | 0.45 | 0.5 | 0.55 | 0.6 | 0.65 | 0.7 |
| BC1-Strong-Loma | N | N | S | M | M | M | M | E | E | E | C | C | C | C |
| BC1-Avg-Nep | N | N | S | M | M | E | E | E | C | C | C | C | C | C |
| BC1-Avg-chi | N | S | M | M | M | E | E | E | C | C | C | C | C | C |
| BC1-Avg-Koce | N | S | M | M | E | E | E | C | C | C | C | C | C | C |
| BC1-Weak-Kobe | N | M | M | E | E | C | C | C | C | C | C | C | C | C |
| BC2-Strong-Loma | S | S | M | M | E | E | C | C | C | C | C | C | C | C |
| BC2-Avg-Nep | S | M | M | E | E | C | C | C | C | C | C | C | C | C |
| BC2-Avg-Chi | S | M | M | E | E | C | C | C | C | C | C | C | C | C |
| BC2-Avg-Koce | M | M | M | E | C | C | C | C | C | C | C | C | C | C |
| BC2-Weak-Kobe | E | E | C | C | C | C | C | C | C | C | C | C | C | C |
| BC3-Str-Loma | N | N | N | S | S | M | M | M | E | E | E | E | C | C |
| BC3-Avg-Nep | N | S | S | M | M | E | E | E | C | C | C | C | C | C |
| BC3-Avg-chi | N | S | S | M | M | E | E | C | C | C | C | C | C | C |
| BC3-Avg-Koce | N | S | S | M | E | E | E | C | C | C | C | C | C | C |
| BC3-Weak-Kobe | S | M | M | E | E | C | C | C | C | C | C | C | C | C |
| BC4-Str-Koce | N | N | S | S | M | M | M | E | E | E | E | C | C | C |
| BC4-Avg-Nep | N | S | M | M | E | E | E | C | C | C | C | C | C | C |
| BC4-Avg-Chi | N | S | M | M | E | E | E | C | C | C | C | C | C | C |

| | | | | | | | | | | | | | | |
|---|---|---|---|---|---|---|---|---|---|---|---|---|---|---|
| BC4-Avg-Koce | N | S | M | E | E | E | C | C | C | C | C | C | C | C |
| BC4-Weak-Kobe | S | M | M | E | E | C | C | C | C | C | C | C | C | C |
| BC5-Str-Loma | N | S | M | M | M | M | M | E | E | E | C | C | C | C |
| BC5-Avg-Nep | S | M | M | M | M | E | E | E | E | C | C | C | C | C |
| BC5-Avg-Chi | S | M | M | M | M | E | E | E | E | C | C | C | C | C |
| BC5-Avg-Koce | S | M | M | M | E | E | E | E | C | C | C | C | C | C |
| BC5-weak-Kobe | M | E | E | E | E | E | C | C | C | C | C | C | C | C |
| BC6-Str-Loma | N | S | M | M | M | E | E | E | E | C | C | C | C | C |
| BC6-Avg-Nep | N | S | M | E | E | E | C | C | C | C | C | C | C | C |
| BC6-Avg-Chi | N | S | E | E | E | E | C | C | C | C | C | C | C | C |
| BC6-Avg-Koce | S | M | E | E | E | C | C | C | C | C | C | C | C | C |
| BC6-Weak-Kobe | M | M | E | E | C | C | C | C | C | C | C | C | C | C |
| BC7-str-Loma | N | N | S | S | M | M | M | E | E | E | E | C | C | C |
| BC7-Avg-Nep | N | N | S | M | M | E | E | E | E | E | C | C | C | C |
| BC7-Avg-Chi | N | S | M | M | E | E | E | E | E | E | C | C | C | C |
| BC7-Avg-Kose | N | S | M | M | E | E | E | E | E | C | C | C | C | C |
| BC7-Weak-Kobe | N | S | M | E | E | E | C | C | C | C | C | C | C | C |
| BC8-Str-Loma | S | S | M | M | M | E | E | C | C | C | C | C | C | C |
| BC8-Avg-Nep | S | S | M | E | E | C | C | C | C | C | C | C | C | C |
| BC8-Avg-Chi | S | S | M | E | E | C | C | C | C | C | C | C | C | C |
| BC8-Avg-Koce | S | S | M | E | E | C | C | C | C | C | C | C | C | C |
| BC8-Weak-Kobe | M | E | E | C | C | C | C | C | C | C | C | C | C | C |
| N: Negligible; S: Slight Damage; M: Moderate Damage; E: Extensive Damage; C: Complete Damage | | | | | | | | | | | | | | |

Table 4-5: Number of Cases with Different Damage State for Brick in Cement Buildings with Flexible Floor and Roof for Case 1

| | **Number of Cases at Different PGA (%g)** | | | | | | | | | | | | | |
|---|---|---|---|---|---|---|---|---|---|---|---|---|---|---|
| **Damage Level** | 0.05 | 0.1 | 0.15 | 0.2 | 0.25 | 0.3 | 0.35 | 0.4 | 0.45 | 0.5 | 0.55 | 0.6 | 0.65 | 0.7 |
| None | 14 | 2 | 0 | 0 | 0 | 0 | 0 | 0 | 0 | 0 | 0 | 0 | 0 | 0 |
| Slight | 9 | 15 | 5 | 0 | 0 | 0 | 0 | 0 | 0 | 0 | 0 | 0 | 0 | 0 |
| Moderate | 1 | 7 | 17 | 14 | 7 | 0 | 0 | 0 | 0 | 0 | 0 | 0 | 0 | 0 |
| Extensive | 0 | 0 | 2 | 10 | 16 | 17 | 14 | 9 | 5 | 2 | 0 | 0 | 0 | 0 |
| Complete | 0 | 0 | 0 | 0 | 1 | 7 | 10 | 15 | 19 | 22 | 24 | 24 | 24 | 24 |

Table 4-6: Cumulative Probability of Damage at Different Damage State for Case 1

| | **Cumulative Probability of Damage at Different PGA (%g)** | | | | | | | | | | | | | |
|---|---|---|---|---|---|---|---|---|---|---|---|---|---|---|
| **Damage Level** | 0.05 | 0.1 | 0.15 | 0.2 | 0.25 | 0.3 | 0.35 | 0.4 | 0.45 | 0.5 | 0.55 | 0.6 | 0.65 | 0.7 |
| Slight | 0.04 | 0.29 | 0.79 | 1.00 | 1.00 | 1.00 | 1.00 | 1.00 | 1.00 | 1.00 | 1.00 | 1.00 | 1.00 | 1.00 |
| Moderate | 0.00 | 0.00 | 0.08 | 0.42 | 0.71 | 1.00 | 1.00 | 1.00 | 1.00 | 1.00 | 1.00 | 1.00 | 1.00 | 1.00 |
| Extensive | 0.00 | 0.00 | 0.00 | 0.00 | 0.04 | 0.29 | 0.42 | 0.63 | 0.79 | 0.92 | 1.00 | 1.00 | 1.00 | 1.00 |
| Complete | 0.42 | 0.92 | 1.00 | 1.00 | 1.00 | 1.00 | 1.00 | 1.00 | 1.00 | 1.00 | 1.00 | 1.00 | 1.00 | 1.00 |

Table 4-7: Number of Cases with Different Damage State for Brick in Cement Buildings with Flexible Floor and Roof for Case 2

| | **Number of Cases at Different PGA (%g)** | | | | | | | | | | | | | |
|---|---|---|---|---|---|---|---|---|---|---|---|---|---|---|
| **Damage Level** | 0.05 | 0.1 | 0.15 | 0.2 | 0.25 | 0.3 | 0.35 | 0.4 | 0.45 | 0.5 | 0.55 | 0.6 | 0.65 | 0.7 |

| | | | | | | | | | | | | | | |
|---|---|---|---|---|---|---|---|---|---|---|---|---|---|---|
| None | 22 | 6 | 0 | 0 | 0 | 0 | 0 | 0 | 0 | 0 | 0 | 0 | 0 | 0 |
| Slight | 13 | 20 | 8 | 3 | 1 | 0 | 0 | 0 | 0 | 0 | 0 | 0 | 0 | 0 |
| Moderate | 4 | 11 | 25 | 19 | 13 | 5 | 5 | 1 | 0 | 0 | 0 | 0 | 0 | 0 |
| Extensive | 1 | 3 | 5 | 16 | 22 | 22 | 16 | 14 | 11 | 7 | 3 | 1 | 0 | 0 |
| Complete | 0 | 0 | 1 | 2 | 4 | 13 | 19 | 25 | 29 | 33 | 37 | 39 | 40 | 40 |

Table 4-8: Cumulative Probability of Damage at Different Damage State for Brick in Cement Buildings for Case 2

| | **Cumulative Probability of Damage at Different PGA (%g)** | | | | | | | | | | | | | |
|---|---|---|---|---|---|---|---|---|---|---|---|---|---|---|
| **Damage Level** | 0.05 | 0.1 | 0.15 | 0.2 | 0.25 | 0.3 | 0.35 | 0.4 | 0.45 | 0.5 | 0.55 | 0.6 | 0.65 | 0.7 |
| Slight | 0.45 | 0.85 | 1.00 | 1.00 | 1.00 | 1.00 | 1.00 | 1.00 | 1.00 | 1.00 | 1.00 | 1.00 | 1.00 | 1.00 |
| Moderate | 0.13 | 0.35 | 0.79 | 0.93 | 0.98 | 1.00 | 1.00 | 1.00 | 1.00 | 1.00 | 1.00 | 1.00 | 1.00 | 1.00 |
| Extensive | 0.03 | 0.08 | 0.15 | 0.45 | 0.65 | 0.88 | 0.88 | 0.98 | 1.00 | 1.00 | 1.00 | 1.00 | 1.00 | 1.00 |
| Complete | 0.00 | 0.00 | 0.03 | 0.05 | 0.10 | 0.33 | 0.48 | 0.63 | 0.73 | 0.83 | 0.93 | 0.98 | 1.00 | 1.00 |

**Plotting Fragility Functions**

Latest risk assessment tools like HAZUS (2003) and other damage assessment tools described in Section 2 suggest fragility functions are plotted as a cumulative log normal distribution function. In this study also, the probability of being in or exceeding a given damage state is plotted as a cumulative lognormal distribution.

For structural damage, given the Peak ground acceleration (PGA), the probability of being in or exceeding a damage state (ds) is calculated as:

$$P\,[ds/PGA] = \frac{1}{2}\,[1 + \text{erf}\left(\frac{\ln PGA - \mu}{\beta\sqrt{2}}\right)]$$

Where

erf = complementary error function

$\mu$ = mean = ln $PGA_{,ds}$

$PGA_{,ds}$ = Median value of PGA at which the building reaches the threshold of the damage state ds.

$\beta$ = Standard Deviation of lnPGA

The cumulative probability of the damage at different PGA from Table 4-6 and 4-8 are plotted together with best fit cumulative lognormal distribution are given in Figure 4-27 and 4-28 respectively. The median values and standard deviation for plotting cumulative lognormal distribution of different damage are calculated from Table 4-6 and Table 4-8. The calculated median values and the standard deviations are given in Table 4-9.

Table 4-9: Median Values and Standard Deviation for Cumulative Lognormal Distribution for Brick in Cement Buildings with Flexible Floor and Roof

| Damage States | Case 1 | | Case 2 | |
|---|---|---|---|---|
| | **Median (PGA for 50% Damage)** | **Standard Deviation σ (or β)** | **Median (PGA for 50% Damage)** | **Standard Deviation σ (or β)** |
| Slight | 0.058 | 0.392 | 0.056 | 0.509 |
| Moderate | 0.121 | 0.317 | 0.117 | 0.380 |
| Extensive | 0.214 | 0.237 | 0.213 | 0.334 |
| Complete | 0.363 | 0.190 | 0.358 | 0.304 |

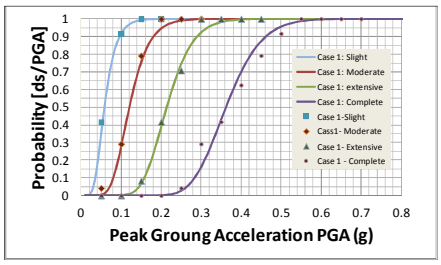


Figure 4-27: Fragility function for Brick in Cement Buildings with Flexible Floor/Roof for Case I

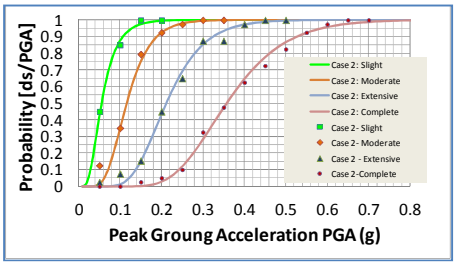


Figure 4-28: Fragility function for Brick in Cement Buildings with Flexible Floor/Roof for Case II

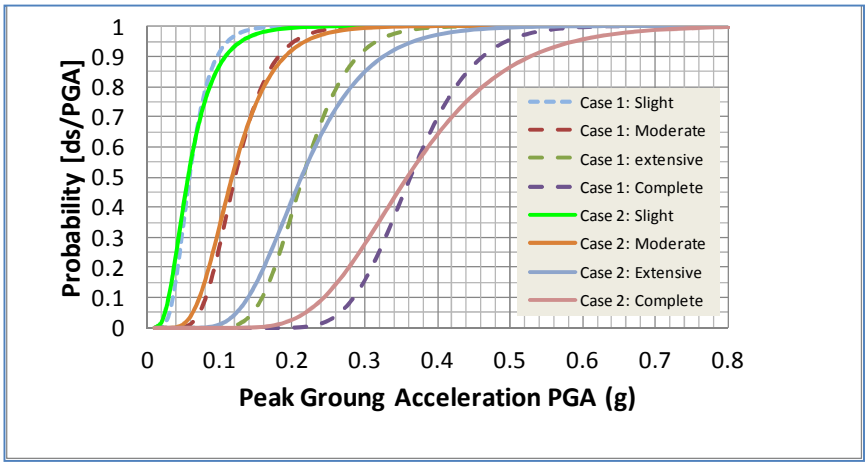


Figure 4-29: Fragility Functions for Brick in Cement Buildings in Nepal with Flexible Floor/Roof

Figure 4-29 shows the fragility functions for brick with cement-sand mortar buildings in Nepal. In each case of the damage state, before the point of intersection case 2 is the upper boundary and case 1 is the lower boundary of the damage while as after the intersection case 1 is the upper boundary and case 2 is the lower boundary of the actual fragility function. So, the actual fragility function will be in somewhere in between these two curves.

### *4.4.2 Fragility Functions for Brick in Mud Mortar Buildings with Flexible Floors and Roof*

**Model preparation and Observation of Damages**

All the 8 buildings as shown in Figure 4-17 were analyzed for mud mortar also. The average mortar strength, 20$^{th}$ percentile to represent weak mortar strength and 80$^{th}$ percentile representing the strong mortar strength were taken based on field test as presented in Table 3-4 in Section 3 of this thesis. The mud buildings got complete damage much sooner than the brick in cement buildings. Figure 4-30 shows damage state at different acceleration of the same building, which is shown in Figure 4-26 with average cement-sand mortar, with average mud mortar. The building was completely damaged at 0.25g.

Figure 4-31 and Figure 4-32 show damage of other two brick masonry buildings with mud mortar. A building with gable wall is taken as an example and is shown Figure 4-31. The building was completely damaged at 0.2g acceleration. Constructing gable is still a common practice for many masonry buildings in Nepal for both the brick masonry and stone masonry. Now-a-days, construction practice of constructing heavy gable wall has been changed to constructing lighter gable walls of wood or tin. Thus, in this study some buildings are considered with gable wall and some without gable wall.

Figure 4-32 shows one of the weakest cases among the 8 representative configurations of buildings which were considered for simulation of brick masonry buildings. In this case, there is a solid wall in one side and there is complete opening for shop purpose. This building, though only one storey, performed very poorly and has collapsed at 0.15g acceleration when the average mortar strength was used. The building was collapsed at 0.1g acceleration with weak mud mortar.

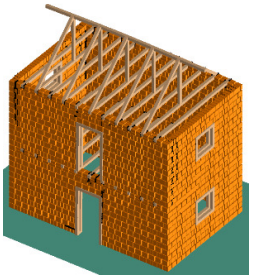

Front side

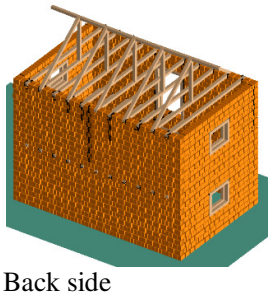

Back side

PGA: 0.05g

- Cracks at corners of building
- Cracks from corners of openings
- Vertical crack at middle of long wall

"Slight Damage"

(a) Damage Patterns and Damage State at 0.05g PGA for building with average mud mortar

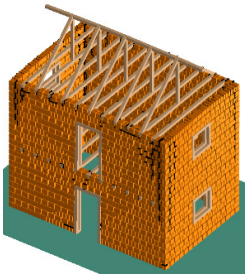

Front side

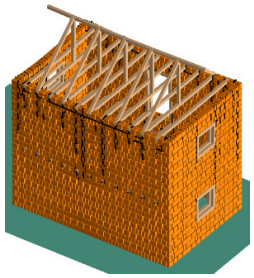

Back side

PGA: 0.10g

- Throughout cracks at the corners of building
- Several vertical cracks at the back side of the building

"Moderate Damage"

(b) Damage Patterns and Damage State at 0.1g PGA for building with average mud mortar

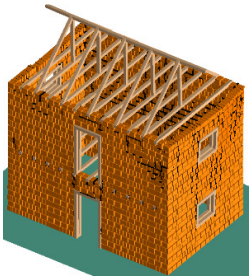

Front side

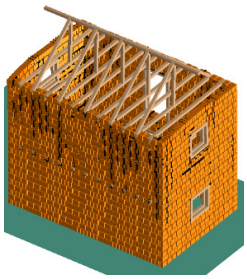

Back side

PGA: 0.15g

- All walls severely cracked
- Significant deformation and damage at corners

"Extensive Damage"

(c) Damage Patterns and Damage State at 0.15g PGA for building with average mud mortar

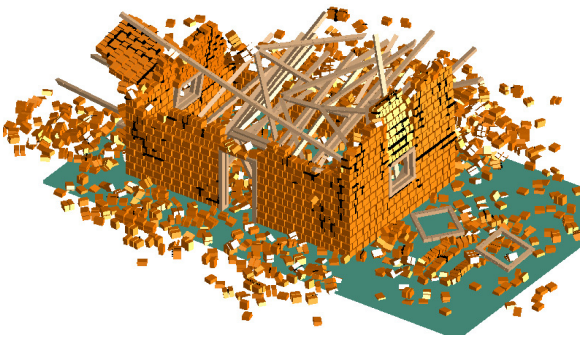

PGA: 0.25g

"Complete Damage"

(d) Damage Patterns and Damage State at 0.25g PGA for building with average mud mortar

Figure 4-30: Damage Patterns and Damage State of Average Strength Mud Mortar Building at Different Acceleration

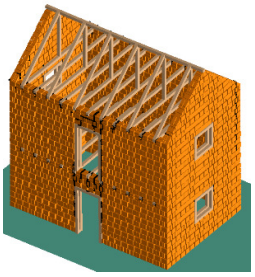

Front side

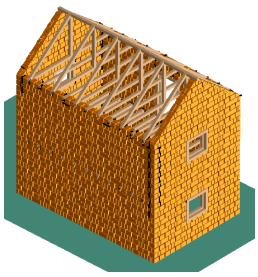

Back side

PGA: 0.05g

- Cracks at corners of building
- Cracks from corners of openings
- Vertical crack at middle of long wall

"Slight Damage"

(a) Damage Patterns and Damage State at 0.05g PGA for gable wall building with average mud mortar

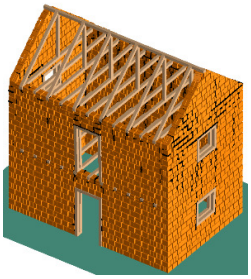

Front side

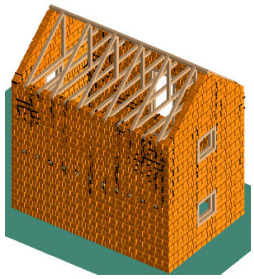

Back side

PGA: 0.10g

- Throughout cracks at the corners of building
- All the walls severely cracked
- Some deformation and separation at corners

"Extensive Damage"

(b) Damage Patterns and Damage State at 0.1g PGA for gable wall building with average mud mortar

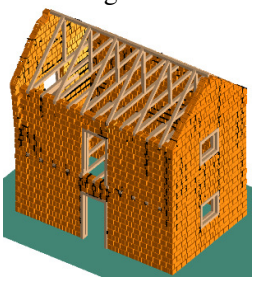

Front side

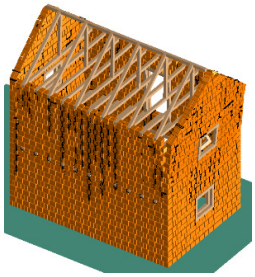

Back side

PGA: 0.15g

- All walls severely cracked
- Significant deformation and damage at corners
- Gable walls are near to collapse

"Extensive Damage"

(c) Damage Patterns and Damage State at 0.15g PGA for gable wall building with average mud mortar

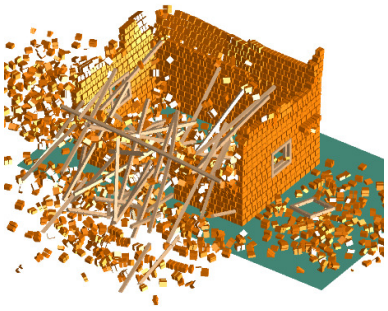

PGA: 0.2g

"Complete Damage"

(d) Damage Patterns and Damage State at 0.20g PGA for gable wall building with average mud mortar

Figure 4-31: Damage Patterns and Damage State of Average Strength Mud Mortar Gable Wall Building at Different Acceleration

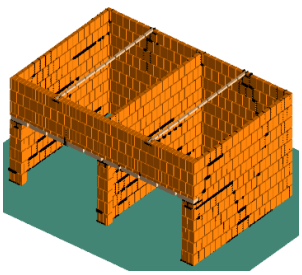

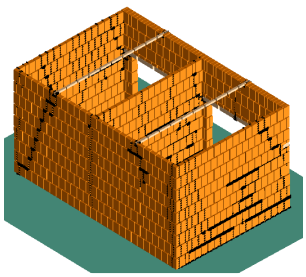

PGA: 0.05g

- Cracks in most of the walls

"Moderate Damage"

Front side Back side

(a) Damage Patterns and Damage State at 0.05g PGA for one side open building with average mud mortar

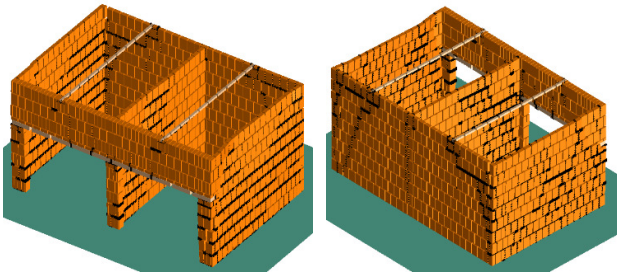

Front side Back side

PGA: 0.10g

- All walls severely cracked
- Orthogonal walls are separated at corners and walls are deformed significantly

"Extensive Damage"

(b) Damage Patterns and Damage State at 0.1g PGA for one side open building with average mud mortar

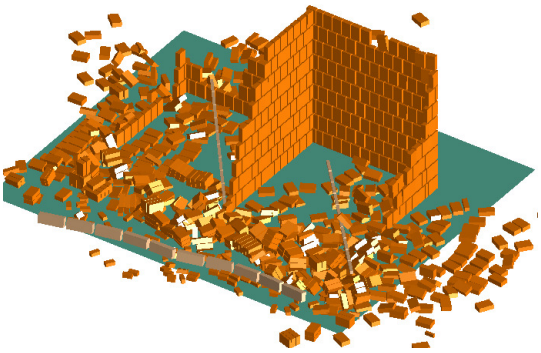

PGA: 0.15g

"Complete Damage"

(c) Damage Patterns and Damage State at 0.150g PGA for one side open building with average mud mortar

Figure 4-32: Damage Patterns and Damage State of Average Strength Mud Mortar One Side Open Building at Different Acceleration

**Compilation of Damage State and Plotting Fragility Functions**

In the mud mortar case also, total of 40 cases for the 8 buildings as shown in Figure 4-17 are analyzed at different PGA using five different input motions of different scale. The buildings were analyzed till complete collapse and the damage state at different PGA are noted. The damage states were noted through observation of cracks, deformed shape and damage level. The damage state noted for each case is presented in Table 4-10.

Table 4-10: Damage State of Different Cases of Brick in Mud Buildings with Flexible Floor and Roof

| | Acceleration (g) | | | | | | | | | | | | | |
|---|---|---|---|---|---|---|---|---|---|---|---|---|---|---|
| Building | 0.05 | 0.1 | 0.15 | 0.2 | 0.25 | 0.3 | 0.35 | 0.4 | 0.45 | 0.5 | 0.55 | 0.6 | 0.65 | 0.7 |
| BM1-Strong-Loma | N | S | M | M | E | E | E | C | C | C | C | C | C | C |
| BM1-Avg-Nep | N | S | M | E | E | C | C | C | C | C | C | C | C | C |
| BM1-Avg-chi | N | S | M | E | E | C | C | C | C | C | C | C | C | C |
| BM1-Avg-Koce | N | S | M | E | C | C | C | C | C | C | C | C | C | C |
| BM1-Weak-Kobe | S | M | E | C | C | C | C | C | C | C | C | C | C | C |
| BM2-Strong-Loma | N | S | M | E | E | E | C | C | C | C | C | C | C | C |
| BM2-Avg-Nep | S | M | C | C | C | C | C | C | C | C | C | C | C | C |
| BM2-Avg-Chi | S | E | C | C | C | C | C | C | C | C | C | C | C | C |
| BM2-Avg-Koce | M | E | C | C | C | C | C | C | C | C | C | C | C | C |
| BM2-Weak-Kobe | E | C | C | C | C | C | C | C | C | C | C | C | C | C |
| BM3-Str-Loma | N | S | S | M | M | E | E | E | C | C | C | C | C | C |
| BM3-Avg-Nep | N | S | M | E | E | E | C | C | C | C | C | C | C | C |
| BM3-Avg-chi | N | S | M | E | E | C | C | C | C | C | C | C | C | C |
| BM3-Avg-Koce | N | M | E | E | E | C | C | C | C | C | C | C | C | C |
| BM3-Weak-Kobe | M | E | E | C | C | C | C | C | C | C | C | C | C | C |
| BM4-Str-Loma | N | S | M | M | E | E | E | C | C | C | C | C | C | C |
| BM4-Avg-Nep | N | M | E | E | C | C | C | C | C | C | C | C | C | C |
| BM4-Avg-Chi | S | M | E | E | C | C | C | C | C | C | C | C | C | C |
| BM4-Avg-Koce | N | M | E | E | C | C | C | C | C | C | C | C | C | C |
| BM4-Weak-Kobe | M | E | C | C | C | C | C | C | C | C | C | C | C | C |
| BM5-Str-Loma | N | S | S | M | E | E | C | C | C | C | C | C | C | C |
| BM5-Avg-Nep | N | S | M | E | C | C | C | C | C | C | C | C | C | C |
| BM5-Avg-Chi | N | S | M | E | C | C | C | C | C | C | C | C | C | C |
| BM5-Avg-Koce | N | S | M | E | C | C | C | C | C | C | C | C | C | C |
| BM5-weak-Kobe | M | E | E | C | C | C | C | C | C | C | C | C | C | C |
| BM6-Str-Loma | N | S | M | E | E | C | C | C | C | C | C | C | C | C |
| BM6-Avg-Nep | S | M | E | C | C | C | C | C | C | C | C | C | C | C |
| BM6-Avg-Chi | S | M | E | C | C | C | C | C | C | C | C | C | C | C |
| BM6-Avg-Koce | S | E | E | C | C | C | C | C | C | C | C | C | C | C |
| BM6-Weak-Kobe | M | E | C | C | C | C | C | C | C | C | C | C | C | C |
| BM7-str-Loma | N | N | S | S | M | M | E | E | C | C | C | C | C | C |
| BM7-Avg-Nep | N | S | M | M | E | E | C | C | C | C | C | C | C | C |
| BM7-Avg-Chi | N | S | M | M | E | E | C | C | C | C | C | C | C | C |
| BM7-Avg-Kose | N | S | M | M | E | C | C | C | C | C | C | C | C | C |
| BM7-Weak-Kobe | N | S | M | E | C | C | C | C | C | C | C | C | C | C |
| BM8-Str-Loma | N | S | M | M | E | E | E | C | C | C | C | C | C | C |
| BM8-Avg-Nep | S | M | C | C | C | C | C | C | C | C | C | C | C | C |
| BM8-Avg-Chi | M | E | C | C | C | C | C | C | C | C | C | C | C | C |
| BM8-Avg-Koce | M | E | C | C | C | C | C | C | C | C | C | C | C | C |
| BM8-Weak-Kobe | E | C | C | C | C | C | C | C | C | C | C | C | C | C |
| N: Negligible; S: Slight Damage; M: Moderate Damage; E: Extensive Damage; C: Complete Damage | | | | | | | | | | | | | | |

The damage state is analyzed further for two different cases as like in brick in cement mortar case earlier. In the first case, only the average cases are considered and in the second case, all cases with strong and weak conditions are also considered. The number of cases for different damage state the corresponding cumulative probability of damages for the first case is presented in Table 4-11 and 4-12 respectively. Similarly, the number of cases for different damage state the corresponding cumulative probability of damages for the second case is presented in Table 4-13 and 4-14.

Table 4-11: Number of Cases with Different Damage State for Brick in Mud Buildings with Flexible Floor and Roof for Case 1

| | Number of Cases at Different PGA (%g) | | | | | | | | | | | | | |
|---|---|---|---|---|---|---|---|---|---|---|---|---|---|---|
| **Damage Level** | **0.05** | **0.1** | **0.15** | **0.2** | **0.25** | **0.3** | **0.35** | **0.4** | **0.45** | **0.5** | **0.55** | **0.6** | **0.65** | **0.7** |
| None | 14 | 0 | 0 | 0 | 0 | 0 | 0 | 0 | 0 | 0 | 0 | 0 | 0 | 0 |
| Slight | 7 | 11 | 0 | 0 | 0 | 0 | 0 | 0 | 0 | 0 | 0 | 0 | 0 | 0 |
| Moderate | 3 | 8 | 11 | 3 | 0 | 0 | 0 | 0 | 0 | 0 | 0 | 0 | 0 | 0 |
| Extensive | 0 | 5 | 7 | 12 | 8 | 3 | 0 | 0 | 0 | 0 | 0 | 0 | 0 | 0 |
| Complete | 0 | 0 | 6 | 9 | 16 | 21 | 24 | 24 | 24 | 24 | 24 | 24 | 24 | 24 |

Table 4-12: Cumulative Probability of Damage at Different Damage State for Brick in Mud Buildings for Case 1

| | Cumulative Probability of Damage at Different PGA (%g) | | | | | | | | | | | | | |
|---|---|---|---|---|---|---|---|---|---|---|---|---|---|---|
| **Damage Level** | **0.05** | **0.1** | **0.15** | **0.2** | **0.25** | **0.3** | **0.35** | **0.4** | **0.45** | **0.5** | **0.55** | **0.6** | **0.65** | **0.7** |
| Slight | 0.42 | 1.00 | 1.00 | 1.00 | 1.00 | 1.00 | 1.00 | 1.00 | 1.00 | 1.00 | 1.00 | 1.00 | 1.00 | 1.00 |
| Moderate | 0.13 | 0.54 | 1.00 | 1.00 | 1.00 | 1.00 | 1.00 | 1.00 | 1.00 | 1.00 | 1.00 | 1.00 | 1.00 | 1.00 |
| Extensive | 0.00 | 0.21 | 0.54 | 0.88 | 1.00 | 1.00 | 1.00 | 1.00 | 1.00 | 1.00 | 1.00 | 1.00 | 1.00 | 1.00 |
| Complete | 0.00 | 0.00 | 0.25 | 0.38 | 0.67 | 0.88 | 1.00 | 1.00 | 1.00 | 1.00 | 1.00 | 1.00 | 1.00 | 1.00 |

Table 4-13: Number of Cases with Different Damage State for Brick in Mud Buildings with Flexible Floor and Roof for Case 2

| | Number of Cases at Different PGA (%g) | | | | | | | | | | | | | |
|---|---|---|---|---|---|---|---|---|---|---|---|---|---|---|
| **Damage Level** | **0.05** | **0.1** | **0.15** | **0.2** | **0.25** | **0.3** | **0.35** | **0.4** | **0.45** | **0.5** | **0.55** | **0.6** | **0.65** | **0.7** |
| None | 23 | 1 | 0 | 0 | 0 | 0 | 0 | 0 | 0 | 0 | 0 | 0 | 0 | 0 |
| Slight | 8 | 19 | 3 | 1 | 0 | 0 | 0 | 0 | 0 | 0 | 0 | 0 | 0 | 0 |
| Moderate | 7 | 9 | 17 | 8 | 2 | 1 | 0 | 0 | 0 | 0 | 0 | 0 | 0 | 0 |
| Extensive | 2 | 9 | 10 | 15 | 14 | 9 | 5 | 2 | 0 | 0 | 0 | 0 | 0 | 0 |
| Complete | 0 | 2 | 10 | 16 | 24 | 30 | 35 | 38 | 40 | 40 | 40 | 40 | 40 | 40 |

Table 4-14: Cumulative Probability of Damage at Different Damage State Considering for Brick in Mud Buildings for Case 2

| | Cumulative Probability of Damage at Different PGA (%g) | | | | | | | | | | | | | |
|---|---|---|---|---|---|---|---|---|---|---|---|---|---|---|
| **Damage Level** | **0.05** | **0.1** | **0.15** | **0.2** | **0.25** | **0.3** | **0.35** | **0.4** | **0.45** | **0.5** | **0.55** | **0.6** | **0.65** | **0.7** |
| Slight | 0.43 | 0.98 | 1.00 | 1.00 | 1.00 | 1.00 | 1.00 | 1.00 | 1.00 | 1.00 | 1.00 | 1.00 | 1.00 | 1.00 |
| Moderate | 0.23 | 0.50 | 0.93 | 0.98 | 1.00 | 1.00 | 1.00 | 1.00 | 1.00 | 1.00 | 1.00 | 1.00 | 1.00 | 1.00 |
| Extensive | 0.05 | 0.28 | 0.50 | 0.78 | 0.95 | 0.98 | 1.00 | 1.00 | 1.00 | 1.00 | 1.00 | 1.00 | 1.00 | 1.00 |
| Complete | 0.00 | 0.05 | 0.25 | 0.40 | 0.60 | 0.75 | 0.88 | 0.95 | 1.00 | 1.00 | 1.00 | 1.00 | 1.00 | 1.00 |

The cumulative probability of the damage at different PGA from Table 4-12 and Table 4-14 are plotted together with best fit cumulative lognormal distribution are given in Figure 4-33 and 4-34 respectively.

The median values and standard deviation for plotting cumulative lognormal distribution of different damage are calculated from Table 4-12 and Table 4-14. The calculated median values and the standard deviations are given in Table 4-15.

Table 4-15: Median Values and Standard Deviation for Cumulative Lognormal Distribution for Brick in Mud Buildings with Flexible Floor and Roof

| Damage States | Case 1 | | Case 2 | |
|---|---|---|---|---|
| | Median (PGA for 50% Damage) | Standard Deviation σ (or β) | Median (PGA for 50% Damage) | Standard Deviation σ (or β) |
| Slight | 0.057 | 0.316 | 0.057 | 0.495 |
| Moderate | 0.095 | 0.313 | 0.100 | 0.495 |
| Extensive | 0.144 | 0.271 | 0.150 | 0.445 |
| Complete | 0.221 | 0.252 | 0.225 | 0.368 |

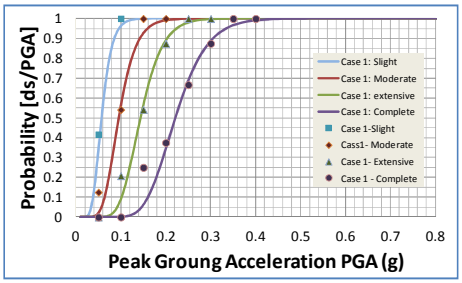


Figure 4-33: Fragility function for Brick in Mud Buildings with Flexible Floor/Roof for Case 1

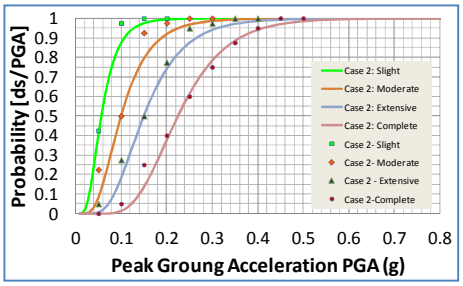


Figure 4-34: Fragility function for Brick in Mud Buildings with Flexible Floor/Roof for Case 2

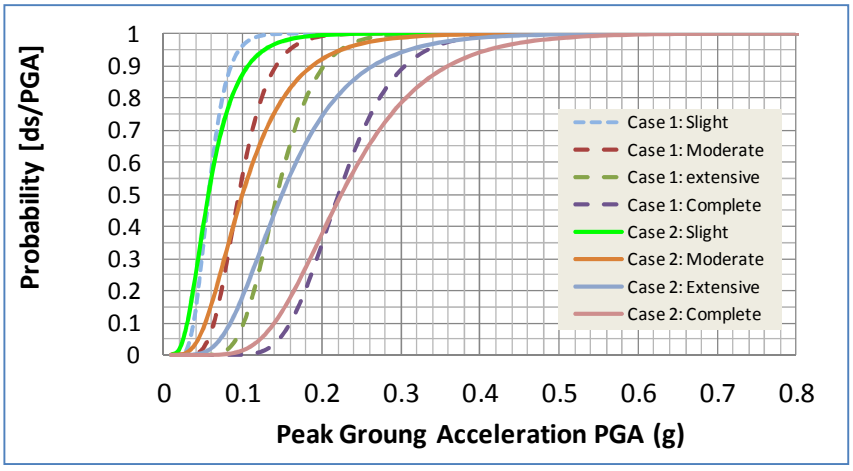


Figure 4-35: Fragility Functions for Brick in Mud Buildings in Nepal with Flexible Floor/Roof

### *4.4.3 Fragility Functions for Brick in Cement Buildings with Rigid Floors and Roof*

**Model preparation and Damage Observation**

Six different buildings with two different configurations and different number of stories are

modeled for numerical simulation. The buildings analyzed are shown in Figure 4-36.

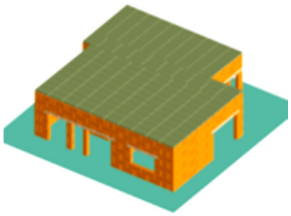

(a) BCL-1: Complex Configuration, Single Storey

(b) BCL-2: Complex configuration, Two Storey

(c) BCL-3: Complex Configuration, Three Storey

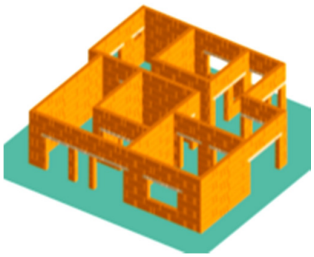

(d) Wall Configuration of Buildings BCL-1, BCL-2 and BCL-3

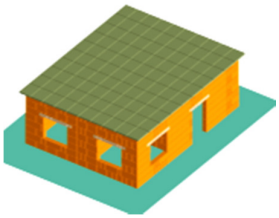

(e) BCL-4: Simple Configuration, Single Storey

(f) BCL-5: Simple Configuration, Two Storey

(g) BCL-6: Simple Configuration, Three Storey

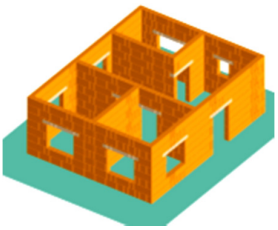

(h) Wall Configuration of Buildings BCL-4, BCL-5 and BCL-6

Figure 4-36: Numerical Models of Brick Buildings with Rigid Floors/Roof

Damage patterns and damage state at different PGA are compared in Figure 4-37, 4-38 and 4-39 respectively. The cases with average mortar strength and same earthquake are presented here for better comparison of storey effect. Figure 4-37 shows the damage patterns and respective damage grades at different PGA of single storey brick in cement building with rigid roof.

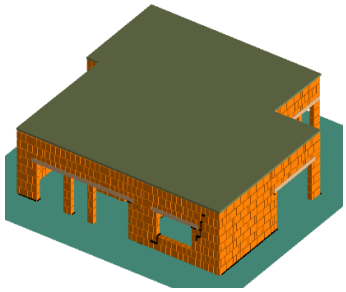

(a) Damage at 0.2g PGA

PGA: 0.2g

- One way diagonal Cracks at corners of openings
- Horizontal crack at some portion of bottom layer

"Slight Damage"

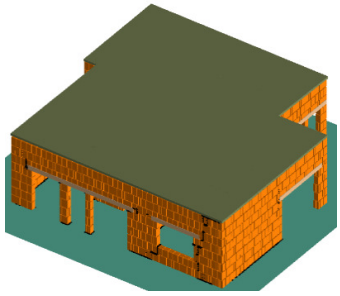

(b) Damage at 0.3g PGA

PGA: 0.3g

- Two way diagonal Cracks at corners of openings
- Horizontal crack at of bottom layer

"Moderate Damage"

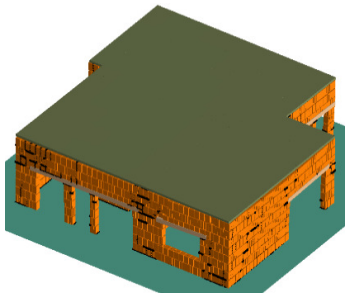

(c) Damage at 0.45g PGA

PGA: 0.45g

- Severe cracks in most of the walls
- Visible separation of walls in different locations

"Extensive Damage"

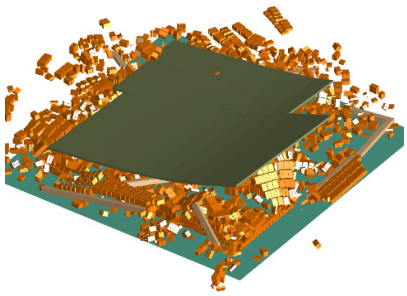

(d) Damage at 0.55g PGA

PGA: 0.55g

"Complete Damage"

Figure 4-37: Damage Patterns and Damage Grades of a Single Storey Brick Building with Rigid Floor/Roof

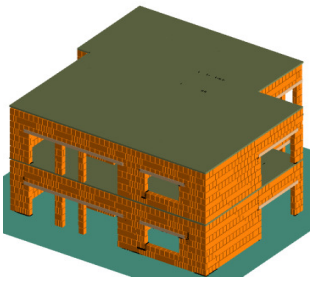

PGA: 0.15g

- One way diagonal Cracks at corners of openings
- Horizontal crack at some portion of bottom layer

"Slight Damage"

(a) Damage at 0.15g PGA

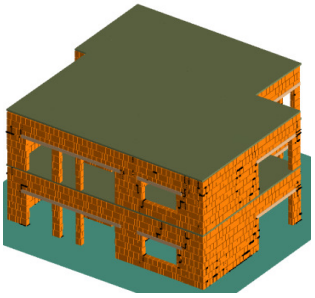

PGA: 0.2g

- Two way diagonal Cracks at corners of openings
- Horizontal crack at of bottom layer

"Moderate Damage"

(b) Damage at 0.2g PGA

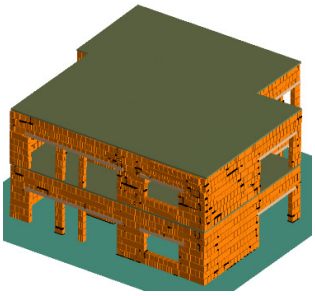

PGA: 0.3g

- Severe cracks in most of the walls
- Visible separation of walls at different locations

"Extensive Damage"

(c) Damage at 0.3g PGA

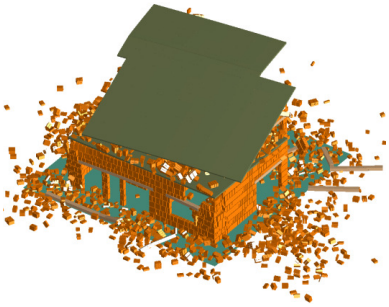

PGA: 0.4g

"Complete Damage"

(d) Damage at 0.4g PGA

Figure 4-38: Damage Patterns and Damage Grades of a Two Storey Brick Building with Rigid Floor/Roof

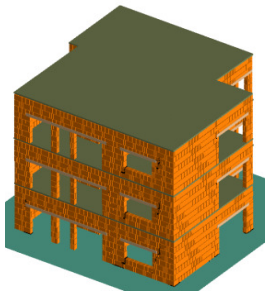

(a) Damage at 0.1g PGA

PGA: 0.1g

- One way diagonal Cracks at corners of openings
- Horizontal crack at some portion of bottom layer

"Slight Damage"

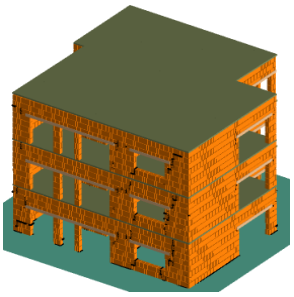

(b) Damage at 0.15g PGA

PGA: 0.15g

- Two way diagonal Cracks at corners of openings
- Throughout horizontal crack at of bottom layer

"Moderate Damage"

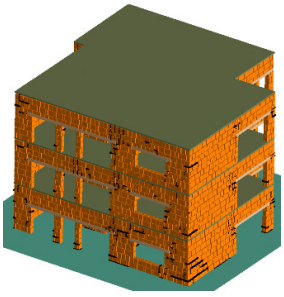

(c) Damage at 0.2g PGA

PGA: 0.2g

- Severe cracks in most of the walls
- Visible separation of walls at different locations

"Extensive Damage"

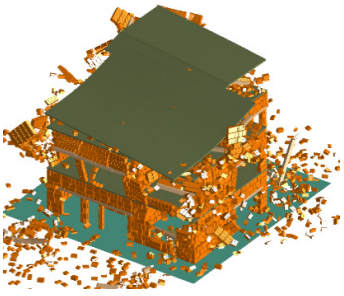

(d) Damage at 0.3g PGA

PGA: 0.3g

"Complete Damage"

Figure 4-39: Damage Patterns and Damage Grades of a Three Storey Brick Building with Rigid Floor/Roof

**Compilation of Damage State and Plotting Fragility Functions**

All six buildings as shown in Figure 4-36 are analyzed with three different mortar strength, average, weak ($20^{th}$ percentile) and strong ($80^{th}$ percentile) from Table 3-1. Thus, total of 30 cases for the 6 buildings analyzed at different PGA using five different input motions of different scale. The buildings were analyzed till complete collapse and the damage state at different PGA are noted. The damage states were noted through observation of cracks, deformed shape and damage level. The damage state noted for each case is given in Table 4-14.

Table 4-16: Damage State of Different Cases of Brick in Cement Buildings with Rigid Floors and Roof

| | Acceleration (g) | | | | | | | | | | | | | | |
|---|---|---|---|---|---|---|---|---|---|---|---|---|---|---|---|
| Building | 0.05 | 0.1 | 0.15 | 0.2 | 0.25 | 0.3 | 0.35 | 0.4 | 0.45 | 0.5 | 0.55 | 0.6 | 0.65 | 0.7 | 0.8 |
| BCL1-Strong-Loma | N | N | N | S | S | S | M | M | E | E | E | E | E | C | C |
| BCL1-Avg-Nep | N | N | N | S | M | M | M | M | E | E | E | C | C | C | C |
| BCL1-Avg-chi | N | N | N | S | M | M | M | M | E | E | E | C | C | C | C |
| BCL1-Avg-Koce | N | N | N | S | S | M | M | E | E | E | C | C | C | C | C |
| BCL1-Weak-Kobe | N | S | M | M | E | E | C | C | C | C | C | C | C | C | C |
| BCL2-Strong-Loma | N | N | N | S | S | M | M | E | E | E | C | C | C | C | C |
| BCL2-Avg-Nep | N | N | S | M | M | E | E | E | C | C | C | C | C | C | C |
| BCL2-Avg-Chi | N | N | S | M | M | E | E | E | C | C | C | C | C | C | C |
| BCL2-Avg-Koce | N | N | S | M | M | E | E | C | C | C | C | C | C | C | C |
| BCL2-Weak-Kobe | N | S | M | E | E | C | C | C | C | C | C | C | C | C | C |
| BCL3-Str-Loma | N | N | S | M | E | E | E | E | E | C | C | C | C | C | C |
| BCL3-Avg-Nep | N | S | M | E | E | E | C | C | C | C | C | C | C | C | C |
| BCL3-Avg-chi | N | S | M | E | E | E | C | C | C | C | C | C | C | C | C |
| BCL3-Avg-Koce | N | S | M | E | E | C | C | C | C | C | C | C | C | C | C |
| BCL3-Weak-Kobe | M | E | E | C | C | C | C | C | C | C | C | C | C | C | C |
| BCL4-Str-Koce | N | N | N | N | S | S | M | M | E | E | E | E | E | C | C |
| BCL4-Avg-Nep | N | N | N | S | M | M | M | M | E | E | E | E | C | C | C |
| BCL4-Avg-Chi | N | N | N | S | M | M | M | E | E | E | E | E | C | C | C |
| BCL4-Avg-Koce | N | N | N | S | M | M | M | E | E | E | E | C | C | C | C |
| BCL4-Weak-Kobe | N | N | S | S | M | M | M | E | E | C | C | C | C | C | C |
| BCL5-Str-Loma | N | N | N | S | S | M | M | M | E | E | E | C | C | C | C |
| BCL5-Avg-Nep | N | N | S | M | M | M | E | E | E | C | C | C | C | C | C |
| BCL5-Avg-Chi | N | N | S | M | M | M | E | E | E | C | C | C | C | C | C |
| BCL5-Avg-Koce | N | N | S | M | M | M | E | E | C | C | C | C | C | C | C |
| BCL5-weak-Kobe | N | S | M | M | E | C | C | C | C | C | C | C | C | C | C |
| BCL6-Str-Loma | N | N | S | M | E | E | E | E | E | E | C | C | C | C | C |
| BCL6-Avg-Nep | N | S | M | M | M | E | E | E | C | C | C | C | C | C | C |
| BCL6-Avg-Chi | N | S | M | M | M | E | E | E | C | C | C | C | C | C | C |
| BCL6-Avg-Koce | N | S | M | M | E | E | E | C | C | C | C | C | C | C | C |
| BCL6-Weak-Kobe | S | M | M | E | C | C | C | C | C | C | C | C | C | C | C |
| N: Negligible; S: Slight Damage; M: Moderate Damage; E: Extensive Damage; C: Complete Damage | | | | | | | | | | | | | | | |

The damage state is analyzed further for two different cases as like in the buildings with flexible floor/roof as described earlier. In the first case, only the average cases are considered and in the second case, all cases with strong and weak conditions are also considered. The number of cases for different damage state and the corresponding cumulative probability of damages for the first case are presented in Table 4-15 and 4-16 respectively. Similarly, the number of cases for different damage state and the corresponding cumulative probability of damages for the second case are presented in Table 4-17 and 4-18.

Table 4-17: Number of Cases with Different Damage State for Brick in Cement Buildings with Rigid Floor and Roof for Case 1

| Damage Level | Number of Cases at Different PGA (%g) | | | | | | | | | | | | | | |
|---|---|---|---|---|---|---|---|---|---|---|---|---|---|---|---|
| | 0.05 | 0.1 | 0.15 | 0.2 | 0.25 | 0.3 | 0.35 | 0.4 | 0.45 | 0.5 | 0.55 | 0.6 | 0.65 | 0.7 | 0.8 |
| None | 18 | 12 | 6 | 0 | 0 | 0 | 0 | 0 | 0 | 0 | 0 | 0 | 0 | 0 | 0 |
| Slight | 0 | 6 | 6 | 6 | 1 | 0 | 0 | 0 | 0 | 0 | 0 | 0 | 0 | 0 | 0 |
| Moderate | 0 | 0 | 6 | 9 | 13 | 9 | 6 | 3 | 0 | 0 | 0 | 0 | 0 | 0 | 0 |
| Extensive | 0 | 0 | 0 | 3 | 4 | 8 | 9 | 10 | 8 | 6 | 5 | 2 | 0 | 0 | 0 |
| Complete | 0 | 0 | 0 | 0 | 0 | 1 | 3 | 5 | 10 | 12 | 13 | 16 | 18 | 18 | 18 |

Table 4-18: Cumulative Probability of Damage at Different Damage State for Brick in Cement Buildings with Rigid Floor and Roof for Case 1

| Damage Level | Cumulative Probability of Damage at Different PGA (%g) | | | | | | | | | | | | | | |
|---|---|---|---|---|---|---|---|---|---|---|---|---|---|---|---|
| | 0.05 | 0.1 | 0.15 | 0.2 | 0.25 | 0.3 | 0.35 | 0.4 | 0.45 | 0.5 | 0.55 | 0.6 | 0.65 | 0.7 | 0.8 |
| Slight | 0.00 | 0.33 | 0.67 | 1.00 | 1.00 | 1.00 | 1.00 | 1.00 | 1.00 | 1.00 | 1.00 | 1.00 | 1.00 | 1.00 | 1.00 |
| Moderate | 0.00 | 0.00 | 0.33 | 0.67 | 0.94 | 1.00 | 1.00 | 1.00 | 1.00 | 1.00 | 1.00 | 1.00 | 1.00 | 1.00 | 1.00 |
| Extensive | 0.00 | 0.00 | 0.00 | 0.17 | 0.22 | 0.50 | 0.67 | 0.83 | 1.00 | 1.00 | 1.00 | 1.00 | 1.00 | 1.00 | 1.00 |
| Complete | 0.00 | 0.00 | 0.00 | 0.00 | 0.00 | 0.06 | 0.17 | 0.28 | 0.56 | 0.67 | 0.72 | 0.89 | 1.00 | 1.00 | 1.00 |

Table 4-19: Number of Cases with Different Damage State for Brick in Cement Buildings with Rigid Floor and Roof for Case 2

| Damage Level | Number of Cases at Different PGA (%g) | | | | | | | | | | | | | | |
|---|---|---|---|---|---|---|---|---|---|---|---|---|---|---|---|
| | 0.05 | 0.1 | 0.15 | 0.2 | 0.25 | 0.3 | 0.35 | 0.4 | 0.45 | 0.5 | 0.55 | 0.6 | 0.65 | 0.7 | 0.8 |
| None | 28 | 19 | 10 | 1 | 0 | 0 | 0 | 0 | 0 | 0 | 0 | 0 | 0 | 0 | 0 |
| Slight | 1 | 9 | 9 | 10 | 5 | 2 | 0 | 0 | 0 | 0 | 0 | 0 | 0 | 0 | 0 |
| Moderate | 1 | 1 | 10 | 13 | 14 | 12 | 11 | 6 | 0 | 0 | 0 | 0 | 0 | 0 | 0 |
| Extensive | 0 | 1 | 1 | 5 | 9 | 11 | 11 | 14 | 15 | 11 | 8 | 4 | 2 | 0 | 0 |
| Complete | 0 | 0 | 0 | 1 | 2 | 5 | 8 | 10 | 15 | 19 | 22 | 26 | 28 | 30 | 30 |

Table 4-20: Cumulative Probability of Damage at Different Damage State for Brick in Cement Buildings with Rigid Floor and Roof for Case 2

| Damage Level | Cumulative Probability of Damage at Different PGA (%g) | | | | | | | | | | | | | | |
|---|---|---|---|---|---|---|---|---|---|---|---|---|---|---|---|
| | 0.05 | 0.1 | 0.15 | 0.2 | 0.25 | 0.3 | 0.35 | 0.4 | 0.45 | 0.5 | 0.55 | 0.6 | 0.65 | 0.7 | 0.8 |
| Slight | 0.07 | 0.37 | 0.67 | 0.97 | 1.00 | 1.00 | 1.00 | 1.00 | 1.00 | 1.00 | 1.00 | 1.00 | 1.00 | 1.00 | 1.00 |
| Moderate | 0.03 | 0.07 | 0.37 | 0.63 | 0.83 | 0.93 | 1.00 | 1.00 | 1.00 | 1.00 | 1.00 | 1.00 | 1.00 | 1.00 | 1.00 |
| Extensive | 0.00 | 0.03 | 0.03 | 0.20 | 0.37 | 0.53 | 0.63 | 0.80 | 1.00 | 1.00 | 1.00 | 1.00 | 1.00 | 1.00 | 1.00 |
| Complete | 0.00 | 0.00 | 0.00 | 0.03 | 0.07 | 0.17 | 0.27 | 0.33 | 0.50 | 0.63 | 0.73 | 0.87 | 0.93 | 1.00 | 1.00 |

The cumulative probability of the damage at different PGA from Table 4-18 and Table 4-20 are plotted together with best fit cumulative lognormal distribution are given in Figure 4-40 and 4-41 respectively. Figure 4-42 shows the fragility functions for brick with cement-sand mortar buildings with rigid floor/roof in Nepal. In each case of the damage state, before the point of intersection case 2 is the upper boundary and case 1 is the lower boundary of the fragility while as after the intersection case 1 is the upper boundary and case 2 is the lower

boundary. So, the actual fragility function will be somewhere in between these two curves. The median values and standard deviation for plotting cumulative lognormal distribution of different damage are calculated from Table 4-18 and Table 4-20. The calculated median values and the standard deviations are given in Table 4-21.

Table 4-21: Median Values and Standard Deviation for Cumulative Lognormal Distribution for Brick in Cement Buildings with Rigid Floor and Roof

| Damage States | Case 1 | | Case 2 | |
|---|---|---|---|---|
| | **Median (PGA for 50% Damage)** | **Standard Deviation σ (or β)** | **Median (PGA for 50% Damage)** | **Standard Deviation σ (or β)** |
| Slight | 0.125 | 0.251 | 0.122 | 0.401 |
| Moderate | 0.175 | 0.223 | 0.175 | 0.376 |
| Extensive | 0.300 | 0.219 | 0.290 | 0.288 |
| Complete | 0.440 | 0.195 | 0.450 | 0.295 |

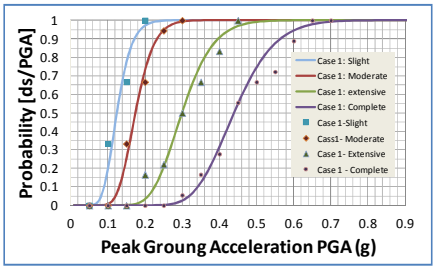


Figure 4-40: Fragility function for Brick in Cement Buildings with Rigid Floor/Roof for Case 1

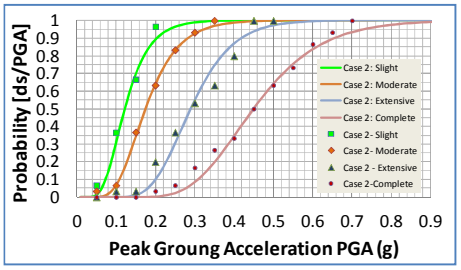


Figure 4-41: Fragility function for Brick in Cement Buildings with Rigid Floor/Roof for Case 2

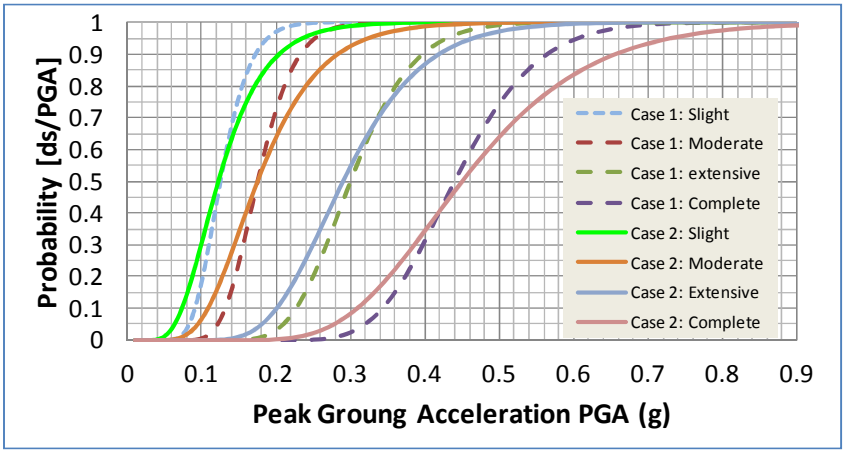


Figure 4-42: Fragility Functions for Brick in Cement Buildings in Nepal with Rigid Floor/Roof

## 4.5 Conclusions

Computation of fragility functions for non-engineered low strength masonry buildings in Nepal through time history analysis using Extreme Loading for Structures (ELS) tool developed in Applied Element Method (AEM) is done. Key parameter required for non-linear analysis like shear strength of existing masonry buildings was obtained through direct shear test in actual field condition. The result obtained from AEM was compared with shaking table test results and a good agreement on experimental and numerical simulation result was found.

Numerical models of several buildings with different configuration and number of stories for three different type of brick masonry were prepared and analyzed with different mortar properties and different input motions. Damage state of all the buildings at the given input motions are recorded according to HAZUS (2003) classification based on observation of cracks, deformed shape and damage. Cumulative probability of damage at each level of PGA starting 0.05g to 0.9g are recorded for all cases for four damage state namely "Slight", "Moderate", "Extensive" and "Complete".

Significant variation in damage level was found among three types of brick masonry buildings. Strength of material, number of stories and configuration was found played vital role on this large variation.

The median value of complete damage for brick in cement buildings with flexible floor and roof was found about 0.36g, for the brick in mud buildings with flexible floor/roof was found about 0.22g and for the brick in cement building with rigid floor and roof was found about 0.45g. This means, about 50% of the brick in mud buildings get complete damage at 0.22g level earthquakes while it requires about 0.45g level of earthquake to get 50% of brick in cement buildings with rigid floor a complete damage. These findings clearly show that only one set of fragility function for low rise brick masonry buildings do not represent the real scenario of buildings fragility in developing countries like Nepal.

The fragility functions were plotted for two different cases considering only the average cases and also considering some extreme cases. Consideration of only average cases shows lower standard deviation and the consideration of extreme cases shows higher standard deviation. Thus, the fragility functions considering the extreme cases can include the cases of some damages at smaller strong motions as well as survival of some buildings even in large accelerations. However, the actual fragility functions will be in between these two cases.

**REFERENCES**

ATC-13(1985), Earthquake Damage Evaluation Data for California, *Applied Technology Council*, 1985.

NBC (1994), Appendix C: Seismic Vulnerability Analysis, The Development of Alternative Buildings Material and Technology for Nepal, Nepal National Building Code (NBC), 1994.

RADIUS(2000) Risk Assessment Tools for Diagnosis of Urban Areas against Seismic Disasters. Geneva, Switzerland: IDNDR Secretariat, United Nations.

GESI(2001): Global Earthquake Safety Initiative Pilot Project, Final report, GHI and UNCRD.

Meguro K. and Tagel-Din H. (2001). Applied Element Simulation of RC Structures under Cyclic Loading. *Journal of Structural Engg.*;127(11):1295-1305

Coburn, A. and Spence, R. (2002). *Earthquake protection*. West Sussex: John Wiley & Sons Ltd.

JICA. (2002). "The study on Earthquake Disaster Mitigation in the Kathmandu valley Kingdom of Nepal." Final report, Vol - II, *Japan International Cooperation Agency*, Kathmandu, Nepal.

HAZUS (2003), Multi-hazard Loss Estimation Methodology: Earthquake Model, Department of Homeland Security, Emergency Preparedness and Response Directorate FEMA, Washington D.C

Mayorca, P. and Meguro, K., (2004). Proposal of an Efficient Technique for Retrofitting Unreinforced Masonry Dwellings. *Proceedings on 13th World Conference on Earthquake Engineering*, Vancouver, Canada.

Pandey, BH. and Meguro, K. (2004). Simulation of Brick Masonry Wall Behavior under Inplane Lateral Loading Using Applied Element Method. *Proceedings on 13th WCEE*, Vancouver, Canada. 2004.

Ramesh GURAGAIN, Kawin WORAKANCHANA, Paola MAYORCA and Kimiro MEGURO (2006); Simulation of Brick Masonry Wall Behavior Under Cyclic Loading Using Applied Element Method; *Seisan Kenkyu*, Vol. 58, No. 6, pp.531-534

Sathiparan, N.(2008), Experimental Study on PP-Band Mesh Seismic Retrofitting for Low Earthquake Resistant Masonry Houses, PhD Dessertation, Institute of Industrial Science, The University of Tokyo, Japan

Ramesh GURAGAIN, Ganesh JIMEE, Amod Mani DIXIT (2008); Earthquake Awareness and Effective Planning through Participatory Risk Assessment: an Experience from Nepal, *14th WCEE*, 12-17 October, 2008, Beijing China

Kawin WORAKANCHANA, Paola MAYORCA, Ramesh GURAGAIN, Sathiparan NAVARATNARAJ and Kimiro MEGURO (2008); 3-D Applied Element Method for PP-

Band Retrofitted Masonry; *Seisan Kenkyu*, Vol. 60 No. 2 pp.128-131

Joonam Park, Peeranan Towashiraporn, James I. Craig and Barry J. Goodnod. (2009). Seismic fragility analysis of low-rise unreinforced masonry structures, *Engineering Structures* **31**. 125-137.

M. Rota, A. Pennab and G. Magenes. (2010). A methodology for deriving analytical fragility curves for masonry buildings based on stochastic nonlinear analyses. *Engineering Structures* **32**, 1312-1323.

# 5. Numerical Simulation of Stone Masonry Buildings and Development of Fragility Functions

## 5.1 Introduction

Large numbers of the residential buildings in developing countries in seismic area are non-engineered type owner built masonry. A building inventory survey conducted in Kathmandu, Nepal shows more than 70% of existing buildings are masonry (JICA, 2002). Unreinforced stone masonry buildings are common in mountain areas in seismic countries around the world. Stone masonry has been constructed for different use starting from simple residential buildings to palaces, temples and monuments. Different type of stone masonry buildings in earthquake prone countries are discussed by Jitendra Bothara and Svetlana Brzev (2011). The performance of masonry buildings during earthquake is very poor. The breakdown of the casualties due to earthquakes in the period of 1900-1990 shows about 75% of the fatalities attributed to earthquakes are caused due to collapse of buildings and the greatest proportion of it is from the collapse of masonry buildings (Coburn, A. and Spence, R., 2002). The performance of stone masonry buildings in different earthquakes shows random shaped stone masonry buildings are more vulnerable than other type of masonry buildings (Robin Spence, 2007). Damage to random shaped stone masonry buildings was highest in 2005 Kashmir earthquake in Pakistan (T. Rossetto and N. Peiris, 2009 and EERI, 2006).

Understanding the failure mechanism and behavior of stone masonry buildings in lateral loads, especially in earthquake ground motions, is therefore important as it helps quantifying the seismic vulnerability of existing buildings and also helps developing proper retrofitting measures. Conducting experiments, like shaking table test, is one of the approaches for understanding the dynamic behavior of structures. In case of masonry, which has a great variability in comparison to other construction materials due to the different characteristics of its components, masonry unit and mortar, and also due the different construction practices, understanding the behavior through limited experiments is difficult. The shape and size of the masonry units has also an influence on the overall behavior of the masonry structures. The great variability of material together with limited resources made it difficult to carryout experimental studies for all types of existing masonry. Numerical tool, in this context, is therefore, one of the good alternatives.

In the field of numerical simulation of masonry buildings, the Applied Element Method (AEM) has shown good result for simulation of masonry as it is capable to follow complete structural response from initial stage of loading until total collapse behavior with reasonable accuracy so that inelastic responses after the cracks occur can be captured (Meguro K. and

Tagel-Din H, 2001). Masonry which is composite of masonry units and mortar and has discrete in nature can easily be modeled in the AEM by a set of elements connected at their contact edges either by 'Element springs' or 'Joint springs' according to their positions (Guragain, R. et al. 2006) and the progressive failure of masonry i.e. cracks initiation, propagation and their distribution can be simulated well in AEM (Guragain, R. et al. 2006).

AEM has shown good results for analysis of brick masonry for different types of loadings. AEM has been used to simulate the behavior of brick masonry by Pandey et al. (2004) and Mayorca et al. (2004) for monotonic load case, Guragain et al. (2006) for cyclic loading 2-D and Worakanchana et al. (2008) for cyclic loading 3-D. However, simulation of shapeless stone masonry in AEM has not been done so far and this study is targeted for it. An AEM tool, Extreme Loading for Structures (ELS) developed by Applied Science International, LLC (ASI), is now available and has been used for this study for simulation of random shaped stone masonry buildings.

First part of this chapter focuses on a new approach of modeling random shaped stone masonry structures in AEM and compares and discuses numerically obtained results with the experimental results. Two experimental models, 1/4 scale stone masonry wallet and 1/4 scale stone masonry house are analyzed by Applied Element Method applying this new approach of modeling stone masonry. Stone masonry modeling in AEM, simulation of stone masonry wallet for monotonic loading and simulation of stone masonry house for earthquake loading are discussed in detail in this chapter.

In the second part, after verification of the new approaches of modeling stone masonry structures is done, several stone masonry buildings available in Nepal are analyzed using this new approach in AEM. The crack patterns, deformed shape and damage level of the each case are noted and the fragility function for stone masonry buildings in Nepal is plotted.

## 5.2 Stone Masonry Modeling in AEM

A new approach of clustering randomly generated triangular meshes to form random shaped stones is proposed in this study. The proposed approach of modeling stone masonry is as: (a) Step 1: Stone masonry wall meshing with randomly generated triangular meshes; (b) Step 2: Clustering certain number of nearby triangles to form a random shape of stones; (c) Step 3: Assigning stone properties inside the cluster and mortar properties around the boundary of the cluster.

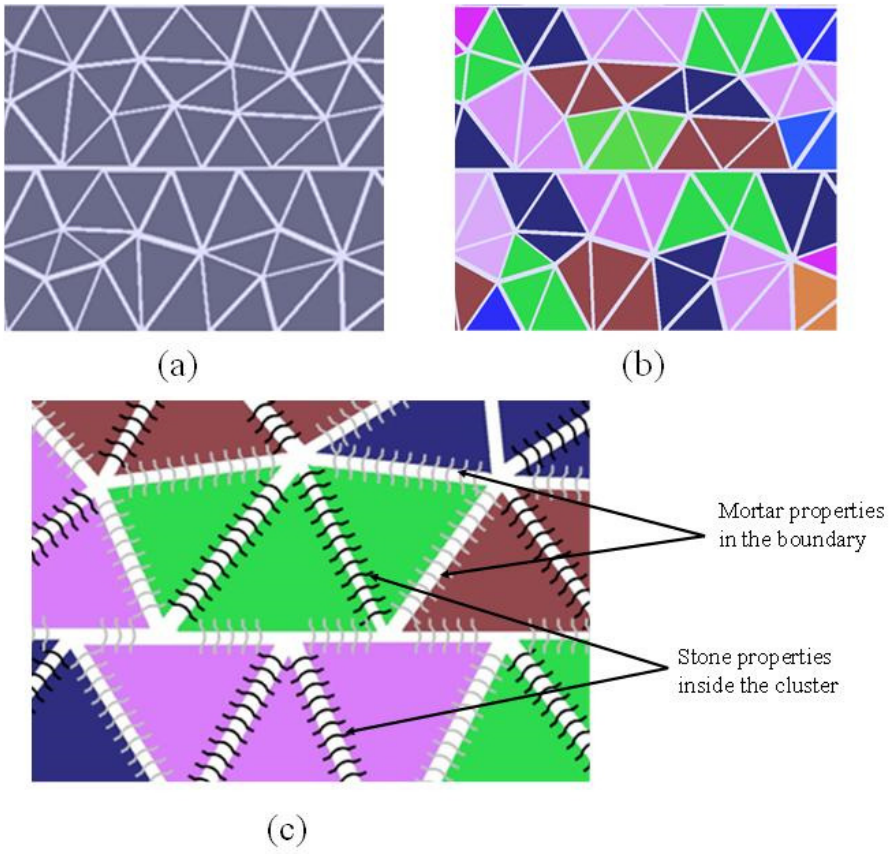


Figure 5-1: Process of stone masonry modeling in AEM

In the first step, the masonry wall is meshed by randomly generated triangular elements and in the second step certain numbers of near-by triangular elements are clustered to generate a random shape of stones. The springs inside the cluster will be assigned with the properties of stone and the connecting springs of one cluster to other clusters, or in other words, one stone to other stones are assigned with the mortar properties.

Figure 5-1 shows the process of stone masonry modeling in AEM which is proposed in this study. As the process starts with randomly generated different shapes and sizes of triangular elements, the further process of clustering more than 2 nearby triangular elements can result to random shapes of stones. Figure 5-1 (b) shows an example of forming different shapes of stones by combining three nearby triangular elements. The number of triangles and orientation of clustering can be chosen based on the size of the stones and the governing shapes of the stones in the real buildings.

## *5.3 Simulation of Stone Masonry Wallet for Monotonic Loading*

The first experimental model simulated using the proposed approach of modeling random shaped stone masonry was a stone masonry wallet of size 0.3m x 0.3m and thickness 0.15m.

This experiment was conducted by Sakurai, K. (2011). Figure 2 shows the schematic diagram of the experimental set-up and the numerical model developed in AEM for monotonic loading. For the numerical simulation model, separate elements at the top and the base of the specimen were modeled to resemble the similar situation of the boundary condition as of the experiment. The top boundary elements were fixed in X and Y displacement and free in Z-displacement. All the rotations were fixed. The base boundary elements were fixed in all displacements and rotations.

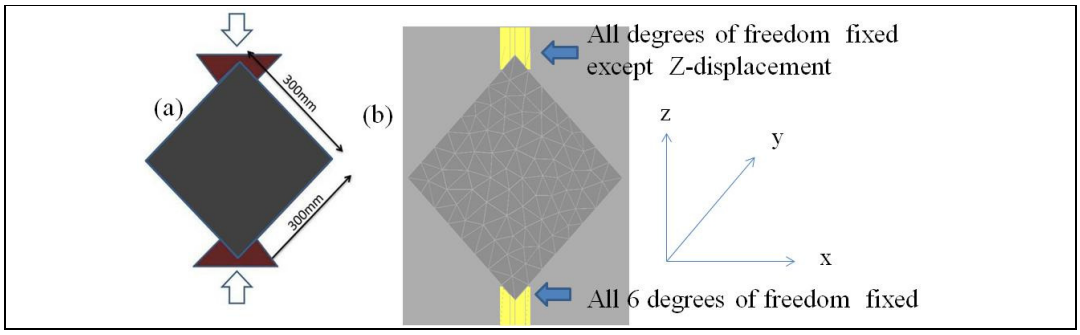


Figure 5-2: (a) Schematic diagram of experimental setup, (b) Numerical model with boundary condition for simulation

Table 5-1 below gives the material properties used in numerical simulation. The properties of the mortar was used from the diagonal shear test carried out by Sakurai, K. (2011) and the stone properties were assumed as more stiff and stronger so that there will be no damage to the stones.

Table 5-1: Material Properties used in Numerical Simulation of Masonry Wallet

| Materials | Tensile Strength (MPa) | Compressive Strength (MPa) | Young's Modulus (GPa) | Friction Coefficient |
|---|---|---|---|---|
| Mortar | 0.078 | 8 | 0.04 | 0.6 |
| Stone | 100 | 1000 | 3 | 0.6 |

The crack patterns and the deformed shape of the numerical results are compared with those obtained from experiment at the displacement of 3 mm and 4.5 mm respectively. Figure 5-3 shows the crack patterns at 3mm displacement and Figure 5-4 shows the crack patterns at 4.5mm displacement in the experiment and the numerical simulation. The crack patterns obtained from numerical simulation is similar to that obtained in experiment. Figure 5-1 gives the comparison of force-displacement relationships obtained from experiment and numerical simulation. The initial stiffness, peak load and post peak response are found matching each other. However, there is relatively rapid drop in case of numerical simulation after the peak load in comparison to the experiment.

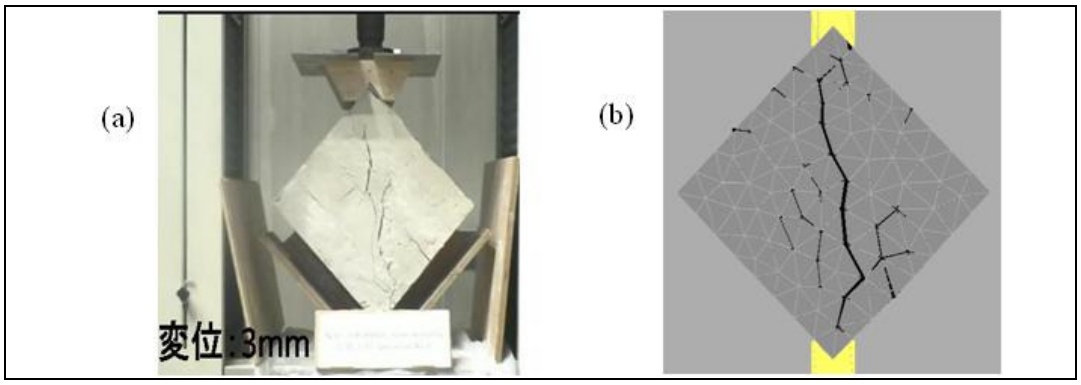


Figure 5-3: (a) Crack patterns at 3 mm vertical displacement from experiment (Sakurai, 2011), (b) Crack patterns at 3 mm vertical displacement from numerical simulation

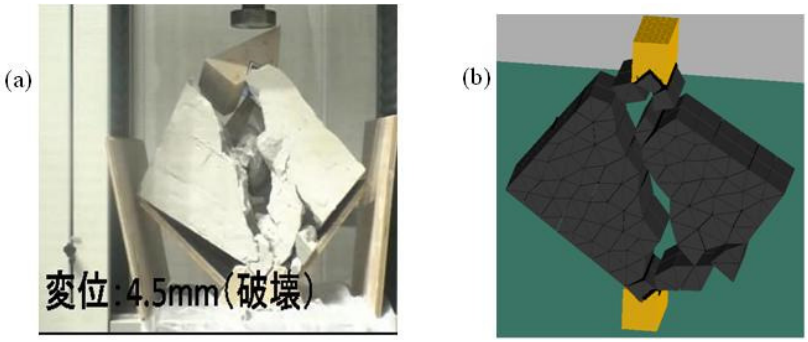


Figure 5-4: (a) Specimen after failure at 4.5 mm vertical displacement in experiment (Sakurai, 2011), (b) Numerical model at 4.5 mm vertical displacement when two parts are completely separated

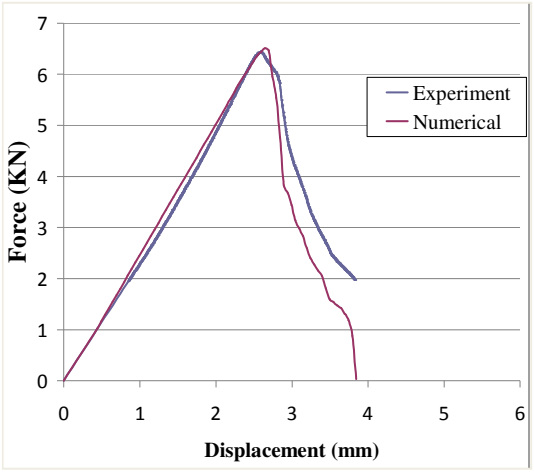


Figure 5-5: Comparison of Force-Displacement Relations Obtained from Experiment and Numerical Simulation

## 5.4 Simulation of Stone Masonry House for Earthquake Loading

Shapeless stone masonry house which was tested on shake table by Sakurai, K. (2011) has been modeled for the verification of the new approach for modeling stone masonry structures. The building size was 950mm x 950mm x 720mm with 100mm thick walls with 10mm plaster on the surfaces of both sides. The sizes of door and window were 290mm x 480mm and 370mm x 240mm, respectively, and were in opposite walls. The test specimen was prepared to represent a simple one-story building with timber framed roof. Modeling of the building in AEM, loading and input motions and result of the simulation in terms of crack initiation and propagation, acceleration output and damage at different stage of loading sequences are discussed in this section.

### 5.4.1 Modeling of Stone Masonry House in AEM

The building was numerically modeled in AEM with randomly generated triangular meshes and three nearby triangles are clustered together to form the random shaped stones. The AEM meshing and clustering was done as per the proposed approach previously discussed in this paper. Photo 1 below gives the experimental model under test and the Figure 5-6 shows the numerical model developed in AEM.

(a) Photo of experimental model house under test (Photo from Sakurai, K., 2011)

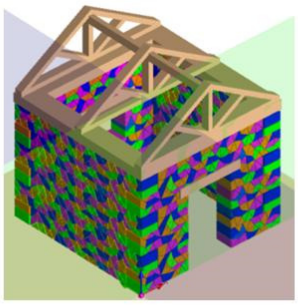

(b) Numerical simulation model prepared in AEM

Figure 5-6: Stone masonry house models used

The properties of stone and mortar are used as given in the Table 1 above as that experiment was conducted to use the same material for the construction of shaking table building model. The roof structure of the real building was wooden roof of 15 kg weight. All the wooden elements were properly connected and damage to the roof was not expected. To simulate the similar situation, same mass of the roofing part was modeled in numerical simulation as well. The material was considered more stiff and strong so that it works like a rigid body and there is no internal damage on it.

### *5.4.2 Input Motions and Boundary Conditions*

Sinusoidal motions of frequencies ranging from 2Hz to 35Hz and amplitudes ranging from 0.05g to 1.0g were applied to obtain the dynamic response of the structures in the experiment. Figure 5-7 shows the typical shape of the applied sinusoidal wave. The numbers given in the Table 5-2 shows the loading sequence followed in tests. General trend of loading was from high frequency to low frequency and from lower amplitude to higher amplitude.

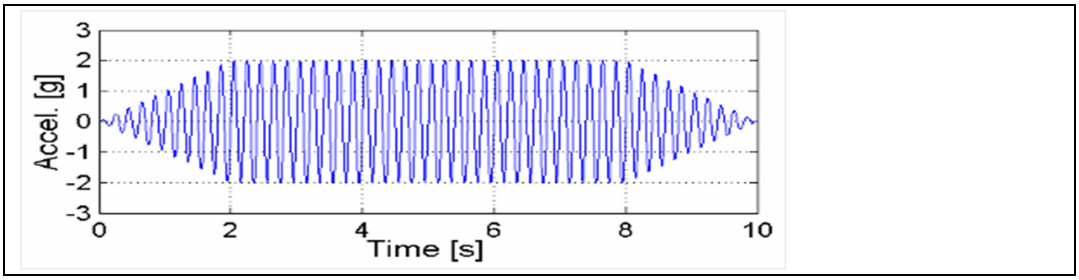


Figure 5-7: Typical Shape of the Applied Sinusoidal Wave

There was no significant damage to run 28 in experiment, thus, the numerical simulation was performed only from run 28 to run 48. During experiment, there was some gap between consequent run so that the model was in a static condition before another run of input motion. However, in case of numerical simulation the input motion was continuously provided one after another and the model was still in motion when the next input motion was provided.

Table 5-2: Loading Sequence of Input Motions

| Amplitude | Frequency | | | | | | | |
|---|---|---|---|---|---|---|---|---|
| | 2 Hz | 5Hz | 10Hz | 15Hz | 20Hz | 25Hz | 30Hz | 35Hz |
| 1.0g | | 48 | | | | | | |
| 0.8g | | 47 | 43 | 40 | 37 | 34 | 31 | 28 |
| 0.6g | | 45 | 42 | 39 | 36 | 33 | 30 | 27 |
| 0.4g | | 44 | 41 | 38 | 35 | 32 | 29 | 26 |
| 0.2g | 46 | 25 | 24 | 23 | 22 | 21 | 20 | 19 |
| 0.1g | 18 | 17 | 16 | 15 | 14 | 13 | 12 | 11 |
| 0.05g | 10 | 09 | 08 | 07 | 06 | 05 | 04 | 03 |
| sweep | 01,02 | | | | | | | |

In the experiment, the bottom layer was fixed with concrete frame with strong mortar. In order to make the similar condition as much as possible, the bottom layer elements were fixed in displacement and rotation in the numerical model.

### *5.4.3 Results Comparison*

The result of the experiment in terms of crack patterns and acceleration response and extent of

damage which are documented by Sakurai, K. (2011) are compared with numerical simulation result. Natural frequency of the building after each run of the input motions is calculated using Eigen value analysis. The first mode natural frequency of the building after each run of input motions is shown in Figure 5-8. The natural frequency of the building is significantly dropped after the runs 35, 38, 41 and 44 before it collapsed at 48 run. The drop in natural frequency is because of significant cracking on that stage of input motions. Therefore, the results obtained from numerical simulations, are compared with the experimental results after the runs when there is significant drop on natural frequency. In addition, the acceleration output from numerical simulation and experiment are also compared for the run 29 before significant cracks are occurred.

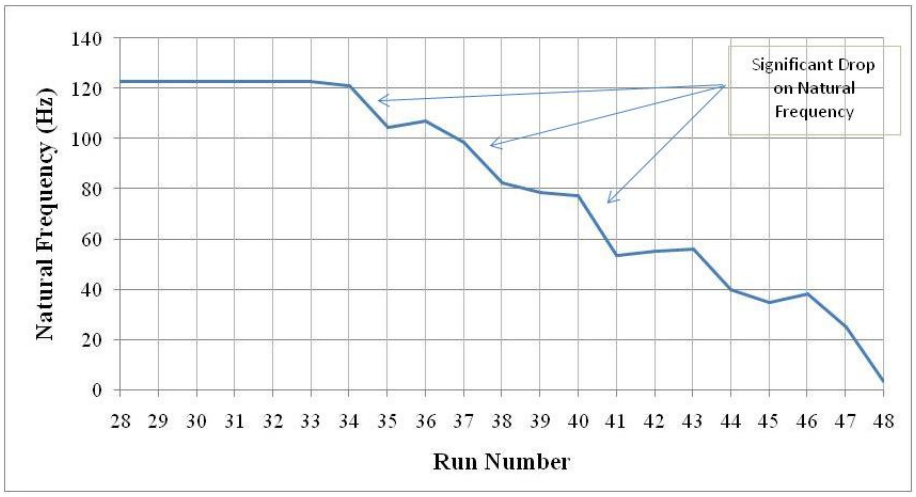


Figure 5-8: Natural Frequencies of the Building after each Run of Input Motions in Numerical Simulation

Figure 9 (a) shows the location where the accelerations are measured and Figures 5-9 (b) and (c) show comparison of the acceleration output from experiment and numerical simulation for the run 29. The numerically obtained acceleration output is very close to the acceleration measured during experiment in terms of the value and also the overall shape of the time-history. Some difference can be seen at the initial part of the acceleration, this is mainly due to the continue input motions in numerical simulation when the inputs were given just one after another without bringing back to static condition.

The crack patterns and the acceleration output for run 35 are compared and shown in Figure 5-10. Figure 5-10 (a) shows the crack patterns mapped during experiment. Diagonal cracks from all 4 corners of the window and two diagonal cracks at top corners of the door were observed in the experiment. Horizontal cracks at the bottom layer from the side of the door were also observed. Similar crack patterns were obtained in numerical simulation as well.

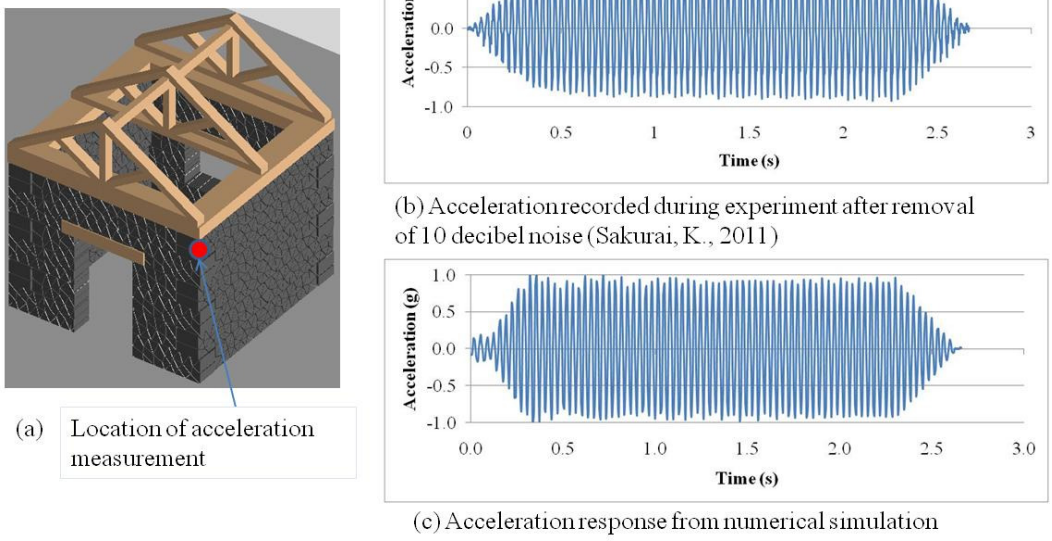


Figure 5-9: Comparison of acceleration output for the run 29 (0.4g at 30 Hz)

Figure 5-10 (b) shows the numerically obtained crack patterns after run 35. Diagonal cracks from all 4 corners of the window were also observed in the numerical simulation and was similar to the experimental cracks but one diagonal crack from the top corner of the window was propagated more horizontally than the experimental crack. On the door side, the diagonal cracks at the top corners of the door and also at the bottom layer to the side of the door were observed in numerical simulation as well. However, the extent of the cracks to the door side was relatively less in numerical simulation. There were no cracks at side walls at this stage.

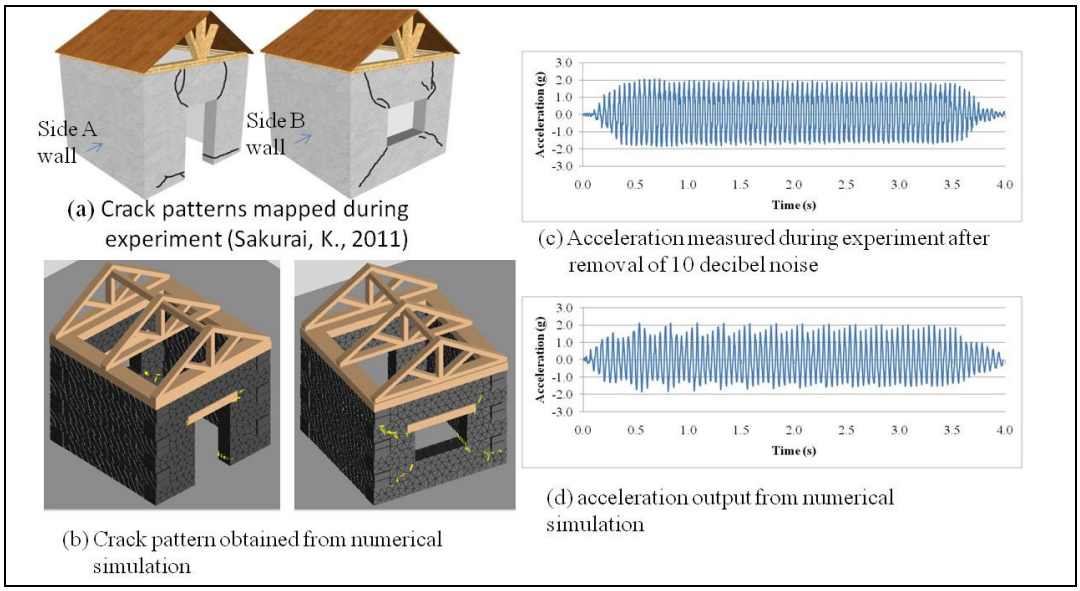


Figure 5-10: Crack Patterns and Acceleration Output Comparison for the Run 35 (0.4g-20Hz)

Figures 5-10 (c) and (d) give the measured acceleration during experiment and the acceleration response in numerical simulation. The maximum value of the acceleration both the cases are around 2.0g and very close to each other. Figure 5-11 compares the result after run 38 (0.4g-15Hz) from the experiment and the numerical simulation. Extensive diagonal cracks from all 4 corners of the window and two diagonal cracks at the top corners of the door were recorded in experimental and numerical cases. One horizontal crack at bottom layer of side-A wall was also observed in both the cases. The horizontal crack at bottom layer of the side of door was propagated to the side-A wall and it was also matching in both the cases. However, a small horizontal crack at bottom layer of the side B wall was observed in the experiment (Figure 5-11(a)) while a complete horizontal crack at the bottom layer was obtained in numerical simulation (Figure 5-11(b)). Figure 5-11(c) and (d) compare the acceleration output for the 38 run from the experiment and the numerical simulation respectively. The maximum positive acceleration values in both the cases are around 1.5g while the negative value in case of experiment is slightly less than the numerical one.

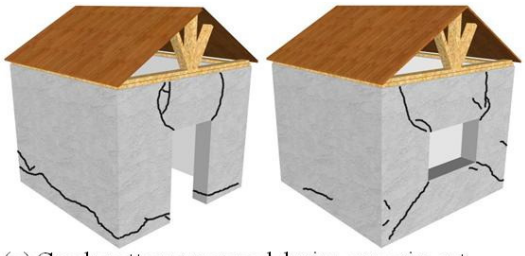

(a) Crack patterns mapped during experiment (Sakurai, K., 2011)

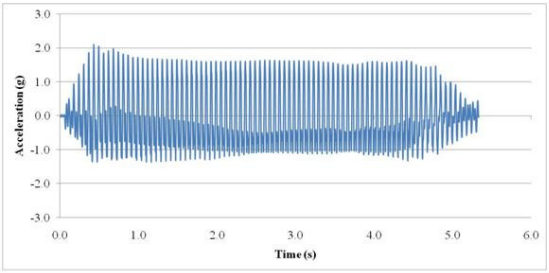


(c) Acceleration measured during experiment after removal of 10 decibel noise

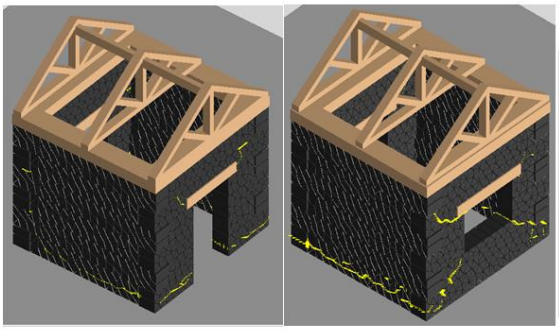

(b) Crack pattern obtained from numerical simulation

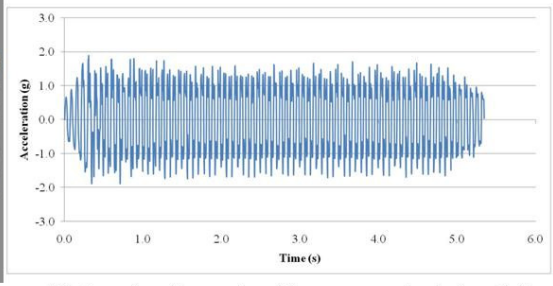


(d) Acceleration output from numerical simulation

Figure 5-11: Crack patterns and acceleration output comparison for the run 38 (0.4g-15Hz)

The comparison of the results in terms of crack patterns and the acceleration is also done for run 41 (Figure 5-12). The diagonal cracks from the openings were more widened, some more cracks were observed at the top corner of the window and there were horizontal cracks at the bottom layer on both side walls until this stage of loading in experiment (Figure 5-12(a)). Similar to the experimental cracks, numerical simulation also shows some additional cracks

around openings and the horizontal cracks at the bottom layer of both side walls. In addition to the experimental cracks, one horizontal crack at the lintel level on the side A wall was obtained in the numerical simulation (Figure 5-12 (b)). The acceleration comparison from the experiment and the numerical gives similar result to that of run 38. The maximum value of acceleration is about 2.0g in both cases. However, negative acceleration in case of experiment is lower than in case of numerical.

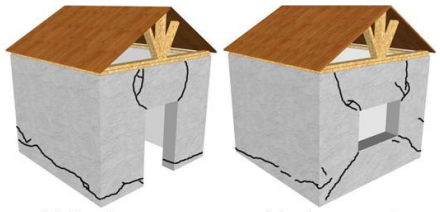

(a) Crack patterns mapped during experiment (Sakurai, K., 2011)

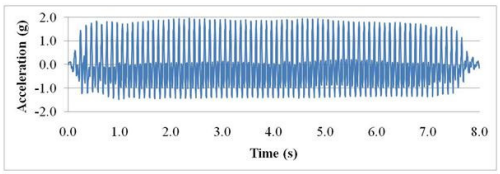


(c) Acceleration measured during experiment after removal of 10 decibel noise

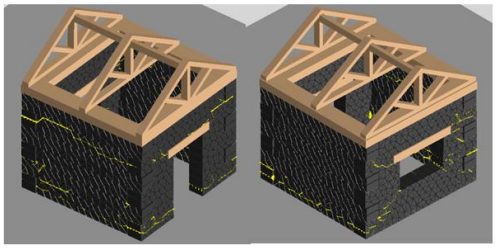

(b) Crack patterns obtained from numerical simulation

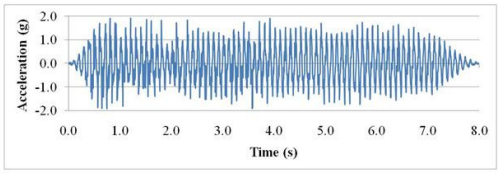


(d) Acceleration output from numerical simulation

Figure 5-12: Crack Pattern and Acceleration Output Comparison for the Run 41 (0.4g-10Hz)

(a) Damage to door side of the building during experiment (Photo from Sakurai, K., 2011)

(b) Damage to window side of the building during experiment (photo from Sakurai, K., 2011)

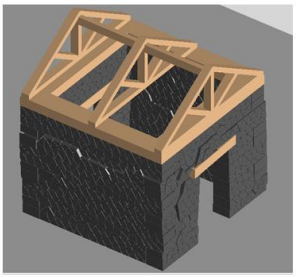

(c) Damage to door side of the building during in numerical simulation

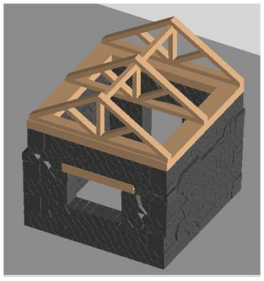

(d) Damage to window side of the building during in numerical simulation

Figure 5-13: Damage Comparison after Run 46 (0.2g-2Hz)

At the later stage of loadings, the deformed shape and crack patterns obtained from numerical simulation is compared with the experiment. Figure 5-13 compares the damage state of the experimental model after run 46 with the damage state in numerical simulation. Some small stones near to the openings were separated and dropped at this stage in experiment. The diagonal cracks were widened significantly and wall above the door was significantly distorted. Some small stones in window side were also dropped and the diagonal and horizontal cracks were completely separated. Similar to the experiment, cracks are widened and models are distorted significantly in numerical simulation as well. There was more damage observed near to the openings.

The building was collapsed in 48 run at 5Hz-1.0g in experiment. The building was collapsed on 48 run in numerical simulation also. Figure 5-14(a) shows the collapsed building at 48 run in experiment and the Figure 5-14(b) shows the collapse of the building on run 48 in the numerical simulation.

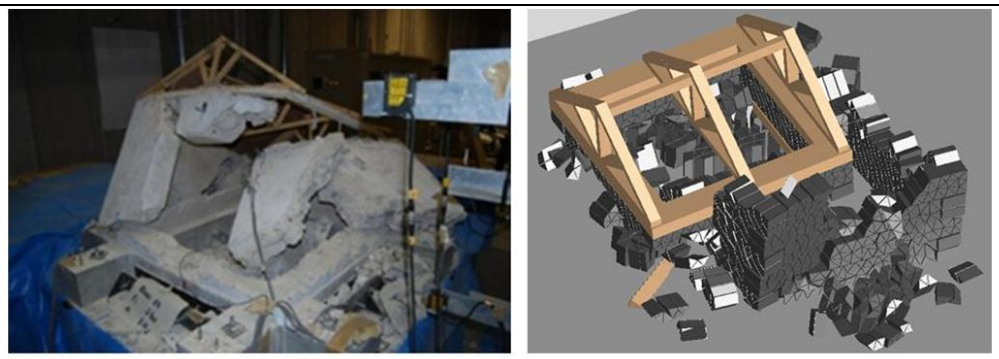

(a) Photograph after collapse of the building at 48 run in experiment (Photo by Sakurai, K., 2011)

(b) Collapse of the building at 48 run in numerical simulation

Figure 5-14: Damage comparison after run 48 (5Hz-1.0g)

## 5.5 Simulation of Stone Masonry Buildings and Development of Fragility Function

**Model preparation**

Six different buildings with different configurations and single and double stories are modeled based on construction practices of stone masonry buildings in Nepal. Both the buildings with gable wall and without gable wall are considered. Figure 5-15 shows different stone masonry buildings model prepared for numerical simulation. Small and big size, one storey and two storeys, without cross wall and with cross wall has been considered based on field observation of major configuration of stone masonry buildings in Nepal. The result of numerical simulation will be presented in the preceding sections of this chapter.

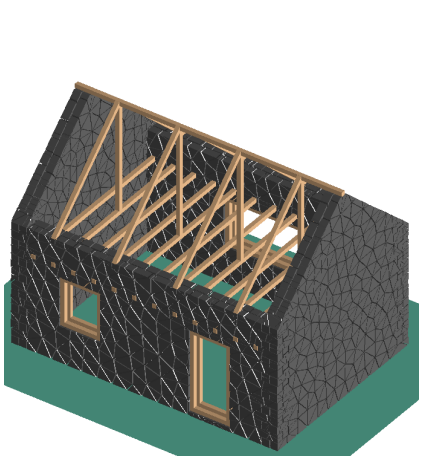

(a) SM-1: Small size, one storey with gable

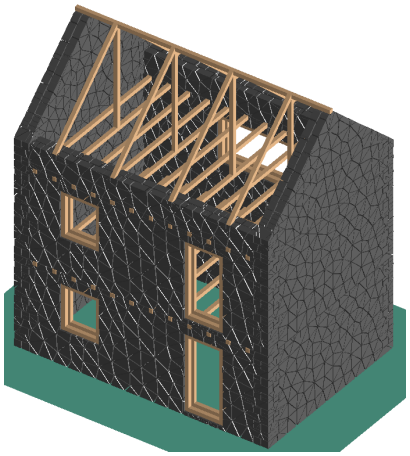

(b) SM-2: Small size, two storey gable

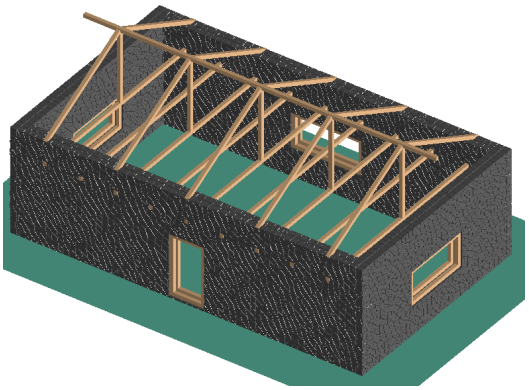

(c) SM-3: Big size, One room, one storey, no gable

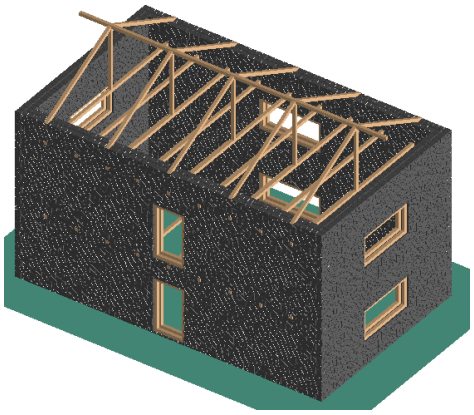

(d) SM-4: Big size, One room, two storey, no gable

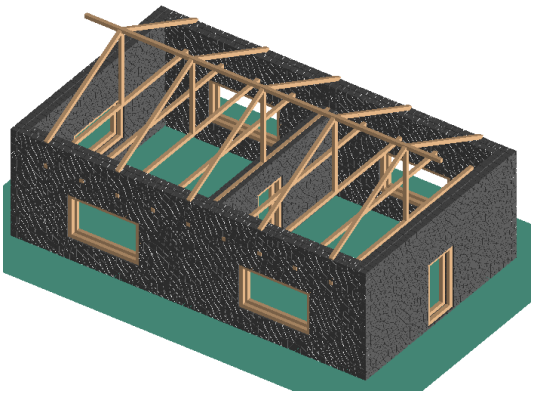

(e) SM-5: Big size, two room, one storey, no gable

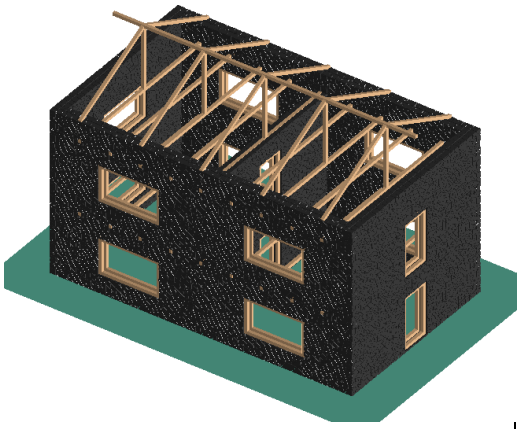

(f) SM-6: Big size, two room, two storey, no gable

Figure 5-15: Numerical Models of Stone in Mud Buildings with Rigid Floors/Roof in Nepal

Damage patterns and damage state at different PGA are compared in Figure 5-16 and 5-17 respectively. The cases with average mortar strength and same earthquake are presented here for better comparison. Figure 5-16 shows the damage patterns and respective damage grades at different PGA of two storey building with gable representing weak configuration while as Figure 5-17 shows the damage patterns and damage grades of a single storey building with cross wall representing safer configuration.

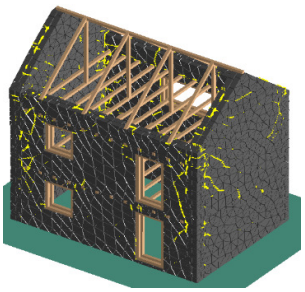

(a) Damage at 0.05g PGA, Average Mortar, Koceli Earthquake

PGA: 0.05g

- Many cracks near corners
- Some cracks are continue throughout the storey height

"Moderate Damage"

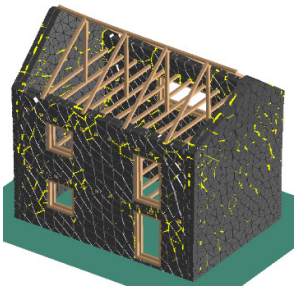

(b) Damage at 0.1g PGA, Average Mortar, Koceli Earthquake

PGA: 0.1g

- Severe cracks in all walls
- Visible deformation and tilting of some portion

"Extensive Damage"

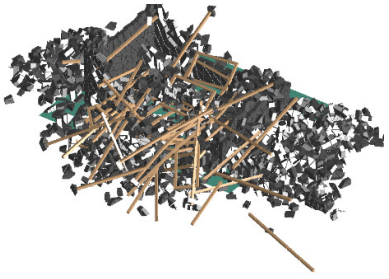

(c) Damage at 0.15g PGA, Average Mortar, Koceli Earthquake

PGA: 0.15g

"Complete Damage"

Figure 5-16: Damage Patterns and Damage Grades of a Double Storey Stone in Mud Building with Rigid Floor/Roof

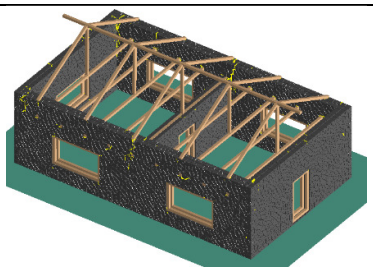

(a) Damage at 0.1g PGA, Average Mortar, Koceli Earthquake

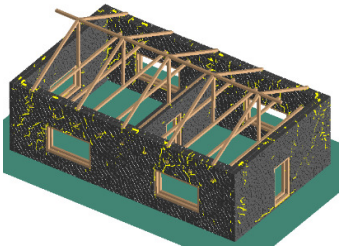

(b) Damage at 0.15g PGA, Average Mortar, Koceli Earthquake

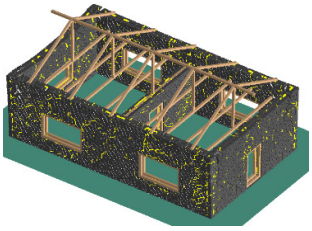

(c) Damage at 0.25g PGA, Average Mortar, Koceli Earthquake

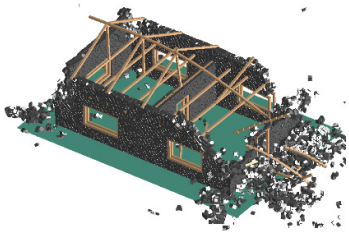

(d) Damage at 0.35g PGA, Average Mortar, Koceli Earthquake

PGA: 0.1g

- Cracks at corners and junctions of walls
- Small cracks near openings

"Slight Damage"

PGA: 0.15g

- Cracks in all walls, some cracks are throughout the storey height
- Small cracks near openings
- No large deformation and tiltinmg of walls

"Moderate Damage"

PGA: 0.25g

- Severe cracks in all walls
- Separation of corners
- Visible deformation and tilting of walls

"Extensive Damage"

PGA: 0.35g

"Complete Damage"

Figure 5-17: Damage Patterns and Damage Grades of a Single Storey Stone in Mud Building with Rigid Floor/Roof

**Compilation of Damage State and Plotting Fragility Functions**

All six buildings as shown in Figure 5-15 are analyzed with three different mortar strength, average, weak (20$^{th}$ percentile) and strong (80$^{th}$ percentile) from Table 3-4. Thus, total of 30 cases for the 6 buildings analyzed at different PGA using five different input motions of different scale. The buildings were analyzed till complete collapse and the damage state at different PGA are noted. The damage states were noted through observation of cracks, deformed shape and damage level. The damage state noted for each case is given in Table 5-3.

Table 5-3: Damage State of Different Cases of Brick in Cement Buildings with Rigid Floors and Roof

| Buildings | Acceleration (g) | | | | | | | | | | | |
|---|---|---|---|---|---|---|---|---|---|---|---|---|
| | **0.05** | **0.1** | **0.15** | **0.2** | **0.25** | **0.3** | **0.35** | **0.4** | **0.45** | **0.5** | **0.55** | **0.6** |
| SM1-Strong-Loma | N | S | M | E | E | C | C | C | C | C | C | C |
| SM1-Avg-Nep | S | M | M | E | C | C | C | C | C | C | C | C |
| SM1-Avg-chi | S | M | M | E | C | C | C | C | C | C | C | C |
| SM1-Avg-Koce | S | M | E | C | C | C | C | C | C | C | C | C |
| SM1-Weak-Kobe | M | E | C | C | C | C | C | C | C | C | C | C |
| SM2-Strong-Loma | S | M | E | E | C | C | C | C | C | C | C | C |
| SM2-Avg-Nep | M | E | C | C | C | C | C | C | C | C | C | C |
| SM2-Avg-Chi | M | E | C | C | C | C | C | C | C | C | C | C |
| SM2-Avg-Koce | M | E | C | C | C | C | C | C | C | C | C | C |
| SM2-Weak-Kobe | E | C | C | C | C | C | C | C | C | C | C | C |
| SM3-Str-Loma | N | N | S | S | S | M | E | E | C | C | C | C |
| SM3-Avg-Nep | N | S | M | E | E | C | C | C | C | C | C | C |
| SM3-Avg-chi | N | S | M | E | C | C | C | C | C | C | C | C |
| SM3-Avg-Koce | N | S | M | M | C | C | C | C | C | C | C | C |
| SM3-Weak-Kobe | M | E | E | C | C | C | C | C | C | C | C | C |
| SM4-Str-Loma | N | S | S | M | E | E | C | C | C | C | C | C |
| SM4-Avg-Nep | S | M | M | E | C | C | C | C | C | C | C | C |
| SM4-Avg-Chi | S | M | M | E | C | C | C | C | C | C | C | C |
| SM4-Avg-Koce | S | M | E | C | C | C | C | C | C | C | C | C |
| SM4-Weak-Kobe | M | E | C | C | C | C | C | C | C | C | C | C |
| SM5-Str-Loma | N | N | N | S | S | M | E | E | C | C | C | C |
| SM5-Avg-Nep | N | N | S | M | E | E | E | C | C | C | C | C |
| SM5-Avg-Chi | N | S | S | M | E | E | E | C | C | C | C | C |
| SM5-Avg-Koce | N | S | M | M | E | E | C | C | C | C | C | C |
| SM5-weak-Kobe | S | M | E | E | C | C | C | C | C | C | C | C |
| SM6-Str-Loma | N | N | S | S | M | E | E | C | C | C | C | C |
| SM6-Avg-Nep | N | S | M | E | E | C | C | C | C | C | C | C |
| SM6-Avg-Chi | N | S | M | E | E | C | C | C | C | C | C | C |
| SM6-Avg-Koce | N | M | M | E | C | C | C | C | C | C | C | C |
| SM6-Weak-Kobe | M | M | E | C | C | C | C | C | C | C | C | C |

N: Negligible; S: Slight Damage; M: Moderate Damage; E: Extensive Damage; C: Complete Damage

The damage state is analyzed further for two different cases as like in the buildings with flexible floor/roof as described earlier. In the first case, only the average cases are considered and in the second case, all cases with strong and weak conditions are also considered. The number of cases for different damage state and the corresponding cumulative probability of damages for the first case are presented in Table 5-4 and 5-5 respectively. Similarly, the number of cases for different damage state and the corresponding cumulative probability of damages for the second case are presented in Table 5-6 and 5-7.

Table 5-4: Number of Cases with Different Damage State for Stone in Mud Buildings with Flexible Floor and Roof for Case 1

| | **Number of Cases at Different PGA (%g)** | | | | | | | | | | | |
|---|---|---|---|---|---|---|---|---|---|---|---|---|
| **Damage Level** | **0.05** | **0.1** | **0.15** | **0.2** | **0.25** | **0.3** | **0.35** | **0.4** | **0.45** | **0.5** | **0.55** | **0.6** |
| None | 7 | 1 | 0 | 0 | 0 | 0 | 0 | 0 | 0 | 0 | 0 | 0 |
| Slight | 8 | 4 | 2 | 0 | 0 | 0 | 0 | 0 | 0 | 0 | 0 | 0 |
| Moderate | 3 | 10 | 8 | 3 | 0 | 0 | 0 | 0 | 0 | 0 | 0 | 0 |
| Extensive | 0 | 3 | 5 | 6 | 3 | 2 | 0 | 0 | 0 | 0 | 0 | 0 |
| Complete | 0 | 0 | 3 | 9 | 15 | 16 | 18 | 18 | 18 | 18 | 18 | 18 |

Table 5-5: Cumulative Probability of Damage at Different Damage State for Stone in Mud Buildings with Flexible Floor and Roof for Case 1

| | **Cumulative Probability of Damage at Different PGA (%g)** | | | | | | | | | | | |
|---|---|---|---|---|---|---|---|---|---|---|---|---|
| **Damage Level** | **0.05** | **0.1** | **0.15** | **0.2** | **0.25** | **0.3** | **0.35** | **0.4** | **0.45** | **0.5** | **0.55** | **0.6** |
| Slight | 0.61 | 0.94 | 1.00 | 1.00 | 1.00 | 1.00 | 1.00 | 1.00 | 1.00 | 1.00 | 1.00 | 1.00 |
| Moderate | 0.17 | 0.72 | 0.89 | 1.00 | 1.00 | 1.00 | 1.00 | 1.00 | 1.00 | 1.00 | 1.00 | 1.00 |
| Extensive | 0.00 | 0.17 | 0.44 | 0.83 | 1.00 | 1.00 | 1.00 | 1.00 | 1.00 | 1.00 | 1.00 | 1.00 |
| Complete | 0.00 | 0.00 | 0.17 | 0.50 | 0.83 | 0.89 | 1.00 | 1.00 | 1.00 | 1.00 | 1.00 | 1.00 |

Table 5-6: Number of Cases with Different Damage State for Stone in Mud Buildings with Flexible Floor and Roof for Case 2

| **Damage Level** | **Number of Cases at Different PGA (%g)** | | | | | | | | | | | |
|---|---|---|---|---|---|---|---|---|---|---|---|---|
| | **0.05** | **0.1** | **0.15** | **0.2** | **0.25** | **0.3** | **0.35** | **0.4** | **0.45** | **0.5** | **0.55** | **0.6** |
| None | 12 | 4 | 1 | 0 | 0 | 0 | 0 | 0 | 0 | 0 | 0 | 0 |
| Slight | 10 | 6 | 5 | 3 | 1 | 0 | 0 | 0 | 0 | 0 | 0 | 0 |
| Moderate | 7 | 12 | 9 | 4 | 2 | 2 | 0 | 0 | 0 | 0 | 0 | 0 |
| Extensive | 1 | 7 | 7 | 9 | 5 | 4 | 3 | 2 | 0 | 0 | 0 | 0 |
| Complete | 0 | 1 | 8 | 14 | 22 | 24 | 27 | 28 | 30 | 30 | 30 | 30 |

Table 5-7: Cumulative Probability of Damage at Different Damage State for Stone in Mud Buildings with Flexible Floor and Roof for Case 2

| | **Cumulative Probability of Damage at Different PGA (%g)** | | | | | | | | | | | |
|---|---|---|---|---|---|---|---|---|---|---|---|---|
| **Damage Level** | **0.05** | **0.1** | **0.15** | **0.2** | **0.25** | **0.3** | **0.35** | **0.4** | **0.45** | **0.5** | **0.55** | **0.6** |
| Slight | 0.60 | 0.87 | 0.97 | 1.00 | 1.00 | 1.00 | 1.00 | 1.00 | 1.00 | 1.00 | 1.00 | 1.00 |
| Moderate | 0.27 | 0.67 | 0.80 | 0.90 | 0.97 | 1.00 | 1.00 | 1.00 | 1.00 | 1.00 | 1.00 | 1.00 |
| Extensive | 0.03 | 0.27 | 0.50 | 0.77 | 0.90 | 0.93 | 1.00 | 1.00 | 1.00 | 1.00 | 1.00 | 1.00 |
| Complete | 0.00 | 0.03 | 0.27 | 0.47 | 0.73 | 0.80 | 0.90 | 0.93 | 1.00 | 1.00 | 1.00 | 1.00 |

The cumulative probability of the damage at different PGA from Table 5-5 and Table 5-7 are plotted together with best fit cumulative lognormal distribution are given in Figure 5-18 and 5-19 respectively. Figure 5-20 shows the fragility functions for stone in mud buildings with flexible floor/roof in Nepal. In each case of the damage state, before the point of intersection case 2 is the upper boundary and case 1 is the lower boundary of the fragility while as after the intersection case 1 is the upper boundary and case 2 is the lower boundary. So, the actual fragility function will be somewhere in between these two curves. The median values and standard deviation for plotting cumulative lognormal distribution of different damage state are calculated from Table 5-5 and Table 5-7. The calculated median values and the standard deviations are given in Table 5-8.

Table 5-8: Median Values and Standard Deviation for Cumulative Lognormal Distribution for Stone in Mud Buildings with Flexible Floor and Roof

| | **Case 1** | | **Case 2** | |
|---|---|---|---|---|
| **Damage States** | **Median (PGA for 50% Damage)** | **Standard Deviation σ (or β)** | **Median (PGA for 50% Damage)** | **Standard Deviation σ (or β)** |
| Slight | 0.033 | 0.423 | 0.031 | 0.718 |
| Moderate | 0.080 | 0.375 | 0.079 | 0.572 |
| Extensive | 0.157 | 0.261 | 0.150 | 0.439 |
| Complete | 0.200 | 0.233 | 0.206 | 0.383 |

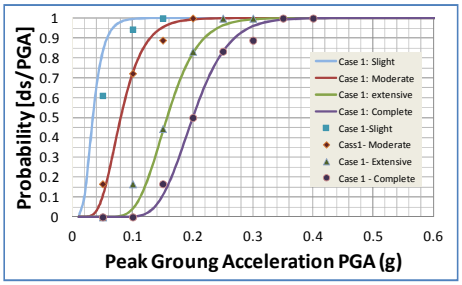


Figure 5-18: Fragility Function for Stone in Mud Buildings with Flexible Floor/Roof for Case 1

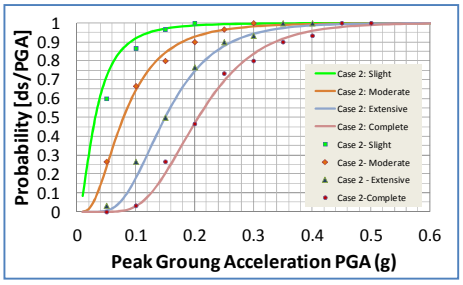


Figure 5-19: Fragility Function for Stone in Mud Buildings with Flexible Floor/Roof for Case 2

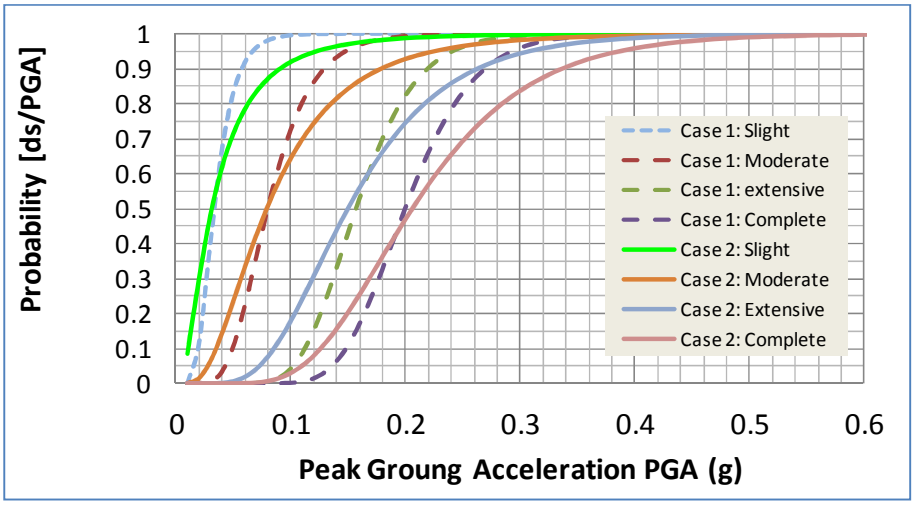


Figure 5-20: Fragility Functions for Stone in Mud Buildings in Nepal with Flexible Floor/Roof

## 5.6 Conclusions

Numerical simulation of shapeless stone masonry structures were done with a new approach of clustering randomly generated triangular meshes to form random shaped stones. 1/4 scale masonry wallet and 1/4 scale stone masonry house were numerically modeled for diagonal tension test to compare monotonic loading and dynamic loading respectively. The numerical models were prepared using proposed new approach of modeling stone masonry in AEM. The numerical simulation results obtained were compared with the experimental results. In monotonic loading case, the force-displacement relation and the crack patterns were compared with experimental results and a good agreement was found. While, in case of the

shaking table test, the initiation and propagation of cracks, acceleration output at different stage of loading and overall damage of the building till collapse were compared. The experimental and numerical results showed a good agreement in all these compared parameters. The study found that the stone masonry structures can be simulated accurately in AEM using this technique of triangular meshing and clustering.

Numerical models of several buildings with different configuration and number of stories were prepared and analyzed with different mortar properties and different input motions. Damage state of all the buildings at the given input motions are recorded according to classification based on observation of cracks, deformed shape and damage. Cumulative probability of damage at each level of PGA starting 0.05g to 0.6g are recorded for all cases for four damage state namely "Slight", "Moderate", "Extensive" and "Complete". Median value of complete damage state for stone in mud buildings is found about 0.2g which is the lowest among all type of masonry buildings analyzed and shows the very high vulnerability during earthquake loading.

**REFERENCES**

Meguro K. and Tagel-Din H. (2001). "Applied Element Simulation of RC Structures under Cyclic Loading".*Journal of Structural Engg*.; 127(11): 1295-1305

Coburn, A. and Spence, R. (2002). Earthquake Protection, West Sussex: John Wiley & Sons Ltd.

JICA. (2002). "The study on Earthquake Disaster Mitigation in the Kathmandu valley Kingdom of Nepal." Final report, Vol - II, *Japan International Cooperation Agency*, Kathmandu, Nepal.

Mayorca, P. and Meguro, K., (2004). Proposal of an Efficient Technique for Retrofitting Unreinforced Masonry Dwellings. *Proceedings on 13th World Conference on Earthquake Engineering*, Vancouver, Canada.

Pandey, BH. and Meguro, K. (2004). Simulation of Brick Masonry Wall Behavior under Inplane Lateral Loading Using Applied Element Method. *Proceedings on 13th WCEE*, Vancouver, Canada. 2004.

Ramesh GURAGAIN, Kawin WORAKANCHANA, Paola MAYORCA and Kimiro MEGURO (2006); "Simulation of Brick Masonry Wall Behavior Under Cyclic Loading Using Applied Element Method"; *Seisan Kenkyu*, Vol. 58, No. 6, pp.531-534

EERI, (2006). "Learning from earthquakes, The Kashmir Earthquake of October 8, 2005:

Impacts in Pakistan". *EERI special earthquake report,* EERI, Oakland, CA 94612-1934 USA

Ramesh GURAGAIN, Kawin WORAKANCHANA, Paola MAYORCA and Kimiro MEGURO (2006); "Simulation of Brick Masonry Wall Behavior Under Cyclic Loading Using Applied Element Method"; *Seisan Kenkyu*, Vol. 58, No. 6, pp.531-534

Robin Spence. (2007). "Saving lives in earthquakes: successes and failures in seismic protection since 1960", *Bulletin of Earthquake Engineering*, Volume 5, Number 2 (2007), 139-251

Kawin WORAKANCHANA, Paola MAYORCA, Ramesh GURAGAIN, Sathiparan NAVARATNARAJ and Kimiro MEGURO (2008); 3-D Applied Element Method for PP-Band Retrofitted Masonry; *Seisan Kenkyu*, Vol. 60 No. 2 pp.128-131

T. Rossetto and N. Peiris. (2009). "Observations of damage due to the Kashmir earthquake of October 8, 2005 and study of current seismic provisions for buildings in Pakistan", *Bulletin of Earthquake Engineering*, 7:681–699

Sakurai, K. (2011). "Experimental Study on Retrofitting of Masonry Houses Using PP-band Method for Shapeless Stone Masonry and 2-story Adobe Masonry Houses", *MSc Dissertation*, IIS, The University of Tokyo, Japan

Jitendra Bothara and Svetlana Brzev.(2011). "A TUTORIAL: Improving the Seismic Performance of Stone Masonry Buildings", Earthquake Engineering Research Institute, EERI Publication Number WHE-2011-01, Oakland, CA 94612-1934 USA

# 6. Shaking Table Experiment of Retrofitted Stone Masonry Buildings

## *6.1 Introduction*

Locally available masonry has been used as a construction material since ancient times and can be found all over the world, be it in residential houses, palaces, temples or important community and cultural buildings.

With the advent of new construction materials and techniques, the use of these materials has substantially decreased in the last few decades; however it is still used abundantly for residential buildings in rural and remote areas of Nepal. In areas accessible by road and in the plain terrains of the south, brick is widely used, and in other northern hilly and mountainous remote areas where alternate materials are unaffordable, abundantly available stone is used. Those masonry buildings are laid in weak cement sand, mud mortar, or even dry in some cases. The quality of mortar and masonry units and the level of workmanship are poor, due to lack of awareness and economic restraints on the people. The stone masonry walls mainly consist of irregularly placed undressed stones, mostly rounded. Such buildings are of the most vulnerable categories of housing due to the nature of the material (high mass, low strength, brittle) and, in the case of low-cost housing, also the lack of proper detailing and maintenance.

Given the large number of existing masonry housing at risk in rural areas of Nepal, it is necessary to retrofit the existing dwellings rather than reconstruct. Several masonry retrofitting techniques have been developed around the world with the appropriateness of each dictated by the local topographical, economical and cultural conditions. However, dissemination of these techniques to the many communities at risk is a very challenging task. The methods used to effectively meet the needs of the large population in danger of non-engineered masonry collapse must be simple and inexpensive, working with the available resources and skill. Some examples of low-cost retrofitting techniques suitable for non-engineered, non-reinforced, masonry dwellings may not necessarily save the house, however it may prevent collapse and save lives.

Seismic retrofitting of low strength masonry buildings are started in Nepal under School Earthquake Safety Program of National Society for Earthquake Technology-Nepal (NSET) since 1997 (Bothara J. K. , Pandey B. and Guragain R., 2004). There is different type of retrofitting methods applied for retrofitting of masonry buildings in Nepal since then. All type of retrofitting techniques applied for retrofitting of masonry buildings in Nepal are compared by Shrestha, Pradhan and Guragain (2012).

(a) Building under retrofit by splint-bandage method

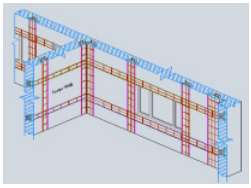

(b) schematic drawing of split and bandage system

(c) Building after second layer of concrete retrofitted by splint-band system

Figure 6-1: Process of retrofitting by Splint and bandage method

The most common retrofitting technique has been splint and bandage system. It is a system of horizontal and vertical bands of thin reinforced concrete. This method is good for masonry buildings with cement mortar. Figure 6-1 shows the process of retrofitting masonry buildings by splint-bandage method.

(a) Jacketing by reinforced concrete mesh

(b) Jacketing by galvanized wire mesh

Figure 6-2: Example of retrofitting of masonry buildings by full wall jacketing in Nepal

In case of masonry buildings with very weak mortar like mud mortar or poor quality cement-sand mortar, this method is not enough and the full wall jacketing has been implemented either with reinforced-concrete jacketing or by galvanized wire mesh jacketing. Figure 6-2 shows the example of retrofitting masonry buildings by full jacketing in Nepal. However, jacketing all the walls with reinforced concrete or galvanized wire mesh both is very

expensive in comparison to the cost of similar new buildings construction.

More economic retrofitting technique by PP-band mesh retrofitting technique is implemented as a pilot in one of the building and the experiences are documented by Macabuag, Guragain and Bhattacharya (2012). Figure 6-3 shows the process and example of PP-band mesh retrofitted building in Nepal.

(a) Low strength masonry building after installation of PP-band mesh

(b) Mud plaster work after PP-band mesh installed

(c) PP-band mesh retrofitted building after completion

Figure 6-3: PP-band mesh retrofitted building in Nepal

However, majority of school buildings are two stories and considering possible large deformation of PP-band retrofitted buildings, this method has not been applied in schools so far. So, a method of combining two system of retrofitting vertical-horizontal reinforced concrete bands and PP-band mesh has been proposed in this study. The overall concept is the reinforced concrete bands will enhance the overall strength and stiffness of the building while as the PP-band mesh will prevent the out of plane failure and provide the ductility in the system.

Shaking table test of two ¼ scale two story stone masonry with very weak mortar are constructed and shaking table test was carried out. This chapter provides the details of the model construction, the input motions and loading sequence and compares the result of the shaking table test for the two cases.

## 6.2 Model Construction

Two identical stone masonry models with weak stone masonry are constructed in ¼ scales. Figure 6-4 shows the process of construction as well as the overall dimension of the building. The models were constructed to simulate the worst case scenario in the field. Small size stones of 2-4 cm size with smooth surface and round-oval shape were used to get the worst case type of stones. Weak mortar of 1 lime: 4 sand mix of mortar was used to resemble mud mortar. The ratio of the mortar over ratio of stones in the wall was also high as about 5mm-7mm of mortar thickness was used for construction and this also made the buildings a weak case. The building has 960mm x 960mm in outer dimension at base and a height of 1300mm.

(a) Model under construction

(b) Layout of stones

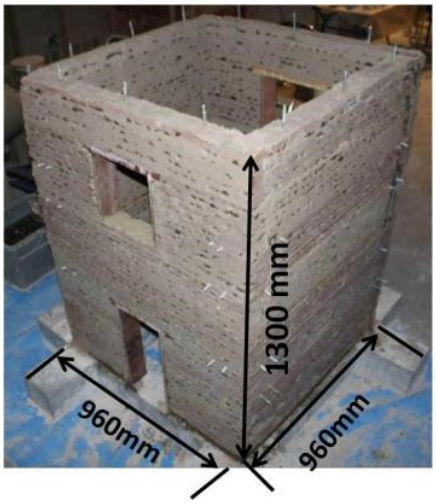


(c) Stone masonry building with overall dimension

Figure 6-4: Construction of shaking table test models

## 6.3 Retrofitting of the Models

In the first case, among the two buildings model one building was retrofitted with the same process of retrofitting stone masonry buildings in the field by splint and band system. At first the corners and the places where the horizontal bands are installed is cleaned with scraping some part of mortar to have proper bond of the added concrete to the existing wall. After all the mortar at the places of installing vertical and horizontal bands is cleaned, first coat of the mortar was used. ASTM Type-N mortar with mix ratio of 1: 1: 6, Cement: Lime: Sand was used with average compressive strength of about 5.0 MPa (750 psi). After that, 3mm diameter plain bar steel mesh was placed and the second coat of the plaster over the mesh was done. In the real retrofit construction, 8-10mm diameter deformed steel reinforcement with about 20 MPa strength is used generally in retrofitting of real buildings in Nepal. As the plain bar of small diameter and weak plaster is used the retrofitting was also weaker than the real

construction in the field. Figure 6-5 shows the construction process of the building model with splint and bandage system.

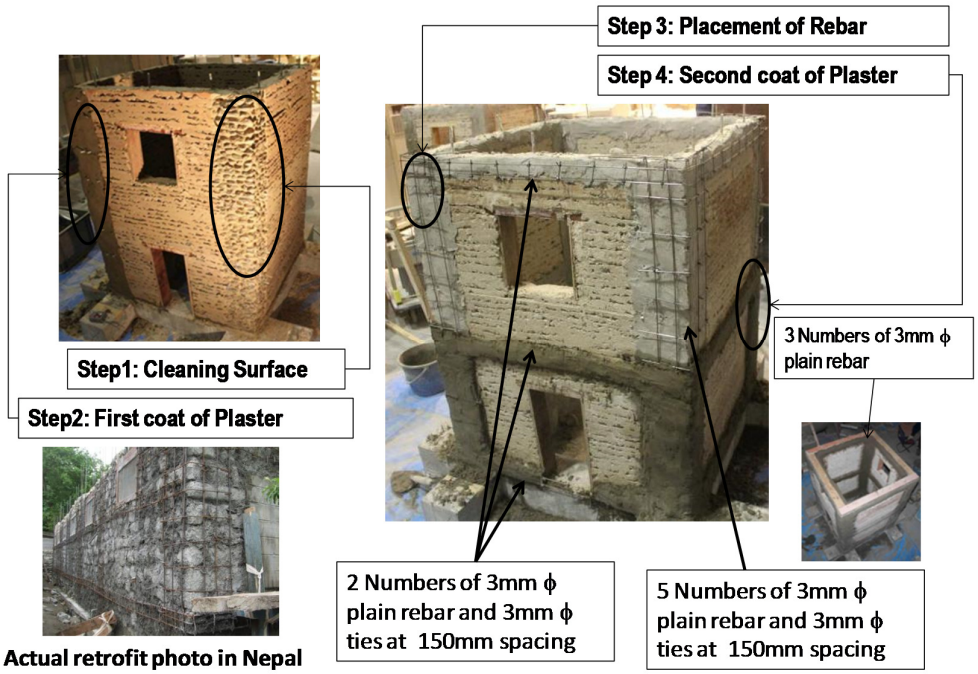


Figure 6-5: Retrofit process for the first case only with splint and bandage

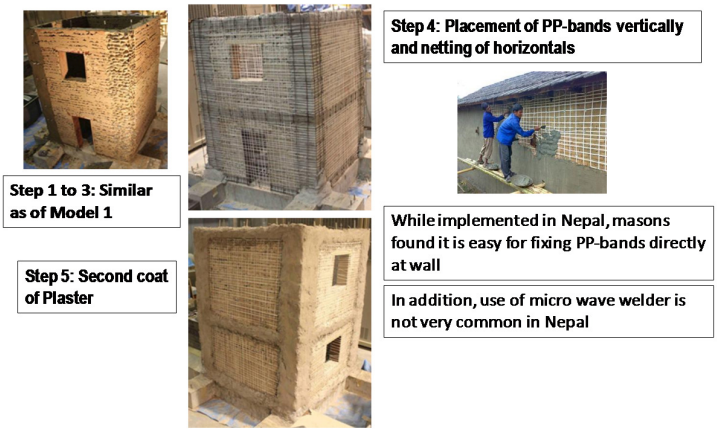


Figure 6-6: Retrofit process for the second case with splint-bandage and PP-mesh

In the second case, the other model was retrofitting by combined method using splint-band and PP-mesh together. The construction process from step 1 to 3 was similar as of Figure 6-5. After the reinforcement is placed, vertical and horizontal PP bands are placed. First, the vertical pp-bands are installed and the horizontal bands are woven in and out without using micro-wave welder. Once the placement of the PP-bands is finished, the second coat of the plaster was applied. This second coat of plaster binds all the pp-bands at the places of the

plaster bands. In the real construction, it will be the concrete covering the reinforcement which will binds the PP-meshes. No, micro-wave welder is used considering the difficulty of use it in the rural Nepal where electricity is not available.

## 6.4 Input Motions and Direction of Shaking

Sinusoidal motions of frequencies ranging from 5Hz to 35Hz and amplitudes ranging from 0.05g to 0.8g were applied to obtain the dynamic response of the structures in the experiment. Figure 6-7 shows the typical shape of the applied sinusoidal wave and Figure 6-8 shows the direction of shaking.

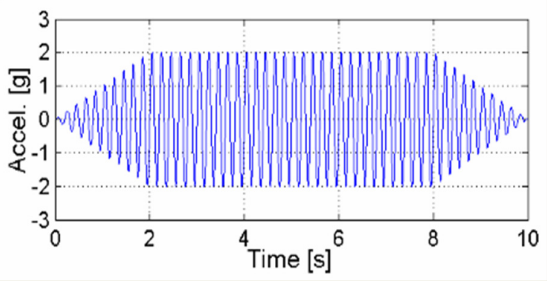


Figure 6-7: Typical Shape of the Applied Sinusoidal Wave

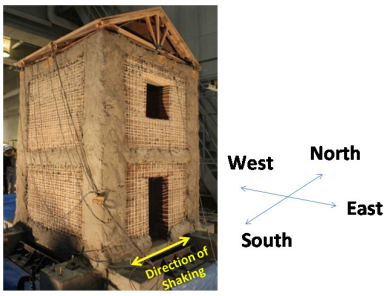


Figure 6-8: Direction of Shaking

The numbers given in the Table 6-1 shows the loading sequence followed in tests. General trend of loading was from high frequency to low frequency and from lower amplitude to higher amplitude considering the total energy content of each input motion. The direction of shaking was in parallel to door and windows. The direction of shaking is shown in Figure 6-8.

Table 6-1: Loading Sequence of Input Motions

| Amplitude | Frequency | | | | | | |
|---|---|---|---|---|---|---|---|
| | 5Hz | 10Hz | 15Hz | 20Hz | 25Hz | 30Hz | 35Hz |
| 0.8g | | 43 | 40 | 37 | 34 | 31 | 28 |
| 0.6g | | 42 | 39 | 36 | 33 | 30 | 27 |
| 0.4g | | 41 | 38 | 35 | 32 | 29 | 26 |
| 0.2g | 25 | 24 | 23 | 22 | 21 | 20 | 19 |
| 0.1g | 17 | 16 | 15 | 14 | 13 | 12 | 11 |
| 0.05g | 09 | 08 | 07 | 06 | 05 | 04 | 03 |
| sweep | 01,02 | | | | | | |

## 6.5 Results Comparison

### 6.5.1 Crack Patterns and Collapse

Both the models started getting minor cracks from corner of the openings at Run 21 with the frequency of 25Hz and acceleration of 0.2g amplitude. The cracks started from windows above the door in both the cases. The cracks were slightly wider in case of case 1 retrofitted case. Figure 6-9 shows the initial diagonal cracks appeared in the models at the 21st run.

(a) Damage to Case-1 retrofit case (b) Damage to Case-2 retrofit case

Figure 6-9: Comparison of Cracks at Run 21 (25 HZ, 0.2g)

At the run 28 with frequency of 35Hz and acceleration of 0.8g amplitude the diagonal cracks near openings were widened with losing some stones in case of case 1. In addition some portion of the south wall was also collapsed in the case of case-1 retrofit. Figure 6-10 shows the comparison of the damage level at the 28th run.

(a) Damage to case-1 retrofit case (b) Damage to Case-2 retrofit case

Figure 6-10: Comparison of Cracks at Run 28 (35 HZ, 0.8g)

The damage to the buildings continues with additional shakings. At the stage of 31st run, significant portion of the south wall of the Case-1 retrofit case was collapsed. In case of the Case-2 retrofit, the same wall, upper storey south wall was severely cracked but all the stones

were hold by the pp-bands. So, the positive effect of the PP-bands is already started seen from this stage. Similarly, there was loss of more stones near-by windows and doors in the case-1 retrofit and there was no loss of stones in the Case-2 retrofit. Figure 6-11 compares the level of damage in two types of retrofit cases after 31st run with 30Hz frequency and 0.8g acceleration.

(a) Damage to case-1 retrofit case

(b) Damage to Case-2 retrofit case

Figure 6-11: Comparison of Cracks at Run 31 (30 HZ, 0.8g)

The loss of walls increased further with additional loading. Most portions of east, west and south walls of the second storey in the Case-1 retrofit were failed completely at this stage of loading at Run-34 with 25Hz frequency and 0.8g amplitude of acceleration. In the Case-2 retrofit, all walls on the second floor severely cracked; there was significant crashing and loss of mortar but all of the stones were still hold by the PP-bands. As, this case was one of the worst case with large ratio of mortar in comparison to the quantity of stones, the case will be much better in the real case where the portion of mortar is relatively less in comparison of the stones.

(a) Damage to case-1 retrofit case

(b) Damage to Case-2 retrofit case

Figure 6-12: Comparison of Cracks at Run 34 (25 HZ, 0.8g)

Damage to the buildings is further done at the run 37 with 20Hz and acceleration of 0.8g amplitude. At this stage of loading, all four walls of the second storey of the first case of retrofitting completely collapsed. In addition, the door and window side of the walls at the 1st floor also get damaged. However, in the second case of retrofit, loss of mortar in all these walls continue but there was not loss of almost all stones. Few small stones were loss from the gap of the PP bands in case of second retrofitting. The models were not plastered to get the worst case, but in reality these buildings will be plastered after application of PP-bands and plastering will prevent loss of mortar as well as prevent falling of small stones enhancing the behavior much better.

(a) Damage to case-1 retrofit case (b) Damage to Case-2 retrofit case

Figure 6-13: Comparison of Cracks at Run 37 (20 HZ, 0.8g)

At the Run 40, 15 Hz frequency and 0.8g acceleration, Case-1 got damaged all seven walls all four side walls of second floor and three walls at the first floor. However, In Case-2, all the walls got cracked, stones got loosened but hold by the PP-bands.

(a) Damage to Case-1 retrofit case (b) Damage to Case-2 retrofit case

Figure 6-14: Comparison of Cracks at Run 40 (15 HZ, 0.8g)

The Case-2 retrofitted model was tested for two more runs till Run 42, with 10Hz and 0.6g acceleration. The damage level at the Run 42 is shown in Figure 6-15. Loss of more mortar

and some small stones continue. The governing behavior of the model also continues as previous case. More than 95% of the stones which are completely loosened were hold well by the PP-bands.

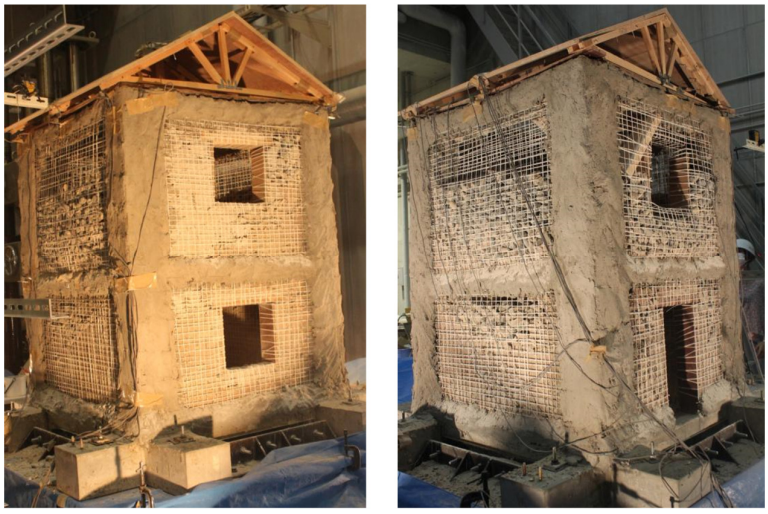

Figure 6-15: Level of Damage at Run 42 for Case-2 Retrofit

Table 6-2 gives the approximate loss in mass of the building models at different stage of loadings. The reduced mass has been considered for calculation of base shear while comparing the force displacement relation of these two models.

Table 6-2: Loss of Mass at Different Stage of Loading based on Observation

| Model | Loss of Mass at Different Stage of Loading at Different Run (% of Total Mass) | | | | | | | | | | | | | |
|---|---|---|---|---|---|---|---|---|---|---|---|---|---|---|
| | 29 | 30 | 31 | 32 | 33 | 34 | 35 | 36 | 37 | 38 | 39 | 40 | 41 | 42 |
| Model-1 | 1 | 1 | 7 | 9 | 10 | 20 | 30 | 40 | 40 | 40 | 45 | 50 | | |
| Model-2 | 0 | 0 | 0 | 0 | 0 | 0 | 1 | 3 | 3 | 3 | 4 | 6 | 12 | 12 |

### *6.5.2 Comparison of Lateral Drift and Hysteresis Curves*

The lateral drift and hysteresis curve of both the models are shown in Figure 6-16 and Figure 6-17. The hysteresis curve is plotted at the same runs where significant additional damages were recorded as described in Section 6.5.1. At the initial stage of loading when the cracks started, the lateral drift and behavior are similar in both the cases. From the Figure 6-16, it is observed that both the models behave similar till run 28. At the Run 31, stiffness of the model-1 is reduced in comparison to the model-2. The reduction in force as well as in the lateral drift is noticed in the Model-1 case mainly because of loss in mass. After significant loss in mass, which reaches up to about 50% of the total mass at the loading stage of Run 40, the model-2 loses only about 6% and thus the base shear and displacement are more in model-2.

| Model-1 | Model-2 |
|---|---|
| 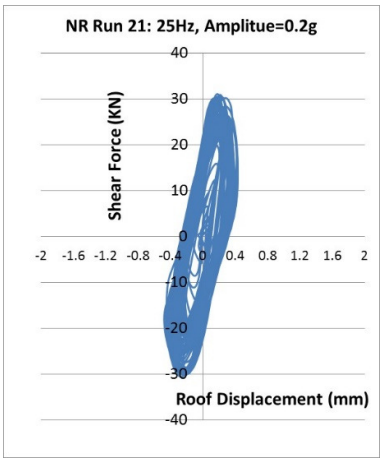 | 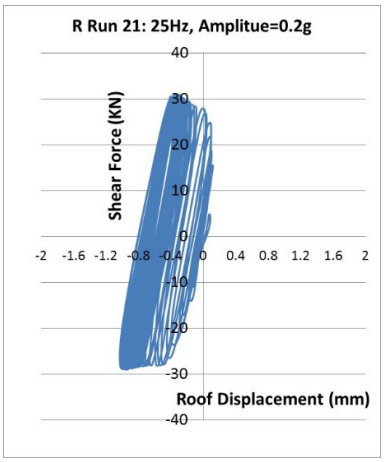 |
| 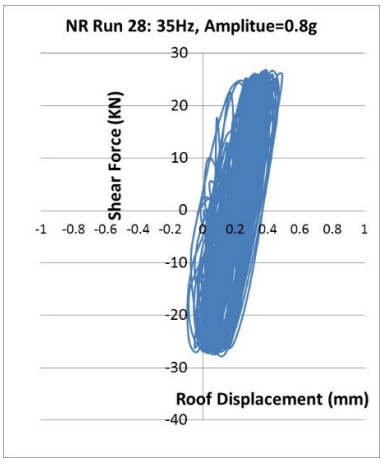 | 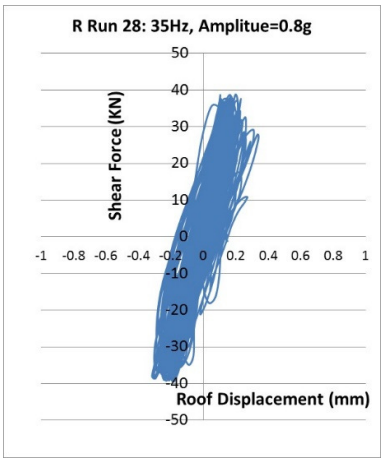 |
| 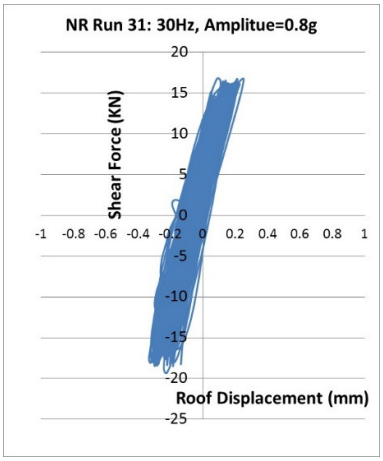 | 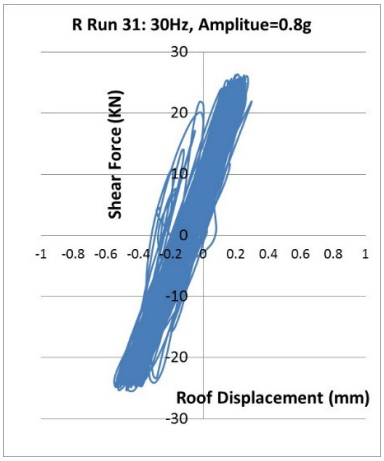 |

Figure 6-16: Comparison of Hysteresis behavior of two models at initial stage of loading

| Model-1 | Model-2 |
|---|---|
| 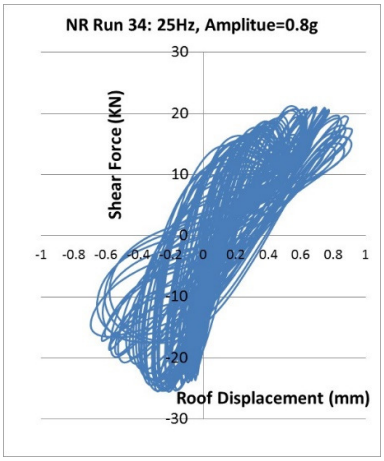 | 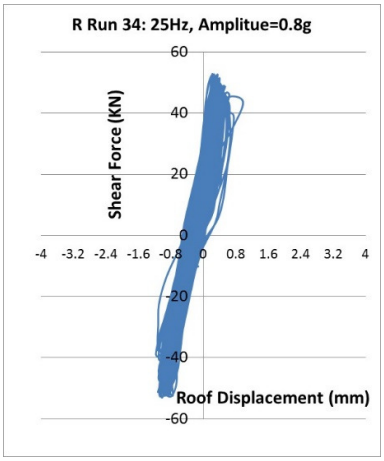 |
| 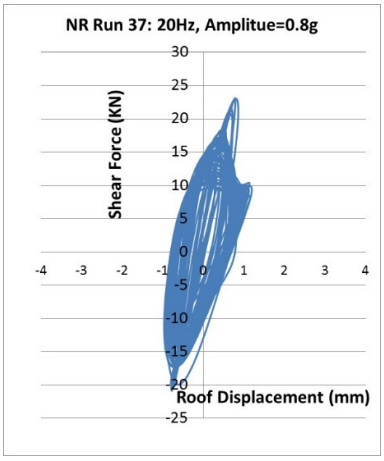 | 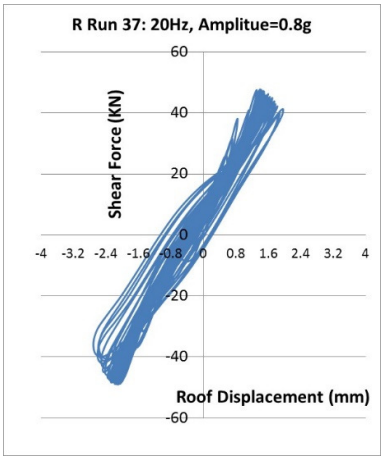 |
| 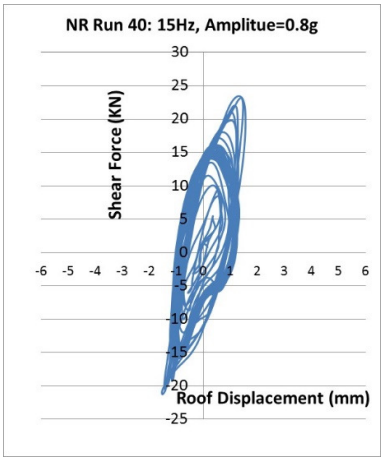 | 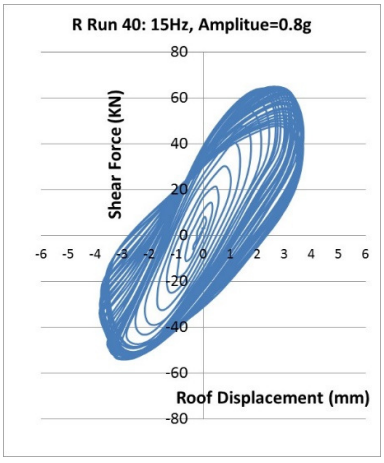 |

Figure 6-17: Comparison of Hysteresis behavior of two models at later stage of loading

### *6.5.3 Comparison of Energy Dissipation of House Models*

Energy dissipation capacity is computed by calculating the area enclosed by each hysteresis loop at the end of each run. Figure 6-18 shows the cumulative energy dissipation by two models. Until run 40, up to when both the models were tested in shaking table, there is 3.6 times difference in the energy dissipation. This clearly shows better energy dissipation capacity of the model 2 which was retrofitted by combined system of splint and bandage plus PP-bands.

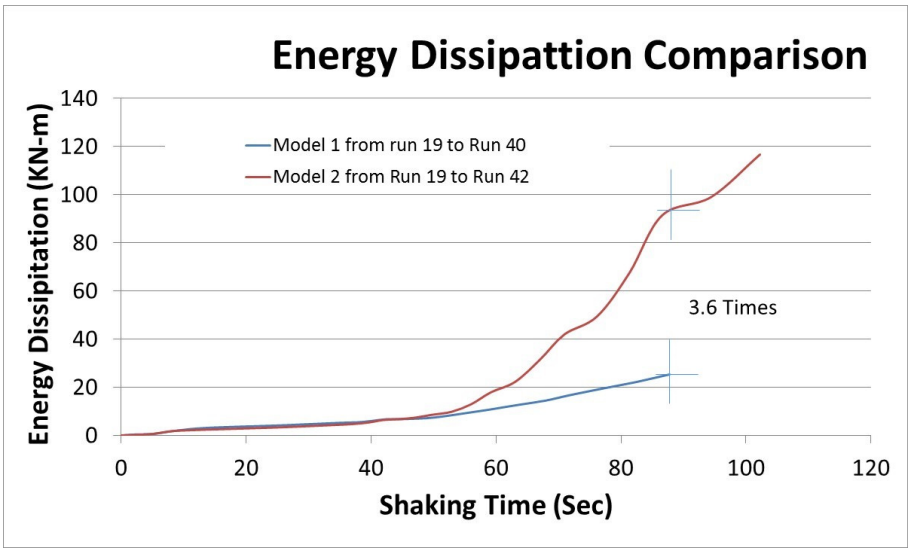


Figure 6-18: Comparison of Energy Dissipation in by Two Models

## *6.6 Conclusions and Recommendations*

Retrofitting of masonry buildings in developing country like Nepal is a challenge because of the retrofitting cost. Different retrofitting techniques are in practice in Nepal. The most common one is split and bandage system which provides thin horizontal and vertical bands of reinforced concrete at the critical location. However, this method is applicable only with those buildings which have relatively strong mortar like good quality cement-sand mortar, especially for important structures like schools. Other retrofitting methods like full walls jacketing are also in practice to prevent collapse of any part of the walls. However, those full jacketing are generally expensive.

Some more economical options like PP-band mesh retrofitting was also applied in one building. However, it could not be applied to 2 stories school buildings considering large potential deformation. So, a combined system of using reinforced concrete bands and PP-

bands together is proposed so that it can be used for 2-3 stories buildings also which are the dominant buildings in Nepal.

Two identical stone masonry models are constructed to compare the benefit of this proposed concept of retrofitting through shaking table test. Due attention was given to prepare the models as the worst case in the field. Majority of stones used were rounded shape, relatively high mortar/stone ration was used, very weak mortar was used to simulate the mud mortar, plain bars are used for retrofitting than the deformed bar, no micro-wave welder is used to attach the pp-bands together and no plaster was applied over PP-bands. Thus, all the weaker conditions are considered.

Both the models are tested on shaking table with sinusoidal motions of different frequencies and amplitude. The general trend of input motions was from higher frequency to lower frequencies considering the total energy content of the input motions. So, the input motions were provided from low energy input motions to high energy input motions.

The result obtained are compared in terms of crack patterns and damage level, total mass loss at different stage of loading, hysteresis behavior and the cumulative energy dissipation. The comparison clearly shows that the model with combined system performed much better in terms of overall damage and loss of mass, better hysteresis behavior and also better energy dissipation capacity. Some loss of mortar and small stones were observed at the later stage of loading, however, in the real situation the proportion of the mortar with the stones will not be as much as in this experimental case and thus the loss of mortar will be less. In addition, in all the cases wherever the PP-band mesh is used for retrofitting, PP-meshes need to be covered by some materials to protect from ultraviolet effect and thus there are no cases without plaster. Plastering over the PP-band meshes enhance the behavior and also prevent such type of loss of crushed mortar.

Analyzing these results and considering the recommend practice of the splint and bandage system of retrofitting, it can be recommended to use this combined system for 2-3 stories buildings including schools in Nepal.

**REFERENCES**

Bothara J.K., Pandey B., Guragain R. (2004). Seismic retrofitting of low strength unreinforced masonry non-engineered school buildings, *Bulletin of the New Zealand Society for Earthquake Engineering ISSN 1174-9857,* vol. 37, No1 (2004), 13-22

Hima Shrestha, Suman Pradhan, Ramesh Guragain (2012), Experiences on Retrofitting of Low Strength Masonry Buildings by Different Retrofitting Techniques in Nepal, *15WCEE*, Portugal, 2012.

Macabuag, Guragain and Bhattacharya (2012), Seismic retrofitting of non-engineered masonry in rural Nepal, *Structures and Buildings* 165, Issue-SB6, 273–286

# 7. Numerical Simulation of Earthquake Resilient Masonry Buildings and Development of Fragility Functions

## *7.1 Introduction*

This chapter focuses on numerical simulation of earthquake resilient buildings. This study focuses on numerical simulation of brick masonry buildings constructed as per Nepal National Building Code. At this first stage, brick in cement buildings are simulated.

## *7.2 Numerical Simulation of Brick Masonry Buildings with Code Recommended Practices and Development of Fragility Functions*

### *7.2.1 Brick in Cement Buildings with Flexible Floors/Roof*

**Models Preparation and Observation of Damages**

Four brick masonry buildings, as per the recommendation of the Nepal National Building Code (NBC), are modeled for numerical simulation was conducted. Figure 7-1 shows the models of the buildings prepared for numerical simulation. NBC recommends for two thin layer of concrete bands at lintel level and sill level, corner stitches (Small piece of corners connection) and single vertical reinforcement bar are each corners and also at side of the openings. Thickness of the concrete bands is considered 6 cm and the width of the bands are equal to the width of the walls. Main longitudinal bars taken as 2 numbers of 10 mm diameter bars and 7 mm diameter bars are considered for transverse reinforcement as per the recommendation by NBC. 16mm diameter bars are considered at 4 corners 12mm diameter bars are considered for side of the doors and windows as the vertical reinforcement bars. 15MPa concrete is considered for bands. The connection between the bands and the masonry is considered as the mortar strength.

The buildings selected are with similar configuration of the buildings simulated for existing buildings without building code implementation in chapter 4. Each of these buildings are simulated with three mortar strength, high strength, average strength and low strength as per the field survey results of the strength of brick masonry bond strength as described in chapter 3. Five time histories, given in chapter 4 are used for the simulation of these buildings also.

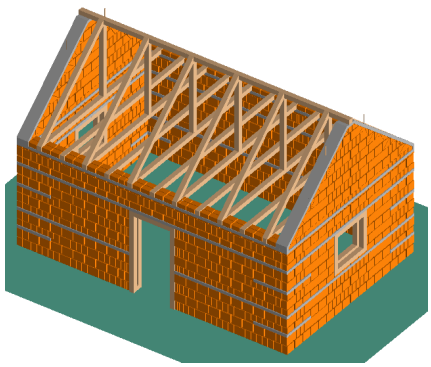

(a) BCER-1: One storey with gable

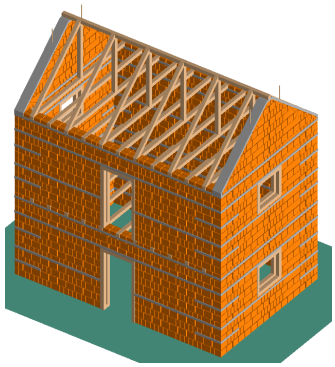

(b) BCER-2: Two storey with gable

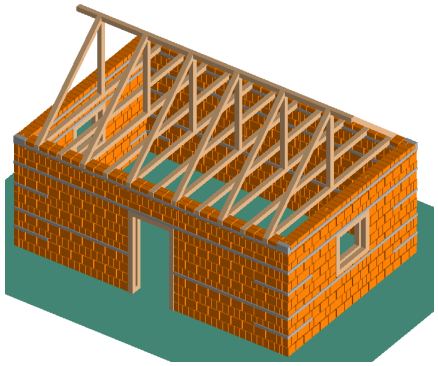

(c) BCER-3: One storey without gable

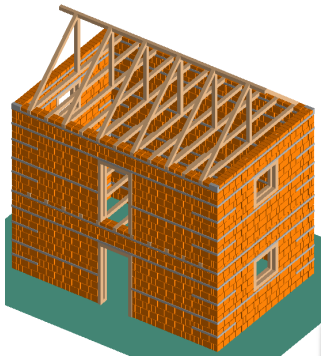

(d) BCER-4: Two storey without gable

Figure 7-1: Numerical Model of Earthquake Resilient Brick Masonry Buildings as Recommended by Nepal Code

Earthquake performance of the buildings has been found significantly enhanced in comparison to the buildings constructed without considering code. Table 7-2 shows a comparison of the performance of same configuration and same masonry mortar strength building with and without considering the building code provisions.

| **Building without Code** | **Building as per Building Code** |
|---|---|
| 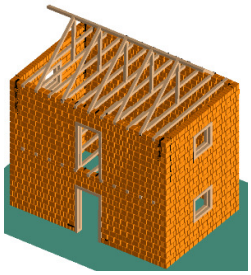 | 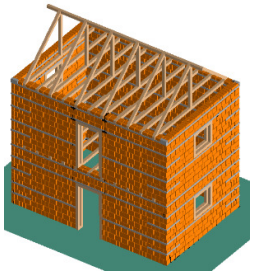 |
| PGA: 0.1g, Slight Damage | PGA:0.4g, Slight Damage |
| 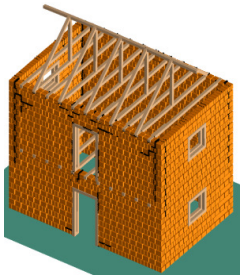 | 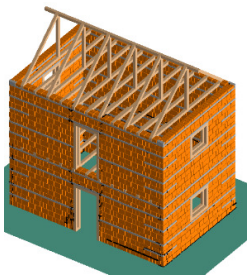 |
| PGA: 0.15g, Moderate Damage | PGA: 0.6g, Moderate Damage |
| 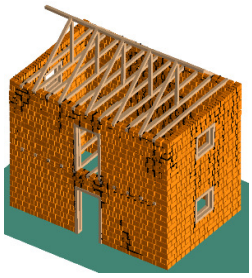 | 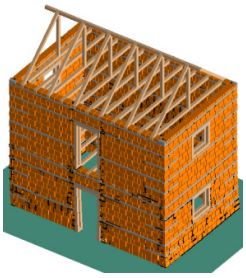 |
| PGA: 0.25g, Extensive Damage | PGA: 0.8g, Extensive Damage |
| 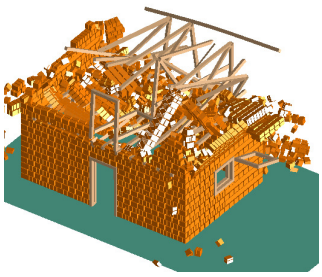 | 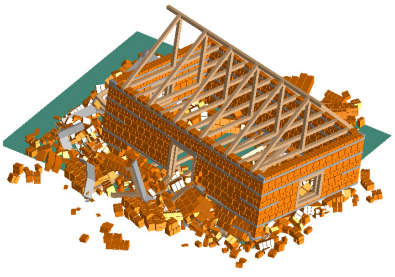 |

| PGA: 0.35g, Complete Damage | PGA: 1g, Complete Damage |
|---|---|

Figure 7-2: Comparison of Damages to Building with and without Building Code

**Compilation of Damage State and Plotting Fragility Functions**

All four buildings as shown in Figure 7-1 are analyzed with three different mortar strength, average, weak ($20^{th}$ percentile) and strong ($80^{th}$ percentile) from Table 3-4. Thus, total of 20 cases for the 4 buildings analyzed at different PGA using five different input motions of different scale. The buildings were analyzed till complete collapse and the damage state at different PGA are noted. The damage states were noted through observation of cracks, deformed shape and damage level.

Table 7-1: Damage State of Different Cases of Brick Masonry as per Provision of Code for Reinforcement

| Buildings | Acceleration (g) | | | | | | | | | | | | | | |
|---|---|---|---|---|---|---|---|---|---|---|---|---|---|---|---|
| | 0.1 | 0.2 | 0.3 | 0.4 | 0.5 | 0.6 | 0.7 | 0.8 | 0.9 | 1.0 | 1.1 | 1.2 | 1.3 | 1.4 | 1.5 |
| BCER1-Avg-Nep | N | N | N | S | M | M | M | M | E | E | C | C | C | C | C |
| BCER1-Avg-chi | N | N | N | S | M | M | M | M | E | E | C | C | C | C | C |
| BCER1-Avg-Koce | N | N | S | M | M | M | M | E | E | E | C | C | C | C | C |
| BCER1-Weak-Kobe | N | N | S | M | M | M | E | C | C | C | C | C | C | C | C |
| BCER2-Strong-Loma | N | N | N | N | S | S | S | M | M | E | C | C | C | C | C |
| BCER2-Avg-Nep | N | N | N | N | S | S | M | M | E | C | C | C | C | C | C |
| BCER2-Avg-Chi | N | N | N | N | S | S | M | M | E | C | C | C | C | C | C |
| BCER2-Avg-Koce | N | N | N | S | S | M | M | E | C | C | C | C | C | C | C |
| BCER2-Weak-Kobe | N | S | M | M | E | C | C | C | C | C | C | C | C | C | C |
| BCER3-Str-Loma | N | N | N | N | S | S | S | S | M | M | E | E | E | E | C |
| BCER3-Avg-Nep | N | N | N | N | S | S | S | M | M | E | E | E | C | C | C |
| BCER3-Avg-chi | N | N | N | N | S | S | S | M | M | E | E | E | C | C | C |
| BCER3-Avg-Koce | N | N | N | S | S | M | M | M | E | E | E | C | C | C | C |
| BCER3-Weak-Kobe | N | N | S | S | M | M | E | E | C | C | C | C | C | C | C |
| BCER4-Str-Koce | N | N | N | S | S | S | S | M | M | M | E | E | C | C | C |
| BCER4-Avg-Nep | N | N | N | S | S | S | M | M | E | C | C | C | C | C | C |
| BCER4-Avg-Chi | N | N | N | S | S | S | M | M | E | C | C | C | C | C | C |
| BCER4-Avg-Koce | N | N | N | S | S | M | M | E | E | C | C | C | C | C | C |

| | | | | | | | | | | | | | | | |
|---|---|---|---|---|---|---|---|---|---|---|---|---|---|---|---|
| BCER4-Weak-Kobe | N | S | M | M | E | E | C | C | C | C | C | C | C | C | C |
| BCER1-Avg-Nep | N | N | N | S | M | M | M | M | E | E | C | C | C | C | C |
| N: Negligible; S: Slight Damage; M: Moderate Damage; E: Extensive Damage; C: Complete Damage | | | | | | | | | | | | | | | |

In the similar way described in previous sections, the cumulative probability damage for different damage state at the given acceleration is calculated and plotted as the fragility function.

The fragility function developed for brick masonry buildings with flexible floor/roof and cement mortar with building code implementation is given in Figure 7-3.

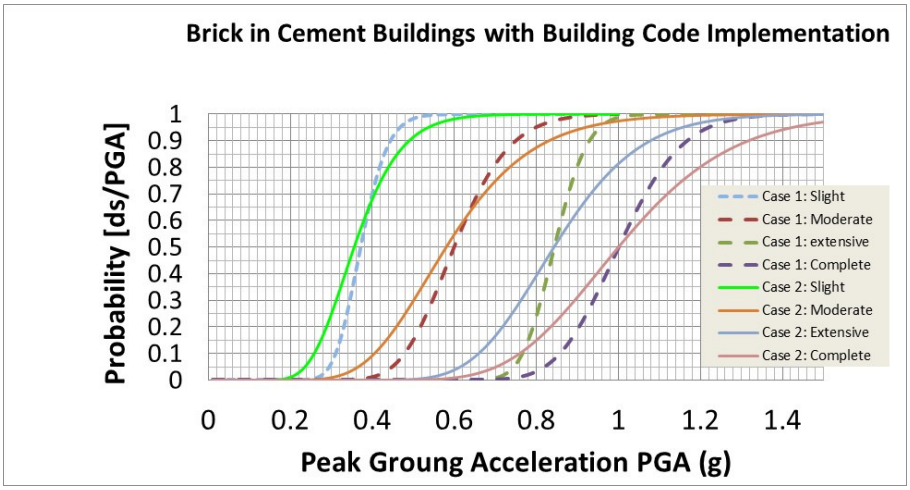


Figure 7-3: Fragility Functions Developed for Brick Masonry Buildings with Building Code Implementation

## *7.3 Conclusions*

Numerical simulation of limited number of brick masonry buildings with cement mortar and flexible floor/roof with building code implementation are conducted and fragility functions are plotted as per the method described earlier. It clearly shows that for the same category of buildings the buildings with building code implementation survived about 3 time larger amplitude earthquakes.

# 8. Use of Fragility Function Developed under this Study for Damage Estimation at City Level

## *8.1 Introduction*

The newly developed fragility functions for different type of masonry buildings were applied in one of the city in Nepal. Possible damage to buildings at the scenario earthquake is calculated using four different set of fragility functions. Three existing set of fragility functions and one set of new fragility functions developed under this study was used for the damage estimation. This chapter gives the comparison of the damage by using different fragility functions used for damage estimation.

## *8.2 Information on Case Study City*

Vyas Municipality in western region of Nepal was chosen as the case study. Figure 8-1 shows location map of the city in Nepal. The size of the city was about 60 sq. km and total number of buildings was about 6500. Figure 8-2 shows the overall buildings distribution in the city. About 15% of the buildings are Reinforced Concrete and about 85% of the buildings are different types of masonry.

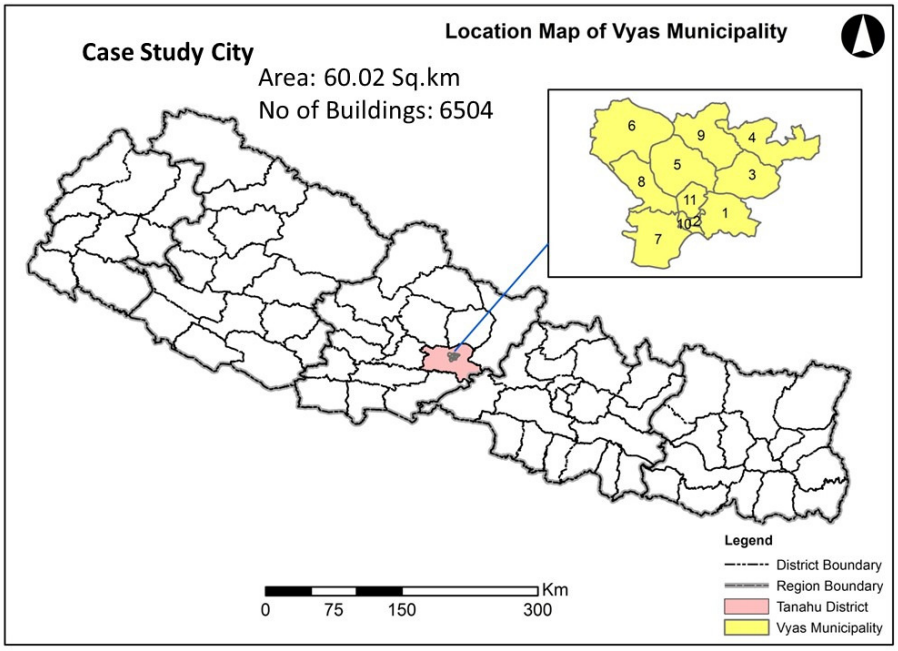


Figure 8-1: Location Map of Case Study City

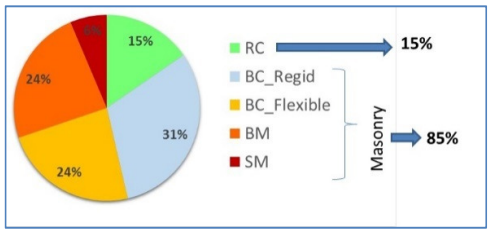


Figure 8-2: Overall Building Stock Distribution

## 8.3 Scenario Earthquake and Buildings Type Distribution

Figure 8-3 and 8-4 show the scenario earthquake and ward-wise buildings distribution in the case study city.

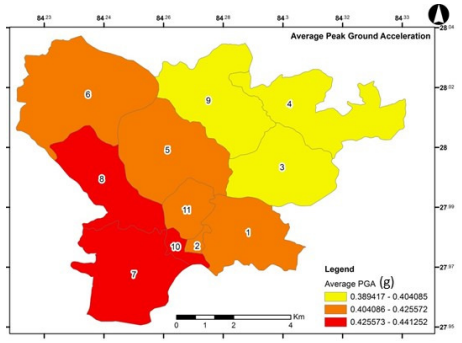


Figure 8-3: Scenario earthquake considered for risk assessment

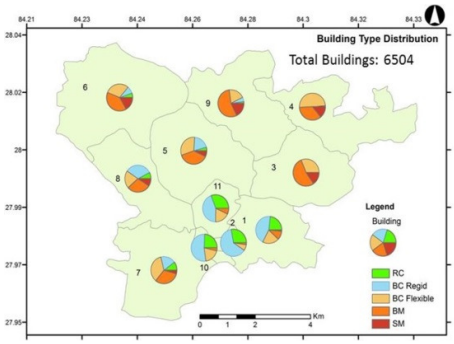


Figure 8-4: Ward-wise buildings distribution

## 8.4 Fragility Functions used for Loss Estimation

Possible damage to buildings at the scenario earthquake is calculated using four different set of fragility functions. Three existing set of fragility functions and one set of new fragility functions developed under this study was used for the damage estimation. Figure 8-5 shows the schematic descriptions of the four type of the fragility functions with their type and details used for the loss estimation.

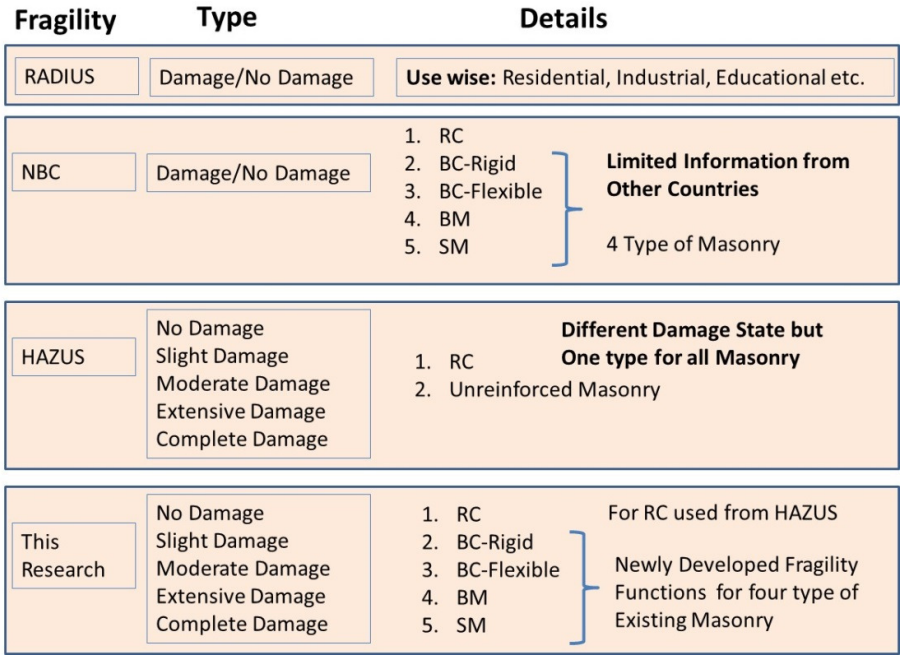


Figure 8-5: Different set of fragility used for loss estimation

## 8.5 Damage Estimation Results

Figure 8-6 and 8-7 show the loss estimation using RADIUS fragility functions and Nepal Building Code (NBC) Fragility Functions respectively.

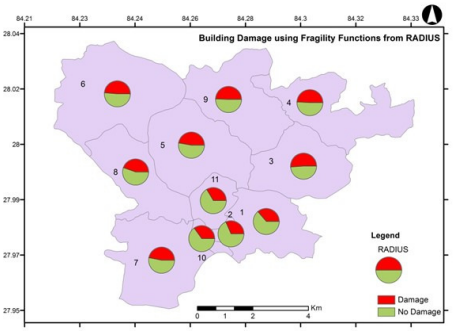


Figure 8-6: Buildings damage using RADIUS fragility functions

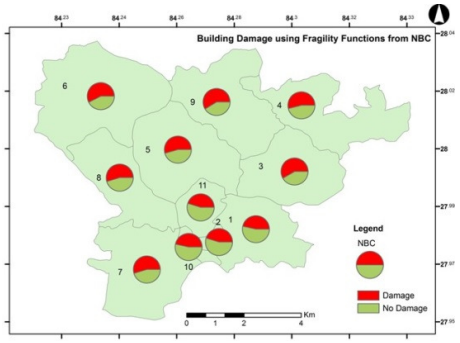


Figure 8-7: Buildings damage using NBC fragility functions

Figure 8-8 and 8-9 show the damage obtained using HAZUS fragility functions and newly developed fragility functions under this study.

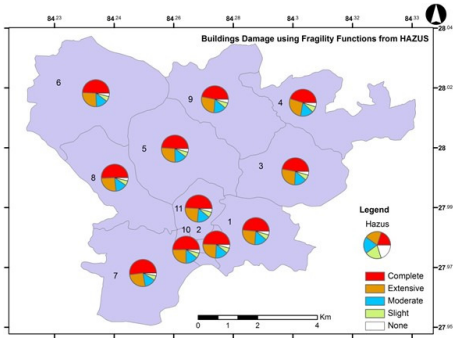


Figure 8-8: Buildings damage using HAZUS fragility functions

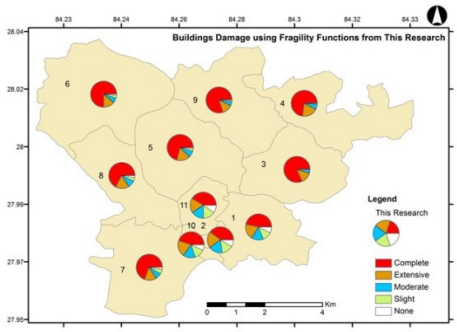


Figure 8-9: Buildings damage using newly developed fragility functions

## 8.6 Conclusions

In case of RADIUS fragility and NBC fragility, the damage are described as "damage" and "no damage" and further details of damages are not available.

In case of HAZUS, though different state of damages are obtained, the damage is average as there is only one type of fragility function for all four types of unreinforced masonry buildings. However, the case of newly developed fragility functions, the damage can be seen more in wards where there are weaker category of buildings like Stone in Mud (SM), Brick in Mud (BM) and Brick in Cement with flexible floor and Roof (BC-Flexible) while there is less damage in wards with larger number of Reinforced Concrete (RC) and Brick in Cement with Rigid Floor/roof category of buildings.

The comparison clearly shows the use of the newly developed fragility functions gives more specific damage at the given location considering the varieties of buildings available in that location.

# 9. Conclusions and Recommendations

Earthquake risk evaluation is the first step for realistic and effective planning and implementation of earthquake risk reduction as well as preparedness initiatives as it helps understanding the underlying problems and its magnitude. Different risk assessment methods are used in Nepal in some cities but the need is to do the risk assessment work at the national level and also at the large number of cities. Therefore, there was a need for a study on development of earthquake risk assessment system in Nepal which suggests appropriate tool/s for conducting earthquake risk assessment at different scale in Nepal, provides/recommend appropriate fragility functions for different types of Nepalese buildings and also suggest how much risk can be reduced if the risk reduction activities are implemented.

So, the overall Goal of this research was "Development of Earthquake Risk Assessment System in Nepal" and the specific objectives were:

1. Study and compare different tool/s for earthquake risk assessment and recommend to use at city and national level
2. Develop and recommend fragility functions for prevalent vulnerable type of buildings in Nepal
3. Compare effectiveness of retrofitted buildings in relation to the developed fragility functions

Conclusions and recommendations of the study under these three objectives are as follows:

**1. Comparison of the different tools and recommendations for city and national level:**

Eight different earthquake risk assessment methodologies and tools used in different cities and communities in Nepal were compared for their characteristics in terms of stakeholders' involvement, provisions of detail input and output, resources required for assessment works, simplicity for use, appropriateness for use at city level and national level and the tools and accessories are open source or not. HAZUS and Open Quake are found better options for national level risk assessment and RADIUS is found comparatively better for cities where there is no GIS information of buildings and infrastructures while as CAPRA GIS is found better for cities where GIS information of individual buildings and infrastructures are available.

**2. Development of fragility functions for existing buildings:**

Computation of fragility functions for non-engineered low strength brick masonry buildings in Nepal through time history analysis using Applied Element Method (AEM) was done. Extreme Loading for Structures (ELS) tool is used for AEM simulation. Key parameter

required for non-linear analysis like shear strength of existing masonry buildings was obtained through direct shear test in actual field condition. The result obtained from AEM was compared with shaking table test results and a good agreement on experimental and numerical simulation result was found. Numerical models of several buildings with different configuration and number of stories for three different category of brick masonry buildings were prepared and analyzed with different mortar properties and different input motions. Damage state of all the buildings at the given input motions are recorded and cumulative probability of damage at each level of Peak Ground Acceleration (PGA) are recorded and a set of fragility functions for four damage state namely "Slight", "Moderate", "Extensive" and "Complete" are computed for three different types of brick masonry buildings prevalent in Nepal.

For the development of fragility functions for stone masonry buildings, a new approach of clustering randomly generated triangular meshes to form random shaped stones is proposed in this study. Numerical models of two experimental cases, one for monotonic load case and the other for dynamic load case, were prepared applying the proposed new approach of modeling. The numerical simulation results obtained were compared with the experimental results. In monotonic loading case, the force-displacement relation and the crack patterns were compared with experimental results and a good agreement was found. While, in case of the shaking table test, the initiation and propagation of cracks, acceleration output at different stage of loading and overall damage of the building till collapse were compared. The experimental and numerical results showed a good agreement in all these compared parameters. The study found that the stone masonry structures can be simulated accurately in AEM using this technique of triangular meshing and clustering. Numerical models of representative stone masonry buildings with different configuration and mortar strength were prepared, analyzed and fragility functions were developed.

**3. Compare effectiveness of retrofitted buildings in relation to the developed fragility functions:**

Retrofitting of masonry buildings in developing country like Nepal is a challenge because of the retrofitting cost. A combined system of using reinforced concrete bands and PP-bands together is proposed in this study and shaking table tests were conducted to compare the effectiveness. Two identical two-story stone masonry buildings of quarter scale were constructed and tested to compare the benefit of this proposed concept of retrofitting through shaking table test. One building model was retrofitted only with reinforced concrete bands and the other with the proposed combined system. Both the models were tested on shaking table with sinusoidal motions of different frequencies and amplitude. The result obtained were compared in terms of crack patterns and damage level, total mass loss at different stage of

loading, hysteresis behavior and the cumulative energy dissipation. The comparison clearly shows that the model with combined system performed much better in terms of overall damage and loss of mass, better hysteresis behavior and also better energy dissipation capacity while the additional cost of PP-bands is negligible.

Numerical Simulation of masonry buildings with code recommended practices were conducted to discuss the change in fragility functions of earthquake resilient masonry buildings with the existing buildings. A remarkable change in safety as well as fragility functions were noticed from the comparison.

Finally, comparative study on earthquake damage assessment at the same scenario earthquake with existing buildings information was conducted using existing fragility functions and the newly developed fragility functions. The comparison clearly shows the use of the newly developed fragility functions gives more specific damage at the given location considering the varieties of buildings available in that location.